Assessment of the Current and Future Saltwater Intrusion Into the Cai River in Nha Trang, Vietnam

B. van Kessel
P.T. Kockelkorn
T.R. Speelman
T.C. Wierikx

TU Delft Delft University of Technology

Assessment of the Current and Future Saltwater Intrusion Into the Cai River in Nha Trang, Vietnam

by

B. van Kessel	4552318
P.T. Kockelkorn	4477499
T.R. Speelman	4448332
T.C. Wierikx	4460510

Final version
Submitted on June 30, 2021

Course:	Civil Engineering Consultancy Project (CIE4061-09)	
Project duration:	April, 2021 – July, 2021	
Project committee:	Dr. T.A. Bogaard	Delft University of Technology
	Dr. ir. A. Blom	Delft University of Technology
	Ir. J.L.F. Eulderink	Delft University of Technology
	Dr. Mai Van Cong	Thuyloi University
	Dr. Dinh Nhat Quang	Thuyloi University
	Dr. Mai Cao Tri	Hanoi University of Civil Engineering

An electronic version of this report is available at `http://repository.tudelft.nl/`.

Cover picture by K. Dobrev, 2019

TU Delft

ĐHTL 1959

Preface

We have written this report for the Civil Engineering Consultancy Project at the Delft University of Technology in the Netherlands in collaboration with the Thuyloi University and the Hanoi University of Civil Engineering in Vietnam. As we are all civil engineering students from different disciplines, we had to study this specific subject extensively before we could make a proper start. In that process, we have learnt a lot. We gained not only hydrological knowledge but also academic skills. Initially, this project was planned to be completely different to us. When the four of us came together for the first time, nobody had heard of Covid-19. We wanted to do this project abroad, but of course, this was not possible anymore after the start of the pandemic. We still wanted to start with the project despite the fact that we were not allowed to go to Vietnam and we have not regretted this choice for a second. Working from home and the university, we were strongly motivated to achieve a great result.

We have received valuable feedback and input from different people towards the completion of this report. Firstly, we would like to thank Ir. Juliette Eulderink for setting up the project and putting us in touch with Vietnam. We are very grateful for all the help of our supervisors. Without the weekly tips, input and enthusiasm of not only Juliette but also Dr. Thom Bogaard and Dr. Ir. Astrid Blom this research would not be as good as it is now. Also, the experience of our Vietnamese supervisors Dr. Mai Van Cong, Dr. Dinh Nhat Quang and Dr. Mai Cao Tri helped us a lot. Especially by being able to collect so much data on the Cai River, they enabled us to perform extensive analyses. It is unfortunate we were not able to meet in person, but maybe we will sometime in the future!

In the process, we also got help from some other people than our supervisors. We would like to thank Prof. Dr. Ir. Hubert Savenije for giving valuable insights into the application of the analytical model and Dr. Ir. Bas van Maren for assisting us with the numerical model. Furthermore, we are grateful to Tung Dao MSc for his help with translating and interpreting Vietnamese documents.

Overall, we are satisfied with the results of this research. It is great to see how much work can be done by four students in two months time. We hope there will be follow-up research capable of validating our models and investigating the other topics that play a role in the Cai River basin. For now, we hope you enjoy the read!

B. van Kessel
P.T. Kockelkorn
T.R. Speelman
T.C. Wierikx

Delft, June 2021

Summary

The Cai River is located in the South Central part of Vietnam, runs through the city of Nha Trang and flows out in the South China Sea. The Cai River basin has a tropical monsoon climate which is characterised by a yearly dry and wet season. Due to this climate, the discharge in the Cai River shows high seasonal fluctuations. In the dry season, the low discharge can lead to significant saltwater intrusion into the Cai River. The saltwater intrusion is undesirable because water with salinity higher than 0.25 kg/m^3 is not usable for domestic and agricultural purposes. Future changes in climate are likely to impact the magnitude and profile of the saltwater intrusion and could possible worsen the negative effects. Therefore, this report analysed what factors influence the magnitude and profile of the saltwater intrusion. Together with projections linked to climate change scenarios, insight was obtained on the development of the saltwater intrusion by applying an analytical and numerical model. Finally, this research analysed the effect of a saltwater intrusion prevention dam.

The river discharge has a significant impact on saltwater intrusion. In order to analyse the river discharge, this research set up the water balance of the Cai River basin and quantified the incoming and outgoing water via respectively precipitation and evapotranspiration. Within the system, the water is used in various ways before it returns to the river or evaporates. A closed water balance on a monthly basis is required in order to link the discharge to the system parameters. However, it was found that 37% more water seemed to leave the basin compared to the water that enters the basin. The discharge data was the most likely source of error. Due to this imbalance error and data gaps, this research did not succeed in closing the water balance.

Besides the discharge, boundary conditions like the seawater level of the South China Sea and the bathymetry of the Cai River determine the magnitude and profile of the saltwater intrusion. The boundary conditions are important input parameters for the models used. Different climatological processes affect the sea level and the tides affect the fluctuations of the sea level. This paper obtained data on all boundary conditions and analysed the tidal spectrum to use as input for the numerical model.

Future expected change in terms of maximum saltwater intrusion was analysed by looking at the projections on the water balance and the boundary conditions. This research concluded that the precipitation and the water demand increases, but the trend of evapotranspiration shows no increase into the future. With some uncertainty, the discharge was expected to slightly increase during all months of the year. Climate change projections expect the sea level to rise by approximately 35-45 cm through to the year 2070, depending on the specific climate change scenario used. The river mouth width was expected to show no natural changes into the future since it is constrained by human construction works. Human interventions can change the future bathymetry, but this was beyond the scope of this research.

The saltwater intrusion was modelled with both an analytical model (based on Savenije, 2006) and a numerical model (in Delft3D). The results of both models were analysed and compared to each other and to in situ measurements. It was concluded that the discharge is the strongest driver in salinity changes based on the results of the models. The most significant change in boundary conditions in the past 20 years is the widening of the river mouth from 130 to 438 m, which potentially increased salinity by 2-3 kg/m^3 at approximately 5 km from the river mouth. The intrusion length is not influenced significantly by changes in the river mouth width. Based on all drivers of saltwater intrusion, freshwater usage has a limited effect and will likely remain as such. Future changes in discharge were expected to have a substantially larger effect, but discharge is mainly human-controlled in the dry season and the extend of saltwater intrusion can therefore also be controlled.

A saltwater intrusion prevention dam showed to be effective in the conceptualized simulations when the gates are at their highest position. For lower positions of the gates, it decreases the salinity values upstream of the dam, but the saltwater intrusion length remains roughly constant. Simulations of different dam positions showed that the dam situated 2.7 km from the river mouth is the most effective. However, the reliability of the effects of the dam on salinity values remains low, because of minor model validation due to a lack of data from measurements. The dam could have a reduced effectiveness in this specific estuary, because the estuary of the Cai River is well-mixed, especially for low discharges (20 m^3/s or lower). The sea level rise can

increase salinity values up to 2.5 kg/m^3 in 2070 till 8 km from the river mouth and saltwater could reach up to 1 km further if all other factors remain constant.

Based on the methods, results and discussion, the authors proposed several ways towards improving the results of this research and further additional research on the same topic. More elaborate in situ measurements of the salinity would contribute greatly to the validation and accuracy of both models. Next to acquiring more in situ data, more accuracy in predictions of the future saltwater intrusion can be obtained by improving the models themselves. Examples of the possible improvements of the models and their results are detailed salinity measurements in the Cai River and real-time operations of the dam during the numerical simulation.

Contents

List of Figures

List of Tables

1

Introduction

The Cai River flows through the Khanh Hoa province in South Central Vietnam. The river flows out into the South China Sea at Nha Trang. The Cai River basin has an area of 1892 km^2 and is shown on the map of Figure 1.1. Khanh Hoa has a tropical monsoon climate with an annual mean temperature of 26.7 °C, every year has a dry season from January to August and a wet season from September to December. These seasonal differences cause a large variation in the river. In the dry season, the mean discharge of the Cai River is about 30 m^3/s and in the wet season, the discharge can be up to 20 times higher [26]. The Cai River serves two main functions for the local population: freshwater supply and shipping. Seasonal differences and freshwater demand pose multiple hydrological problems in the Cai River basin like flooding, saltwater intrusion, coastal erosion and excessive sediment deposition.

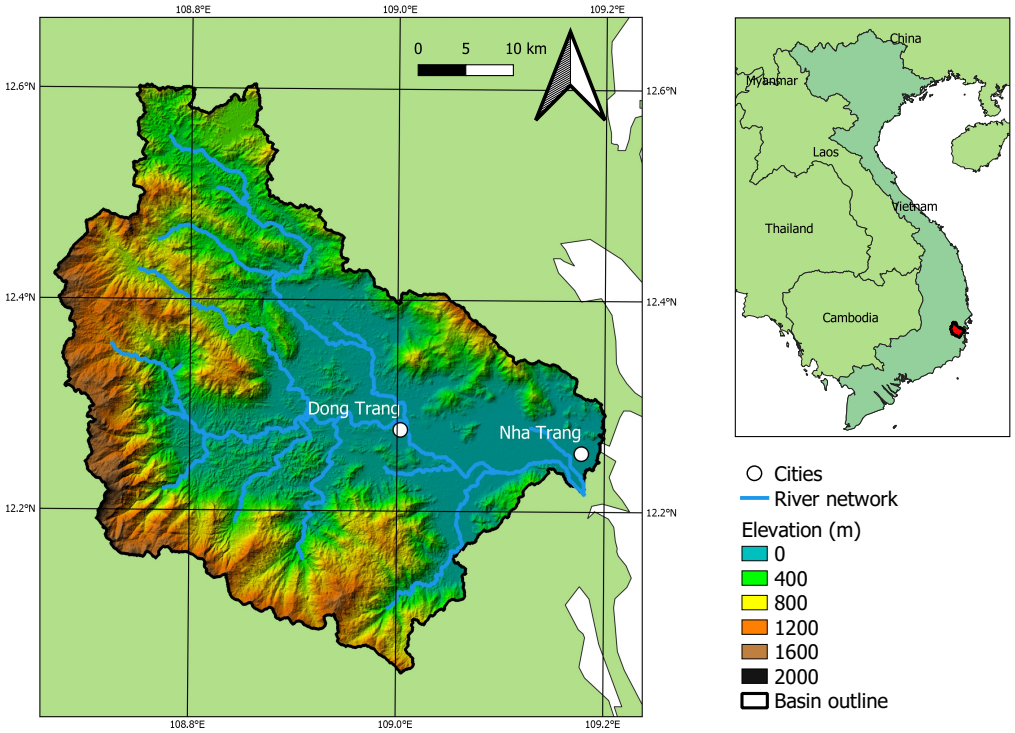

Figure 1.1: Location and DEM of the Nha Trang Cai River Basin in Khanh Hoa, Vietnam.

This research focused on the problem of the saltwater intrusion into the Cai River in Vietnam. In the dry season, the saltwater can intrude the river up to 15 kilometres posing some serious problems regarding freshwater supply (drinking water, irrigation and industrial water). If the river water exceeds the allowable salinity

limit of 0.25 kg/m^3, the water cannot be used for freshwater supply [39]. In the past, the exceedance of this limit has lead to temporary shutdowns of five freshwater pumping stations and some factories creating water scarcity and costing millions of dollars [39]. Figure 1.2 shows the first 15 km of the estuary including the pumping stations.

Tackling these problems requires full comprehension of the saltwater intrusion, its causes and its consequences. If it is understood why and how the saltwater intrusion happens and what influences the magnitude of it, the local government can make educated choices to mitigate or moderate the negative effects. The length of the saltwater intrusion is mainly influenced by the river discharge, river bathymetry, sea level and tidal flows [35]. Especially river discharge plays a crucial role in the saltwater intrusion process as a high discharge is able to push back the saltwater. Several models demonstrate that it is even the most important process impacting the intrusion length [22]. Not only natural processes like rainfall and evapotranspiration but also human interventions like water use and damming influence river discharge. Therefore, analysing the development of the saltwater intrusion requires a complete water balance of the area.

Measures to reduce saltwater intrusion are necessary because future changes in climate and freshwater demand are likely to increase the problem [17]. A rising sea level and an increase in periods of drought by climate change and a lower river discharge by an increasing freshwater demand are believed to worsen the problem of saltwater intrusion [22]. Insight into how the intrusion will exactly change over time is valuable for decision-making. There is already a proposed solution to the saltwater intrusion problem: a dam upstream of Nha Trang (the location of the dam can be seen in Figure 1.2). This dam should prevent the saltwater to intrude further upstream in the dry season and prevent floods in the wet season. Many analyses have been performed to investigate the effects of the dam [10, 39]. However, research on the saltwater intrusion into the Cai River in general and the effect of the dam on the saltwater intrusion is missing. This research provides a first analysis on this subject.

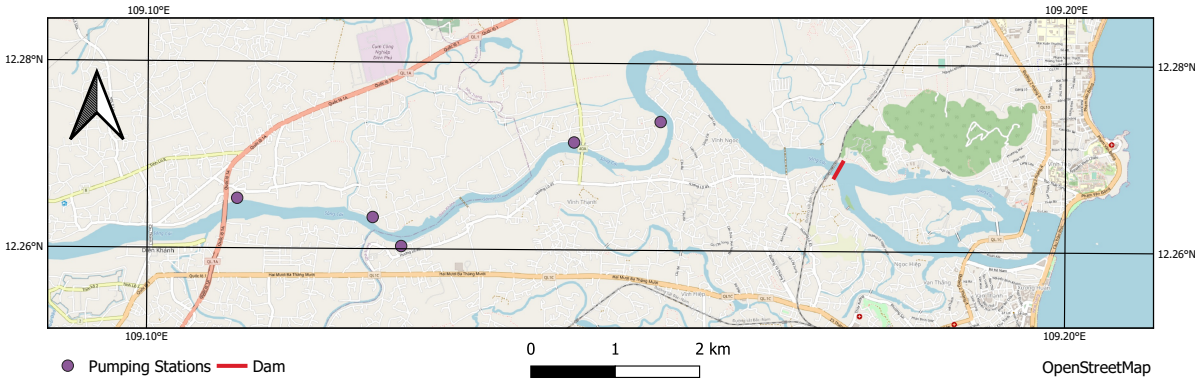

Figure 1.2: The First 15 km of the Cai River Estuary, its Freshwater Pumping Stations and the Location of the Future Dam. The Location of the Pumping Stations and the Dam Follows From the Dam Reports [10, 39].

1.1. Research Goal and Questions

The goal of this research was to make a quantitative hydrological analysis of the development of saltwater intrusion into the Cai River in Nha Trang, Vietnam over the past 30 years and into the future. This goal was achieved with the help of the following research questions:

1. How has the saltwater intrusion changed in the Cai River over the past 30 years?
2. How has the freshwater use in the Cai River basin changed over the past 30 years?
3. What is the local climate in the Cai River basin and (how) has it changed over the past 30 years?
4. What is the Cai River bathymetry and (how) has it changed over the past 30 years?
5. To what extent do (future changes in) freshwater use, local climate and bathymetry influence the saltwater intrusion in the Cai River?
6. What is the expected future change in saltwater intrusion in the Cai River (e.g. by the realisation of a saltwater intrusion dam)?

1.2. Methodology

The proposed research questions in the previous section acted as guidance for obtaining the research goal. The flowchart of Figure 1.3 gives an overview of the research processes. Please note that a period of 30 years was chosen, as this was considered long enough to determine trends, while also still staying within the range of available data.

Question 1 was answered by a literature study. In the past, there have been four salinity measurement campaigns in the Cai River [10, 11, 26]. Data, as presented in the research papers, was analysed to judge its quality and usefulness to this research.

Questions 2, 3 and 4 focus on the drivers of changes in salinity. The freshwater use (question 2) is obtained from official government documents, but this does not span the entire period of interest.

Climate data (question 3) is widely available. Rainfall data was obtained from remote sensing techniques and calibrated with in situ precipitation data. Research in the North of Vietnam has shown that remote sensing is not very accurate for daily precipitation events, but on a monthly basis, it can be considered sufficiently reliable [19]. Within this research, more focus was put on the long term trend and yearly numbers than extreme events, which makes remote sensing data a usable option for obtaining precipitation data with higher temporal and spatial resolution than in situ data.

River bathymetry (question 4) was obtained from drawings provided by Dr. Quang. Furthermore, this research investigated dredging activities in the river estuary and changes in the river mouth width to describe changes in the bed profile.

The data obtained by answering these four questions was used to find a correlation between the driving forces (i.e. freshwater use, local climate and bathymetry) and the resulting saltwater intrusion. A water balance was set up by combining the data obtained from questions 2 and 3. The discharge, resulting from this analysis, was used as input along with the river bathymetry and seaward boundary conditions to model the saltwater intrusion by both an analytical model and a numerical model. Subsequently, salinity data obtained in question 1 was used to calibrate and validate the models.

Question 5 is about the expected future change in saltwater intrusion based on water balance projections by using the correlation between the driving forces and the saltwater intrusion. This was done by changing the input parameters for the analytical and numerical model. The input for the hydrodynamical model was also altered to include the saltwater intrusion prevention dam and a changing bathymetry to answer research question 6.

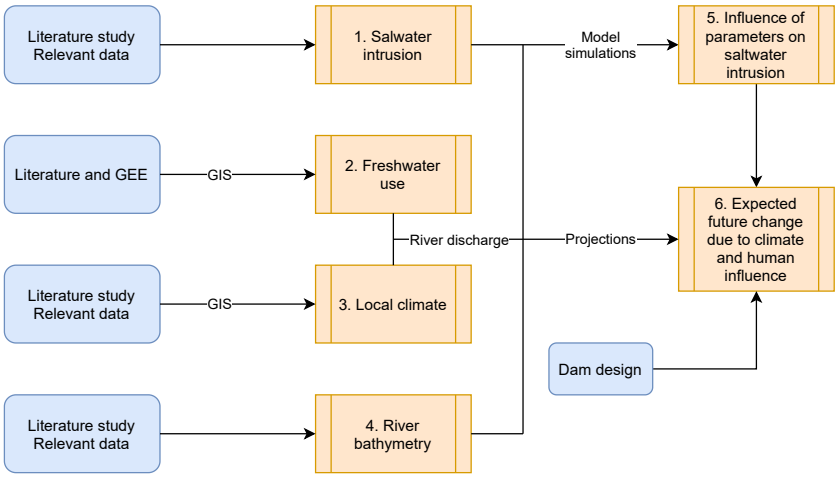

Figure 1.3: A Flowchart of the Research Process. The Blue Cells Indicate the Input Data, the Numbered Orange Cells Indicate the Corresponding Research Questions and the Arrow Text Denotes the Process or Technique Used to Answer the Research Question (GEE Stands for Google Earth Engine).

1.3. Structure of the Report

This report starts with an analysis of the water balance of the Cai River basin in Chapter 2. This chapter gives an overview of the effect of human activities and local climate on river discharge and therefore answers

research questions 2 and 3 by determining trends in freshwater use and local climate. In Chapter 3 the boundary conditions that are required for the models are given. This chapter answers also question 4 about the Cai River bathymetry. In both chapters 2 and 3, also projections for changes in the parameters are given at the end of the chapters. Next, Chapter 4 gives some relevant background information on saltwater intrusion as well as collected salinity data of the Cai River. To answer question 1, an attempt was made to determine a trend in the extend of saltwater intrusion. All the above chapters form the basis to make an analytical and numerical model of the saltwater intrusion. These models are introduced in Chapter 5 and their results are presented and discussed in Chapter 6. The sensitivity of multiple parameters on the model was investigated to make projections of the saltwater intrusion. This was done to answer research questions 5 and 6. Lastly, Chapter 7 provides conclusions and recommendations of this research.

2

Water Balance

The discharge of the Cai River has a significant influence on the extent of the saltwater intrusion. It is, therefore, important to understand and quantify the processes that determine the discharge. The water balance of the Cai River basin was analysed in order to achieve this. All important factors of the water balance are displayed in Figure 2.1. The inflow of the basin consists of precipitation in the catchment area. The outflow of the basin consists of evapotranspiration and river runoff or discharge. The characteristics of the outflow are determined by separate storage mechanisms which are represented by the rectangular boxes. Those specific mechanisms were identified because elaborate data on this was present from The Khanh Hoa Ministry of Agriculture and Rural Development and The Institutes of Water Resources Planning [12]. Many hydrological processes that take place in a basin were not separately treated as the level of detail was too high for the purpose of this research, instead, they were all included in the 'Basin' box. Those processes include, but are not limited to, groundwater flow, infiltration and percolation. The precipitation and evapotranspiration data were measured or estimated using remote sensing and validated and calibrated using in situ ground measurements.

This chapter treats several parameters of the water balance separately. Sections 2.1, 2.2 and 2.3 discuss precipitation, evapotranspiration and runoff respectively. They provide answers to research question 3; *What is the local climate in the Cai River basin and (how) has it changed over the past 30 years?* Section 2.4 presents the water use data, answering research question 2; *How has the freshwater use in the Cai River basin changed over the past 30 years?* The findings of those sections are then combined to obtain a quantified water balance in Section 2.5 and 2.6. Lastly, Section 2.7 discusses the expected future changes in the water balance's main parameters.

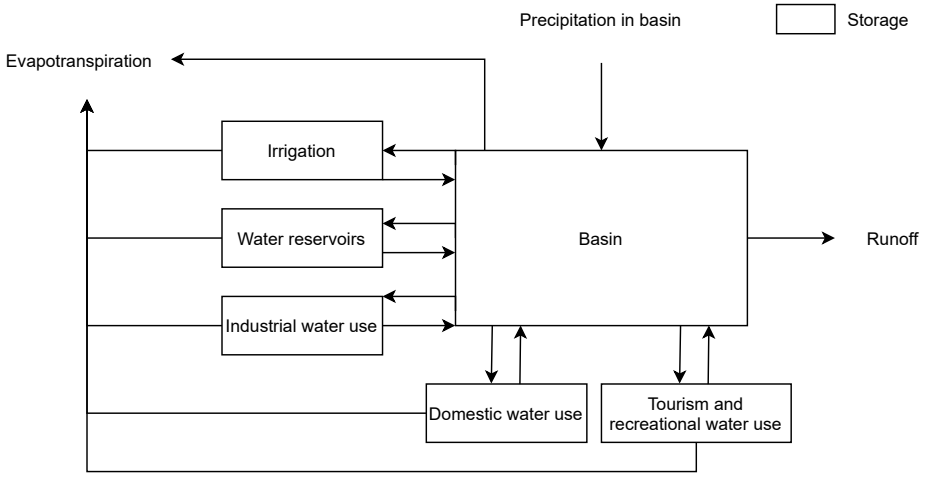

Figure 2.1: Schematization of a Water Balance of a River Basin.

2.1. Rainfall

The rainfall can be measured both in situ as well as using remote sensing. In the Cai River basin, rainfall is measured in situ measured at two locations: Dong Trang and Nha Trang (the locations of the rain gauges are shown in Figure 2.3) [2]. The advantage of in situ data is that it has high temporal availability and is accurate. The downside is its low spatial availability, i.e. it cannot take into account the spatial variability within the region. Remote sensing data, on the other hand, is a more inaccurate estimation but has high spatial availability [19]. This research used the TerraClimate data set for remote sensing rainfall data [3]. It should be noted that this data set does not solely consist of remote sensing data, but combines remote sensing data with reanalysis and ground-based stations. However, since this is a global model, it is considered less accurate than the in situ measurements at Dong Trang and Nha Trang.

2.1.1. Current Situation

Figure 2.2 shows monthly averages for the two measurement locations. The seasonal pattern in the basin is clearly visible: a dry season in the first months of the year and a wet season from September to December. In the figure, the error bars represent the variability (1 σ) between the years. Interestingly, the standard deviations for the in situ measurements were substantially higher. A possible explanation could be that remote sensing did not capture extreme events very well, hence leading to lower variability.

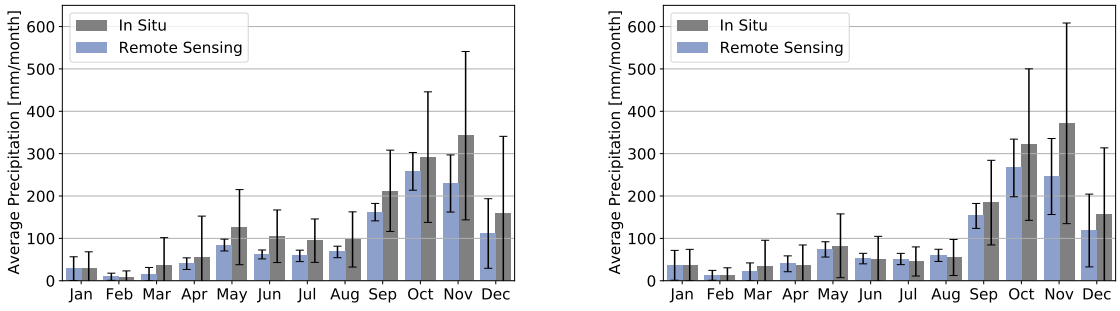

(a) Dong Trang

(b) Nha Trang

Figure 2.2: Monthly Averaged Rainfall Measurements From in Situ and Remote Sensing Data From 1977 to 2015 [2, 3]

Equation 2.1 shows the obtained correlation between in situ and remote sensing data. Herein, p_{IS} and p_{RS} refer to the precipitation from in situ and remote sensing measurements respectively, both in mm. The correlation coefficient R^2 is often used as a measure of correlation, ranging from -1 to 1. 1 indicates perfect correlation, 0 indicates no correlation and -1 indicates perfect negative correlation. The fit had an R^2 of 0.66 in this case, which is not very strong, but still indicates that a correlation is present. The results suggested that remote sensing measurements tend to underestimate the rainfall. Appendix A.3 provides a more elaborate data analysis.

$$p_{IS} = 1.38 \cdot p_{RS} - 6.64 \tag{2.1}$$

Remote sensing is capable of capturing the local differences, although the remote sensing data is considered less accurate. Analysis of the remote sensing data showed that a clear spatial rainfall pattern is present in the basin. Figure 2.3 shows precipitation relative to the measurement station in Dong Trang. In this figure, the western rain gauge is located at Dong Trang and the eastern rain gauge is located at Nha Trang. It is visible that both measurement locations were situated in relatively dry areas of the basin: the Western part of the Cai River basin consists of a mountainous area and rainfall was up to 50% higher there. It was decided to use a combination of in situ and remote sensing data for obtaining a water balance representing the entire research area; the model uses the spatial pattern from remote sensing but calibrated with the correlation from Equation 2.1. After these corrections, the yearly rainfall averaged over the entire basin was computed to be 1635 mm.

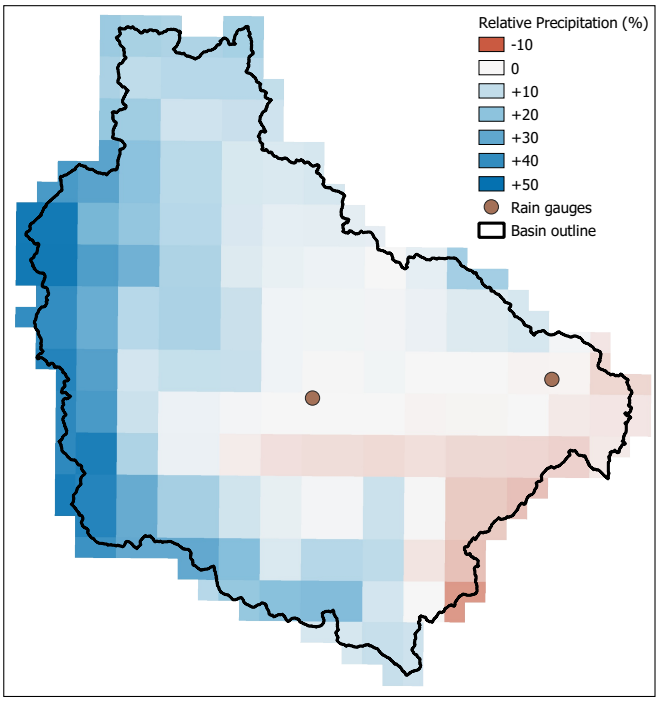

Figure 2.3: Average Yearly Precipitation From 1977 to 2015 in the Cai River Basin Relative to the Precipitation in Dong Trang [3]

2.1.2. Trend Analysis

Yearly averages over the past 30 years were computed to investigate whether the rainfall has changed over the past 30 years, as Figure 2.4 shows. For the purpose of this report, not only yearly trends were considered relevant, but trends in the dry and wet season as well. Therefore, the average monthly rainfall was computed for both the dry and wet season.

The outcome, depicted in the figure, indicated an increase in average rainfall over the years in the wet season. The precipitation in the dry season, which is of most significance for the saltwater intrusion, has remained constant over the years. These trends are quantified in Table 2.1. The R^2 values indicated a very weak correlation between the years and precipitation amounts. The high variability of the precipitation between the years and the relatively small trends caused a low correlation coefficient. However, in this context the goal is not to predict a dependent variable (precipitation) based on an independent variable (time), which makes it hard to evaluate trends based purely on R^2. Therefore, the probability of no trend has also been indicated in the table, as a measure for trend significance. The probability of no trend is defined here as the two-sided

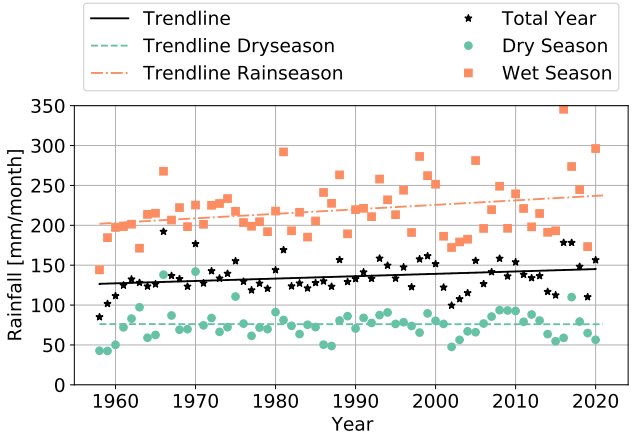

Figure 2.4: Calibrated Yearly Averages From 1977 to 2015 of Precipitation in the Cai River Basin.

p-value for a hypothesis test, where the null hypothesis is a trend of 0. This indication, therefore, pointed out that the trend is significant for the wet season, despite its low R^2.

In conclusion, trends in precipitation are present; the data suggested that rainfall has increased during the wet season, but not during the dry season. An average monthly increase in precipitation of 0.3 mm/month/year amounted to 3.6 mm/year^2. This is in accordance with the literature, where it is mentioned that precipitation increases in the coastal zones and that the precipitation slope in the South-Central area of Vietnam of the past 30 years is around 5 mm/year^2 [20]. This strengthens the likelihood of the data and processing techniques being reliable.

Table 2.1: Trends in Precipitation in the Cai River Basin.

	Trend [mm/month/year]	R^2	Probability of no Trend
Entire Year	0.30	0.044	0.16
Dry Season (Jan-Aug)	-0.003	0.0	0.98
Wet Season (Sep-Dec)	0.56	0.084	0.021

2.2. Evapotranspiration

Remote sensing can also measure actual evapotranspiration, which for simplicity will be called evapotranspiration (ET) in this report. Several methods have been developed that yield estimates. The data set used for this trend analysis made use of the Penman-Monteith equation and used daily meteorological reanalysis data combined with satellite data such as vegetation property dynamics, albedo and land cover [33]. Furthermore, ET was also measured in situ at one location within the Cai River basin [10].

2.2.1. Current Situation

The data from remote sensing was available over the past 20 years with an eight-day time interval. These data were converted to monthly data. Figure 2.5 displays a comparison of the in situ data and the remote sensing data. Their averages amounted to nearly the same of 116.5 and 118.8 mm/month for remote sensing and in situ, respectively. However, on a monthly basis, they did significantly differ. A similar approach as in Subsection 2.1.1 was applied, but the correlation was found to be too weak (R^2 = 0.046) to use for calibration. It was decided to only use the remote sensing data for the water balance analysis. In this way, the spatial gradient of ET was taken into account. Since the yearly totals of in situ and remote sensing measurements were similar, remote sensing was deemed to be reliable enough for water balance analysis. It was found that the total yearly ET on average is 1326 mm/year.

2.2.2. Trend Analysis

To investigate changes, the trend in ET over the years was computed. Averaged over the entire year, the ET showed no long-term trend. Trends did emerge when separating the wet season and dry season, but these were still not significant. Figure 2.6 shows these trends and a quantification is shown in Table 2.2. One can conclude that the overall measured ET has shown no significant change. The ET during the dry season also remained constant. Only ET during the wet season showed a slight increase over the past 20 years.

Table 2.2: Trends in Evapotranspiration in the Cai River Basin.

	Trend [mm/day/year]	R^2	Probability of no Trend
Entire Year	0.0005	0.00	0.91
Dry season (Jan-Aug)	0.0015	0.034	0.75
Wet season (Sep-Dec)	0.0080	0.034	0.45

2.3. Runoff

The runoff in the Cai River basin equals the discharge of the Cai River at the river mouth. No extensive discharge data is available at Nha Trang (near the river mouth). However, daily discharge data was available at Dong Trang, approximately 30 km upstream.

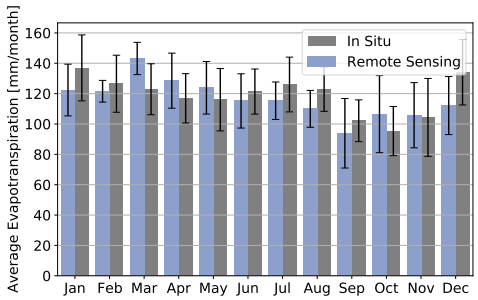

Figure 2.5: Monthly Averages of Evapotranspiration in the Cai River Basin From 2001 to 2016 [10, 33]

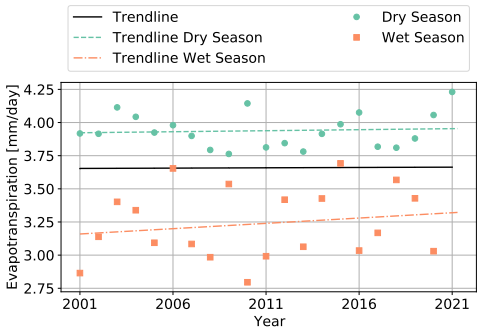

Figure 2.6: Yearly Averages of Evapotranspiration in the Cai River Basin [10, 33].

2.3.1. Current Situation

Discharge data from 1983 to 2012 was analysed and averaged per month [1]. Figure 2.7 visualises the result. A similar pattern as for the precipitation is seen; the lasts months of the year, the wet season, showed the highest discharge values, albeit with a slight delay with respect to the precipitation. The high standard deviations of the monthly averages point out that the discharge had substantial deviations in between years. This can be partially attributed to extreme flood events, where discharge values of more than 1500 m^3/s were often observed.

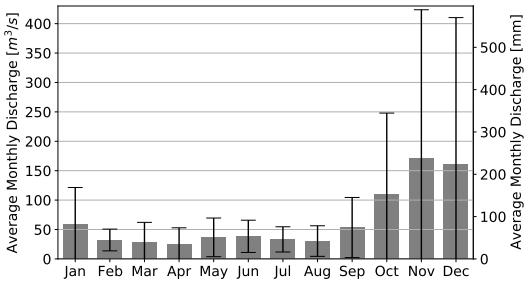

Figure 2.7: Monthly Average Discharge of the Cai River at Dong Trang [1].

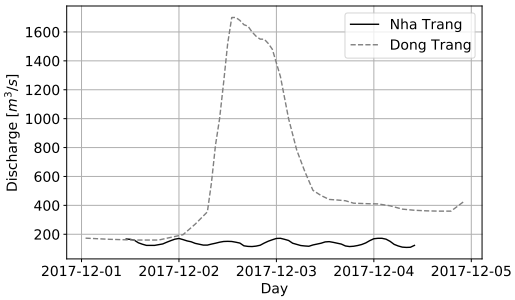

Figure 2.8: Discharge at Dong Trang and Nha Trang During December 2017 [1, 10]

In the ideal situation, data of the discharge at the river mouth is available completely or partially, such that the discharge equals the runoff. For this research, discharge data near the mouth (at Nha Trang) was only available from one measurement campaign of four days, from the 1st of December 2017 to the 4th of December 2017 [10]. Data for both locations are shown in Figure 2.8. It seems that an unusually high flood event occurred in this period; the discharge at Dong Trang ranged between 173 and 1700 m^3/s within a few days. These data were therefore not deemed sufficient to do any calibration by comparing actual values at the same times. The discharge at Nha Trang, i.e. near the mouth, was more constant over time. The average over these four days is 139 m^3/s. This can be compared to the average discharge at Dong Trang in December of 158 m^3/s.

The catchment area sizes upstream of Nha Trang and Dong Trang are 1892 and 872 km^2 respectively, so some difference in discharge can be expected. However, it was hard to find a correction factor to convert discharge measurements from Dong Trang to discharge at the mouth from these data. From the time series at the start of December 2017, it seems that before the flood event, the discharges were somewhat similar. Therefore, the rough assumption was made that the discharge at Dong Trang was approximately equal to the discharge at the mouth. The total amount of runoff per year then amounted $2.07 \cdot 10^9$ m^3 or, when scaled to the basin area, 1080 mm.

In addition to yearly and monthly means, it is also of importance to analyse the probability distribution of the discharge. Figure 2.9 shows the probability density function of the measured daily discharge in the domain of 0 to 250 m^3/s. Although the daily mean was 65 m^3/s, the median (35 m^3/s) and mode (28 m^3/s) were substantially lower due to the positive skewness of the distribution. For modelling the saltwater intrusion, especially the lower extremes are of interest since these usually lead to higher saltwater intrusion.

Figure 2.10 displays the cumulative distribution function of the discharge. From this figure, it can be derived that low discharges, below 10 m^3/s, occurred on approximately 7% of the days. It should be noted, however, that extremely low discharges at Dong Trang are not likely to occur simultaneously at Nha Trang, since low discharges are mitigated by releasing water from water reservoirs downstream of Dong Trang (see Subsection 2.4.4).

The low values are important for saltwater intrusion, but the high values are of more interest for the water balance. The cumulative contribution to the total discharge is shown in Figure 2.11 to further investigate the contribution of high extremes. The figure points out how most runoff in the catchment happened during only a small portion of the days. Only 13% of the days showed discharge values of over 100 m^3/s, but these events contributed to more than 50% of the total discharge.

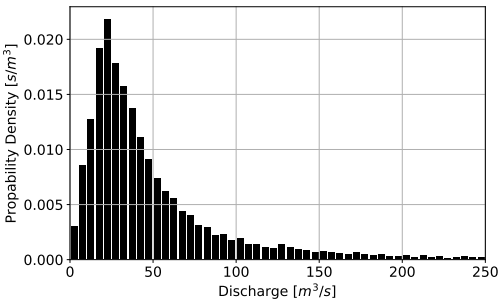

Figure 2.9: Sample Probability Density Function of Daily Averaged Discharge at Dong Trang From 1983 to 2016.

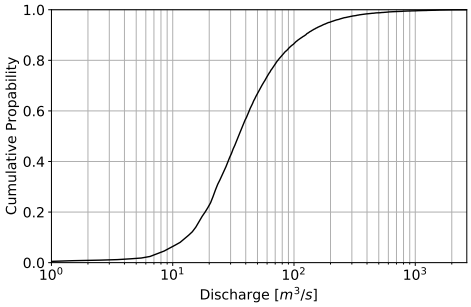

Figure 2.10: Cumulative Distribution Function of Daily Averaged Discharge at Dong Trang From 1983 to 2016.

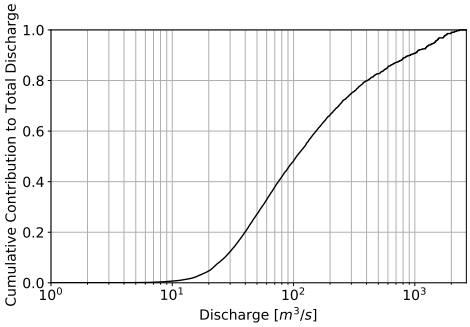

Figure 2.11: Cumulative Contribution to the Total Discharge at Dong Trang From 1983 to 2016.

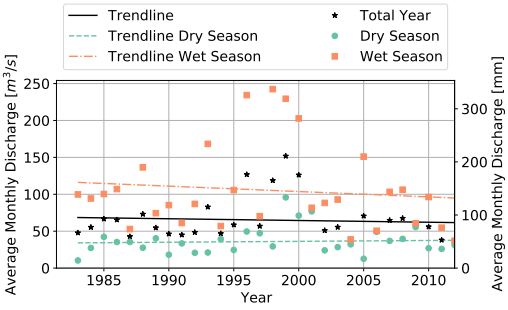

Figure 2.12: Yearly Trends in Runoff at Dong Trang.

2.3.2. Trend Analysis

In a similar way as was done for the precipitation and ET, the runoff data was also further analysed for yearly trends. The yearly averaged values for the entire year, dry season and wet season are plotted in Figure 2.12. Table 2.3 shows The trends and probabilities of no trend. The results displayed in both the figure and the table suggest that the yearly averaged discharge can be assumed to have roughly remained constant. The seasonal trend of the runoff seems to have changed over the past 30 years. The discharge in the wet season had a slight downward trend and in the dry season, an upward trend is visible. However, both trends cannot be considered significant.

A possible explanation for shrinking the difference between the dry and wet season could be reservoir management. Nevertheless, the inflow points of the big reservoirs (Figure 2.15) are located downstream of the measurement location, so the influence of reservoir management is likely to be limited. In previous sections, it was already shown that the precipitation had increased, while the yearly averaged ET remained constant. This would, in theory, lead to an increase in runoff as well, but the data did not show that. Section 2.5 investigates this imbalance more thoroughly.

Table 2.3: Trends in Runoff in the Cai River Basin.

	Trend [$m^3/s/year$]	R^2	Probability of no Trend
Entire Year	-0.071	0.006	0.91
Dryseason (Jan-Aug)	0.38	0.003	0.35
Rainseason (Sep-Dec)	-0.69	0.014	0.58

2.4. Water Demand

The water balance in Figure 2.1 is a simplified diagram of reality where categories are grouped. On the one hand, as described in Section 2.1 and Section 2.2, natural processes such as precipitation and evapotranspiration control the water flow of the system. On the other hand, human influence (partly) controls how the water moves through the system and with what quantities. The human-induced categories of the water balance analysed in this section are:

- **Irrigation:** Cropland in the Cai River basin needs irrigation to grow, especially in the dry season.
- **Aquaculture:** Marine species farmed for food production.
- **Livestock:** Animals farmed for meat production.
- **Domestic:** Water use in the daily lives of people. This ranges from flushing the toilet to drinking water.
- **Tourism:** Water use at touristic attractions and tourists personal water use.
- **Industrial:** Water use in the industrial sector. This includes water used for cooling and cleaning, but also water that is included in the final product.
- **Minimum discharge (DC):** Water reserved to maintain the minimum discharge needed in the Cai River in order to sustain the functions of the river.

This section makes use of data obtained from The Khanh Hoa Ministry of Agriculture and Rural Development and The Institutes of Water Resources Planning [12]. The water demand per category is quantitative, for the exact numbers per category and per month the reader is referred to Appendix A.1. It was not specified how the data was obtained and thus it is unclear what the uncertainty ranges are. Figure 2.13 shows the total expected water demand in the Cai River basin per month of the year 2015. It can be seen that in the dry season, from January to August, the water demand is 3-4 times higher than in the wet season. This is explained by the increased water demand for irrigation and minimum discharge in the dry season as opposed to the wet season, where irrigation and discharge occur naturally.

Figure 2.14 illustrates the distribution of the water demand in the Cai River basin over the different categories in the year 2015. It can be seen that the water demand for irrigation and minimum discharge are dominant. In the dry season the part for minimum discharge significantly increases, while, on the contrary, the other categories contribute less to the total water demand. An explanation for this is that only in the dry season water is needed to maintain the minimum discharge, all other categories are slightly less seasonal. The water demand for aquaculture, livestock and industry are below 1% of the total water demand and were therefore not looked into thoroughly in the rest of the report.

2.4.1. Irrigation

In the area mainly rice and mango are produced covering approximately 15% of the land area in the Cai River basin. According to plans concerning the irrigated land use area, the total farming area is reduced and more focus is placed on the development of tourism services throughout the Khanh Hoa province [12].

2.4.2. Domestic Water Use

Domestic water use consists of all the water extracted from the water source that people use in their homes and gardens. After the water has been used, a part is returned to the source and a part is 'consumed'. The consumed water does not return to the source and is lost due to evaporation or incorporation in products [32].

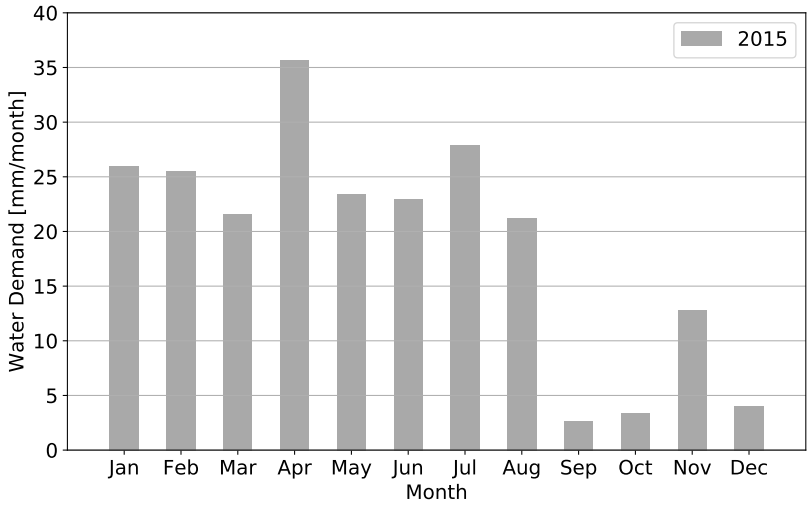

Figure 2.13: Water Demand per Month for the Year 2015 in the Cai River Basin. [12]

2.4.3. Tourism

Tourism is a key sector in the Khanh Hoa province. Tourists mainly visit for relaxation and cultural sites. It results in good economical returns and therefore the Khanh Hoa province exploits its touristic attractions maximally. The result of this is an increased amount of tourists travelling to the Khanh Hoa province and the city of Nha Trang. Tourists use relatively large amounts of water and thus the water demand for the sector has increased. [30]

2.4.4. Water Reservoirs and Minimum Discharge

In the wet season in the Cai River basin there is a water excess, while in the dry season there is a water shortage. To flatten the curve, the provincial government of Khanh Hoa built three water reservoirs with a capacity larger than 1 million m^3 in the Cai River basin in the last 20 years (the locations and capacities are shown in Figure 2.15). Their total effective capacity is 35.3 million m^3. The main purpose of the reservoirs is to serve as a buffer to maintain a sufficient freshwater supply in the dry season. The reservoirs are filled during the wet season. In addition to the water reservoirs, there are also two hydropower plants with a total capacity of 74 MW in the Cai River basin [24]. The discharge of the Cai River is partly human-induced because of the reservoirs and the hydropower plants. This makes it possible to maintain an artificial minimum discharge in the Cai River. All three large reservoirs have their location of outflow downstream of Dong Trang, the location of the measurement campaign of the discharge of the Cai River. Therefore, when the reservoirs are emptied in the dry season, one can expect an underestimation of the discharge at the river mouth compared to the measured data obtained in Dong Trang.

2.4.5. Influence of Anthropogenic Water Demand on the Water Balance

On a yearly basis, the change in storage in a water basin was assumed to be zero, provided that there are no significant changes in the boundary conditions and the characteristics of the basin. On a monthly basis, the change in storage can play a role. This is because from month to month the boundary conditions change significantly. The tropical monsoon climate in Vietnam has large precipitation and lower temperatures in the rainy season compared to the dry season. Different weather conditions provide different water demand patterns, for example, more irrigation is needed in the dry season, as can be seen from Figure 2.13 and Table A.1.

Water demand as depicted in Figure 2.1 takes water away from the basin. During the time that this water is used, it can be considered in storage and will therefore not contribute to the Cai River discharge. After usage, part of the initially captured water is either returned as discharge or 'consumed'. Consumed in this context means that the water has been removed from the basin via evaporation, transport or product incorporation. Water consumption varies between 80% for irrigation and 20% for other domestic/anthropogenic demands [21]. So especially for demand types other than irrigation, a large part is returned to the basin resulting in a discharge. Water use, therefore, does not necessarily always lead to a decrease in discharge, but to a delay in

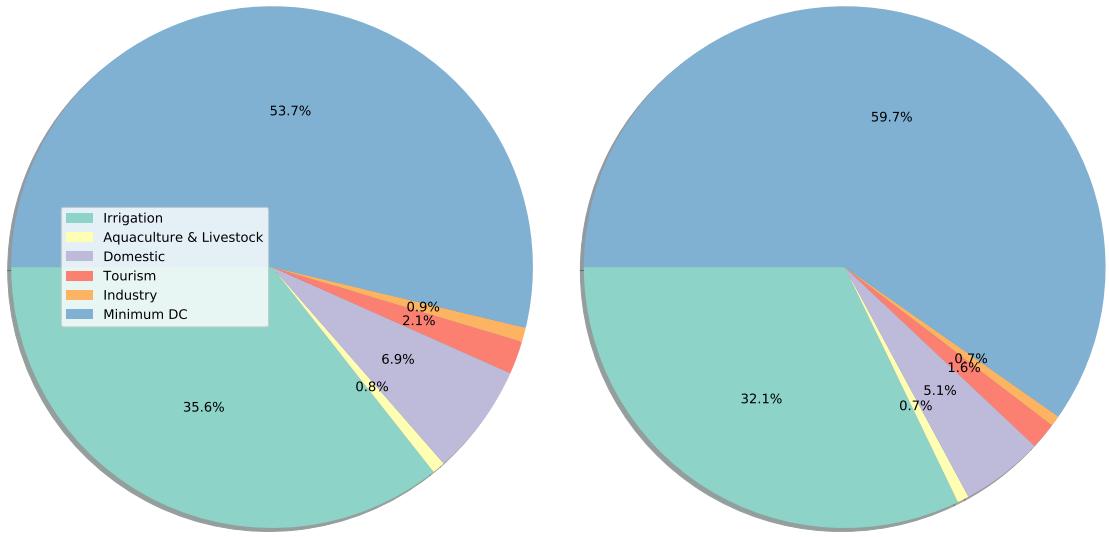

(a) (b)

Figure 2.14: The Ratio of Water Demand per Category in the Cai River Basin in 2015 for the Whole Year (a) and for the Dry Season (b). [12]

discharge. Because of this, extreme meteorological events such as droughts can have a delayed effect on the discharge and the peaks and troughs of such events can be smoothed by storage and reservoirs.

Figure 2.16 shows that irrigation and water reservoirs are the largest water demand and storage mechanisms in the Cai River basin. Domestic, industrial and tourism water demand are 5-75 times smaller than irrigation and water reservoirs and thus were deemed negligible for the purpose of this research. Irrigation and water reservoirs have the most influence on the delay of the discharge, especially in the dry season months (Jan-Aug) where precipitation is low. The delay in discharge of water reservoirs is used to maintain a minimum discharge in the river to prevent excessive saltwater intrusion during the dry season.

2.5. Quantified Yearly Water Balance

The above analysed natural and human processes influence the water balance. Summarising the findings of the previous sections results in a water balance depicted in Figure 2.16. On a yearly basis, the storage rectangles were assumed to have a net change of zero, which can be justified for a basin in equilibrium without significant sudden changes in boundary conditions. The demand per storage category was known from data. However, the distribution of flow resulting out of each category was unknown. On a yearly basis, however, this has no significant influence. On a monthly basis, these processes result in a delay and altered pattern of the discharge and they can therefore influence saltwater intrusion.

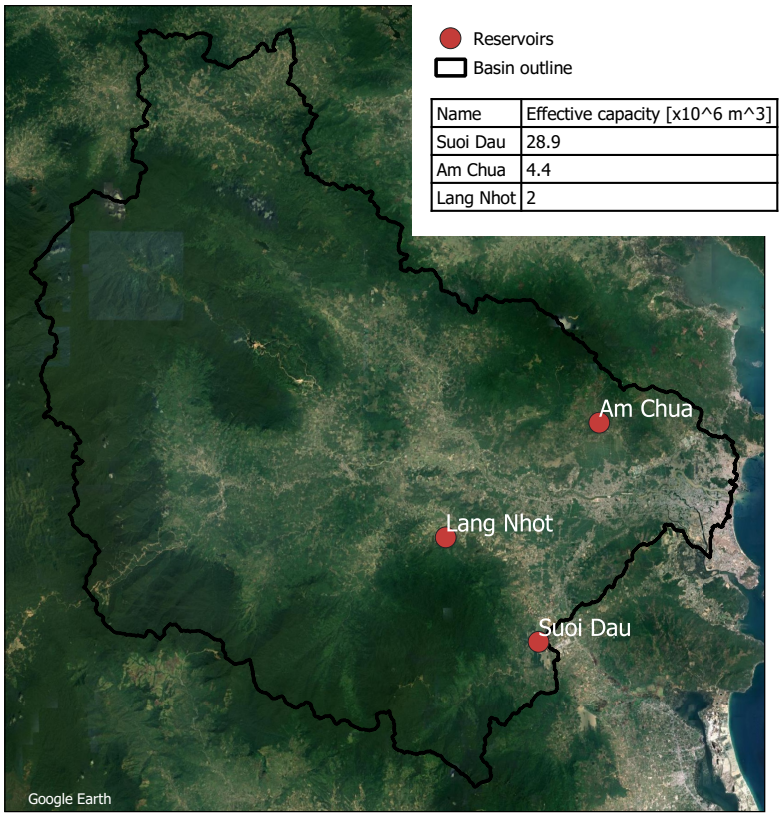

Figure 2.15: The Location and Capacity of the Reservoirs With a Capacity Larger Than 1 Million m^3.

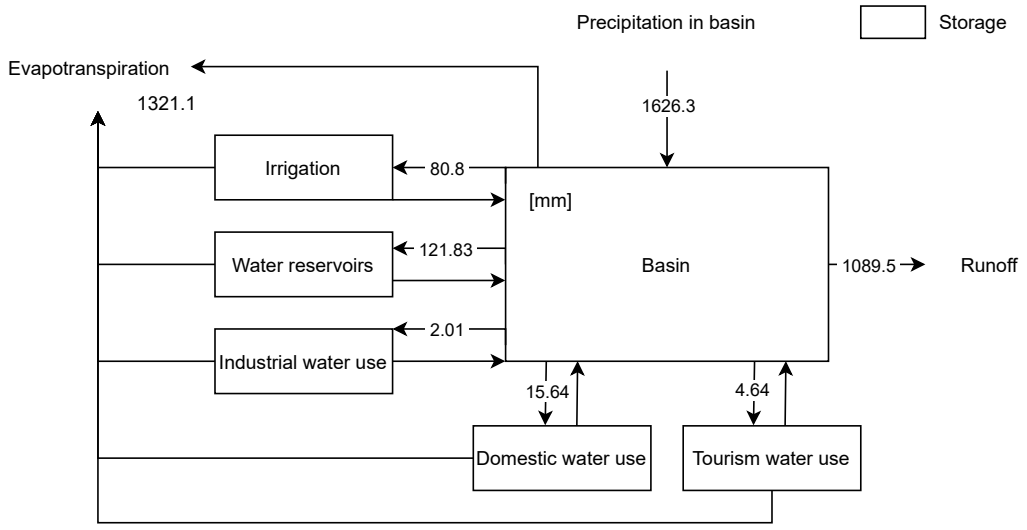

Figure 2.16: Schematization of the Yearly Water Balance of the Cai River Basin.

2.5.1. Discussion

The quantified water balance as shown in Figure 2.16 gives a clear indication of the significance of all factors involved. All values are either supported by measurements, model estimations or literature. On a yearly basis, it was assumed that the storage within the basin remains constant. Therefore, one should expect that the total amount of precipitation equals the sum of evapotranspiration and runoff. In this water balance, this was not the case. The sum of evapotranspiration and runoff far exceeded the precipitation, which would mean that

more water leaves the basin than enters.

The precipitation data is considered reliable, as it was validated with in situ data at two locations over a long period of time. The runoff data is considered reliable to some extent; the observed values seem to be accurate and in agreement with the literature, but they were not measured at the river mouth. Thus, it was not exactly known whether the runoff from the data was an accurate indication of the runoff of the entire catchment. However, this assumption was sustained in this research. The evapotranspiration data is slightly less reliable since the remote sensing and in situ data were not in agreement on a daily and monthly level. Nevertheless, they sum up to approximately the same totals on a yearly basis.

Another possible explanation for the imbalance is an overestimation of the river runoff. If a lot of water was extracted downstream of the discharge measurement, this would mean that not all water left the catchment through runoff, but was perhaps used for irrigation. That implies that the water left mainly as evapotranspiration.

2.6. Quantified Monthly Water Balance

Most data in Figure 2.16 was available on both yearly and monthly timescales. Because of the highly seasonal character of both the water demand and availability, it is useful to assess the water balance on a monthly timescale. The three in and outflows of the Cai River basin are computed in Figure 2.17 (precipitation, evapotranspiration and runoff). The change in storage was also calculated with these inputs. In Subsection 2.5.1 it was already discussed that there is an imbalance which is clearly visible in Figure 2.17; the yearly-averaged change in storage is -49 mm/month, whereas it should be zero. Despite it being incorrect, the monthly water balance does provide a good indication of the differences between the dry and wet season. It suggests that a clear water deficit is present in the first months of the year, which is compensated on a yearly basis by high precipitation from September onward.

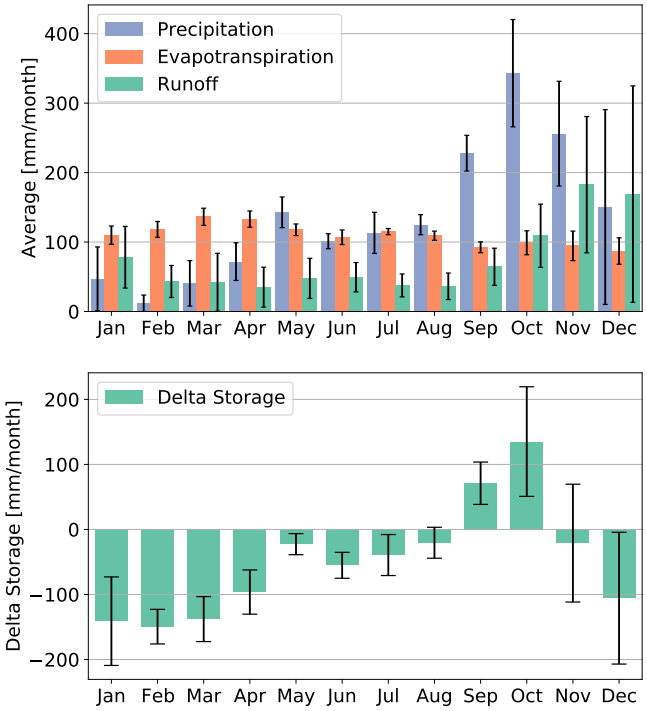

Figure 2.17: Monthly Water Balance.

2.7. Projections

Many pieces of research have been done on the effect of climate change on the factors mentioned in this chapter. Most of the projections are based on the fifth assessment report (AR5) of the Intergovernmental Panel on Climate Change (IPCC). This section describes the projections of the factors previously described in this chapter based on literature.

2.7.1. Temperature and Rainfall

The Vietnamese Ministry of Natural Resources and Environment published a report for policymakers with climate projections for Vietnam [41]. These projections are based on the AR5 and includes projections based on two scenarios, RCP4.5 and RCP8.5. The report describes among other things the expected change in precipitation and temperature. The data was obtained for both scenarios and is presented in Table 2.4 and Table 2.5.

Table 2.4: Projections of Climate Change for the RCP4.5 Scenario for the Khanh Hoa Province Determined by the Ministry of Natural Resources and Environment [41] including 10% and 90% confidence interval.

Period	2016 - 2035	2046 - 2065	2080 - 2099
Temperature [°C]	0.7 (0.4-1.2)	1.4 (0.9-2.0)	1.8 (1.2-2.5)
Precipitation [%]	9.1 (-1.3-19.2)	14.4 (3.9-25.5)	11.0 (-0.2-21.1)

Table 2.5: Projections of Climate Change for the RCP8.5 Scenario for the Khanh Hoa Province Determined by the Ministry of Natural Resources and Environment [41] including 10% and 90% confidence interval.

Period	2016 - 2035	2046 - 2065	2080 - 2099
Temperature [°C]	0.8 (0.5 - 1.2)	1.8 (1.2 - 2.5)	3.2 (2.5 - 4.1)
Precipitation [%]	16.1 (4.9 - 27.2)	8.1 (-1.5 - 18.0)	5.4 (-6.1 - 15.6)

Due to the increasing temperatures and decreasing rainfall in the dry periods, droughts would be more severe. This is mentioned in the climate change report [41] but it does not provide any quantitative data on this issue. Another study researched climate projections providing projections for rainfall and temperatures in the different regions of Vietnam [23]. The research shows that the model used to make the projections cannot capture the pattern of the consecutive dry days. In the climate change report from 2009 [28] some projections were made for the change in precipitation per season. For a medium emission scenario, they computed a change in precipitation in the dry season for South Central Vietnam in 2050 of -5.4% for December-February and -7.4% for March-May.

2.7.2. Water Demand

This subsection uses data from The Institutes of Water Resources Planning [12]. The report is a hydraulic development planning for the Khanh Hoa province. It includes expected data for the years 2015, 2025 and 2035 and projections were made based on climate scenario B2. This scenario emphasises local solutions to economic, social, and environmental sustainability. It also includes a continuously increasing world population and intermediate economic development [31]. The exact numerical values used in this section can be found in Appendix A.1. Due to climate and societal changes described in this chapter, from 2015 to 2035 an increase of 24% in yearly water demand and an increase of 18% in dry season water demand was expected. The lower relative increase during the dry season compared to the whole year is because the initial water demand

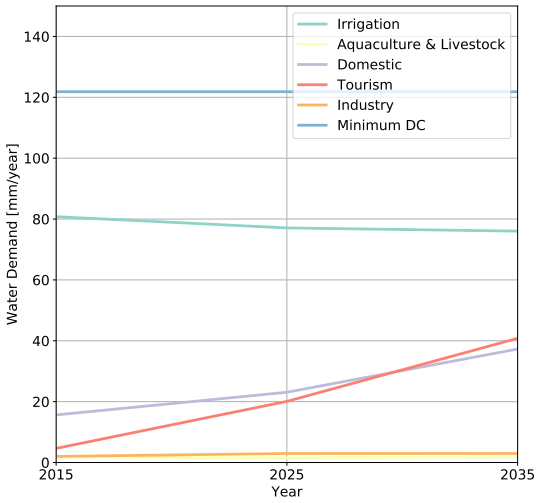

Figure 2.18: Projected Development of the Water Demand per Sector in the Cai River Basin. [12]

in the dry season is higher. Even if the absolute increase was higher, the relative increase can be lower. Figure 2.18 shows the absolute expected increase per sector until 2035. It can be seen that the growth in demand mainly comes from domestic and tourism water demand. Irrigation is projected to slightly decrease and minimum discharge is projected to stay the same. The other categories are insignificant compared with the other categories. This justifies the statement made in Section 2.4 to not treat these categories in more depth.

The demand for minimum discharge is larger in the wet season than in the dry season. More information on this subject can be found in Appendix A.1. Furthermore, it was found that the four main categories contributing to the total demand are irrigation, minimum discharge, domestic and tourism. Of which over the years the part for irrigation and discharge is expected to decrease and the part for tourism and domestic is expected to increase as a portion of the total water demand in the Cai River basin.

Domestic water demand is expected to see an increase due to the continuous growth of population in the basin area (see Figure A.7). Furthermore, one anticipates that the freshwater demand per capita also increases over time due to increasing access to water and quality of living. The average water consumption per capita was slightly above 100 L/day in 2019. The domestic water demand is expected to have an annual growth of 4.5% till 2030 taking into account the growing population count and the increase in water demand per capita. So, in 2030 the expected water demand is 150 L/day/capita [15].

Tourism water demand shows a large projected increase because the province sees the tourism industry as very profitable compared to other industries. Therefore, the province is investing more into the tourism industry and has not shown signs of stopping the increased exploitation of touristic attractions [12].

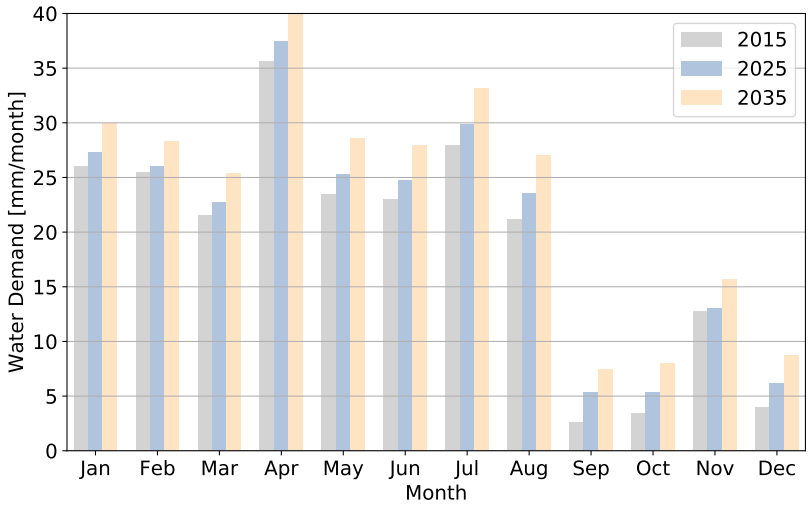

Figure 2.19: (Projected) Water Demand in the Cai River Basin per Month for the Years 2015, 2025 and 2035. [12]

2.8. Conclusions on the Water Balance

This chapter analysed the water balance of the Cai River Basin. In Sections 2.1 to 2.3 the incoming and outgoing water of the basin was investigated and quantified. In Section 2.4 the water use behaviour inside the system was investigated and quantified. After that, in Sections 2.5 and 2.6 the quantitative water balance was made up for the entire Cai River basin. Finally, the projections for the forcings and the characteristics of the basin were determined in Section 2.7. Conclusions on the water balance are drawn in this section.

Precipitation in the Cai River basin occurs mainly in the rainy monsoon months September until December when approximately 63% of the total 1626 mm of rain falls. In the dry season months, January until August, very limited precipitation occurs, leading to almost no water coming into the system naturally. The resulting water balance showed an imbalance, for which the underlying cause was not clearly determined. Approximately 37% more water seemed to be leaving the basin than entering, which is an indication that the numbers

used were not correct. The discharge data is the most likely source of error of all parameters. Nevertheless, the obtained numbers do provide valuable insights in the orders of magnitudes of all factors involved.

Water is used within the basin system in various ways by different sectors such as farming, industry and tourism. Furthermore, water is stored in water reservoirs until needed. On a yearly time scale, the influence of the water demand per sector on the discharge of the Cai River is insignificant, as almost all water returns to the river after use. However, the effect of the water demand on the discharge is notable on a monthly basis. A large part of the runoff in the dry season is human-controlled through the release of water from water reservoirs. The part of the runoff due to water reservoirs is approximately 50% of the total average runoff per month in the dry season. This is a rough estimation and it is not known when the water is released exactly. It was, therefore, not possible with the current data to take into account the outflow of these reservoirs.

Projections and trend analyses of the water demand, precipitation and evapotranspiration gave more insight into the development of the system into the future. It was concluded that precipitation is likely to increase and evapotranspiration is likely to remain constant. The projected increase in precipitation is expected to mainly occur in the wet season. Furthermore, the water demand was projected to increase during all months of the year. Domestic and tourism water are the main increasing sectors, whilst the other sectors approximately remain the same. From the water balance, water demand and the projections it was concluded that in the future there is going to be more discharge running through the Cai River on a yearly basis due to the increased precipitation. The water stress could increase due to an increase in water demand and no significant increase in precipitation in the dry season.

It was not possible to directly model the discharge per month as a function of the system characteristics and the boundary conditions accurately enough to model the saltwater intrusion because of the aforementioned knowledge gaps in the water balance of the Cai River basin. Qualitative analyses can be done as much about the system was known and trends into the future have also been determined. In the remainder of the report, the influence of the system parameters on saltwater intrusion is determined using analytical and numerical models. The link is made between the influence of the discharge on the saltwater intrusion and the qualitative development of the discharge as was explained in this chapter.

3

Boundary Conditions

This chapter describes the factors related to the seaward boundary and river boundaries that influence saltwater intrusion, which is necessary for the saltwater intrusion models. First, Section 3.1 describes the changes in sea level. The bathymetry of the river is described in Section 3.2. Then, Section 3.3 gives projections for the future change of these factors. Lastly, in Section 3.4 the design and location of the saltwater intrusion dam are discussed.

3.1. Sea Level and Tides

The Cai River flows out in the South China Sea, which has a mean water density of 1021 kg/m^3 [38]. Multiple tide gauges recorded the sea level in the South China Sea. A tidal station at Nha Trang measured the water level at the river mouth between the years 1998 and 2017. The average sea levels for each month were computed and are shown in Figure 3.1. In the figure, the error margins represent the standard deviations of the datasets. Sea levels are clearly lowest around July and highest around December. The maximum tidal range found in the dataset has a range of 153 cm during a spring tide on 14 December 2004. This dataset does not span the entire period of interest of 30 years. Therefore, these data are combined with data obtained from a different station close to the river mouth.

The station closest to the area of interest with available historical data is located at Qui Nhon, 150 kilometres north of Nha Trang. The station measured the mean sea level for every month between 1977 and 2013 with a precision of 1 mm [18]. Figure 3.2 shows the computed moving averages of 3 months and 5 years of the entire dataset. The graph clearly shows a seasonal variation and an interannual variation.

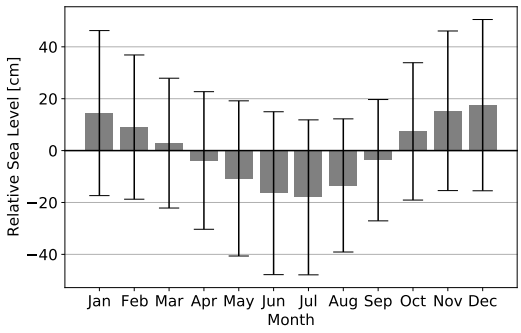

Figure 3.1: Mean Sea Level per Month Relative to Overall Mean Sea Level at Nha Trang.

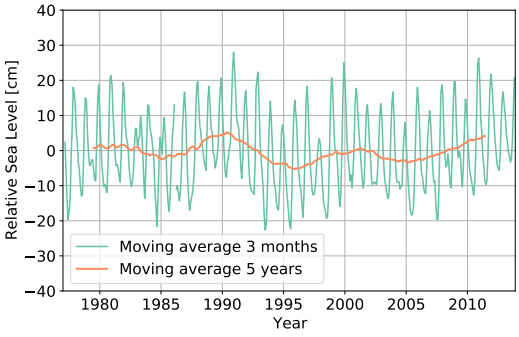

Figure 3.2: Sea Level Relative to Mean Sea Level at Qui Nhon Between 1977 and 2013. Obtained from the Hydro-meteorological and Environmental Station Network Center [18].

Changing wind stresses cause seasonal differences in the South China Sea [37]. The wind stresses have a different direction during the winter and summer monsoon. The stresses drive the surface circulation in the sea, which also changes direction with the seasons. Currents transport the water away from the coast of Central Vietnam during summer, while the current is directed towards the coast during winter. The current

velocities are shown in Figure 3.3. These different transport directions cause seasonal differences in the sea level.

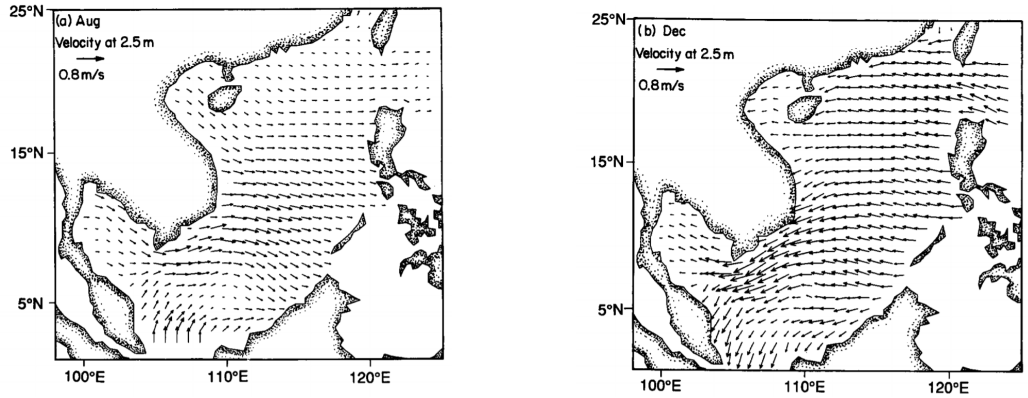

Figure 3.3: Velocity Vectors in the South China Sea Obtained From Shaw and Chao (1994) [37]. Transport Near Central Vietnam is in August in the Eastern Direction (a) and in December in the South-Western Direction (b).

Multiple studies investigated the interannual variations of the sea level in the South China Sea [8, 37]. Their research shows that the interannual variations are caused by El Nino Southern Oscillations (ENSO). Circulation in the Pacific Ocean caused by the ENSO affects the atmospheric circulation in the South China Sea. These changes in atmospheric circulation result in variations in surface wind, air temperature and humidity and therefore also variations in seawater level and temperature [43].

The tide is an important boundary condition on the side of the sea. Increasing the seawater level at the mouth of the estuary results in a larger density-driven force into the estuary. Tidal data obtained from a measurement station in Cau Da, 6 kilometres south of the river mouth, was decomposed in the frequency domain to distinguish different tidal wave frequencies and the corresponding amplitudes. Table 3.1 shows the results of the frequency decomposition, while the frequency graphs and interpretation are shown in Appendix A.5.

Table 3.1: Tidal Constituents and Amplitudes.

		Amplitude [cm]	**Period**	
Long term constituents	S_a	17.44	365.25	
	S_{sa}	2.40	182.62	
	M_m	2.00	27.57	Days
	MS_f	2.84	14.76	
	M_f	1.99	13.65	
Diurnal constituents	Q_1	4.39	26.87	
	O_1	22.31	25.82	
	P_1	8.40	24.07	Hours
	S_1	2.40	24.00	
	K_1	28.43	23.93	
	J_1	0.55	23.10	
Semi-diurnal constituents	μ_2	0.68	12.87	
	N_2	2.33	12.66	
	ν_2	0.52	12.62	Hours
	M_2	9.60	12.42	
	S_2	3.97	12.00	
	K_2	4.61	11.97	

3.2. Bathymetry

The bathymetry of the first 3 km of the river was available at a high resolution with an average spacing of 10 metres between the samples, see Figure 3.4. The approximately 20 km upstream bathymetry data consisted of cross-sections with a spacing of approximately 130 m. Bathymetry data with a high resolution was only available for one particular moment in 2017. Therefore, the changes in the bathymetry of the bottom of the river over the last 30 years were not analysed in this research.

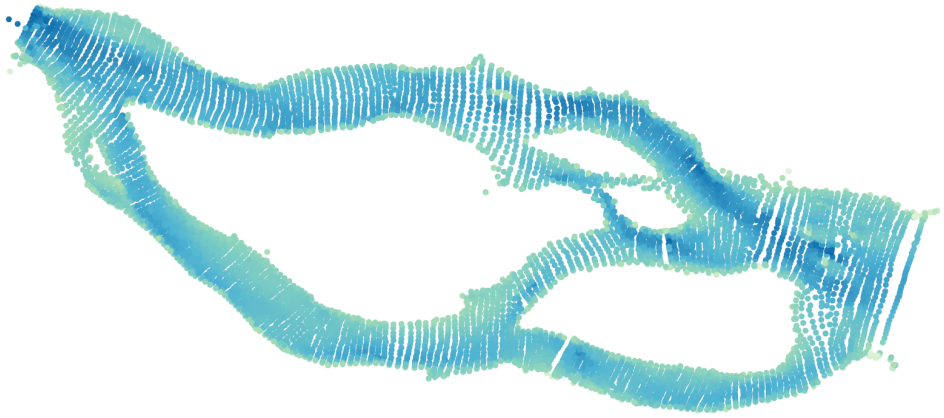

Figure 3.4: Bathymetry of the Cai River Estuary.

Historical satellite images obtained from Google Earth showed the changes over the past 20 years. The bed level could not be extracted from these images, but they showed large differences in the width of the river mouth. Figure 3.5 shows the computed river mouth width for different years. The images were made in different seasons and with different tidal phases, which could influence the differences in river mouth width [29]. These differences are, however, small compared to the total width and the images clearly show that the width of the river mouth increased significantly over the last 20 years.

No changes were visible between 2012 and 2021 in the width of the river mouth. The abutments supporting the ends of the bridge built after 2006 have a fixed location and can cope with the forces coming from the tides and waves. Waves generated by the northeast monsoon caused a longshore sediment transport from north to south. This longshore sediment transport caused a shoreline retreat and the degeneration of the river mouth sand spit [42]. Over time, the sand spit in the river mouth eroded and the river mouth width reached a maximum of 438 m, restricted by the abutments of the bridge.

3.3. Future Expected Change

The climate change report of the Vietnamese Ministry of Natural Resources and Environment [41], gives projections of the sea level rise at the coast of Vietnam. The report gives projections for different scenarios of climate change (RCP4.5 and RCP8.5). The largest increase in sea level is expected to be caused by thermal expansion of the ocean and melting of the glaciers. Projections of the combined effect of these factors on the sea level rise relative to the mean sea level in the period 1986-2005 can be found in Table 3.2.

Table 3.2: Sea Level Rise Projections for the Coast of Vietnam Determined by the Ministry of Natural Resources and Environment [41] with a 10% and 90% confidence interval.

Scenario	Sea Level Rise [cm]				
	2030	2040	2050	2060	2070
RCP4.5	13 (8 - 19)	18 (11 - 26)	23 (14 - 34)	29 (18 - 43)	36 (22 - 53)
RCP8.5	13 (9 - 19)	19 (13 - 27)	26 (17 - 36)	34 (23 - 47)	43 (28 - 59)

Besides sea level rise, the 2016 climate change report by the Vietnamese government [41] also gives projections of the maximum storm surge height that could occur. The maximum observed storm surge height for the coast of Nha Trang is 170 cm. The maximum expected storm surge height that might occur is 220 cm.

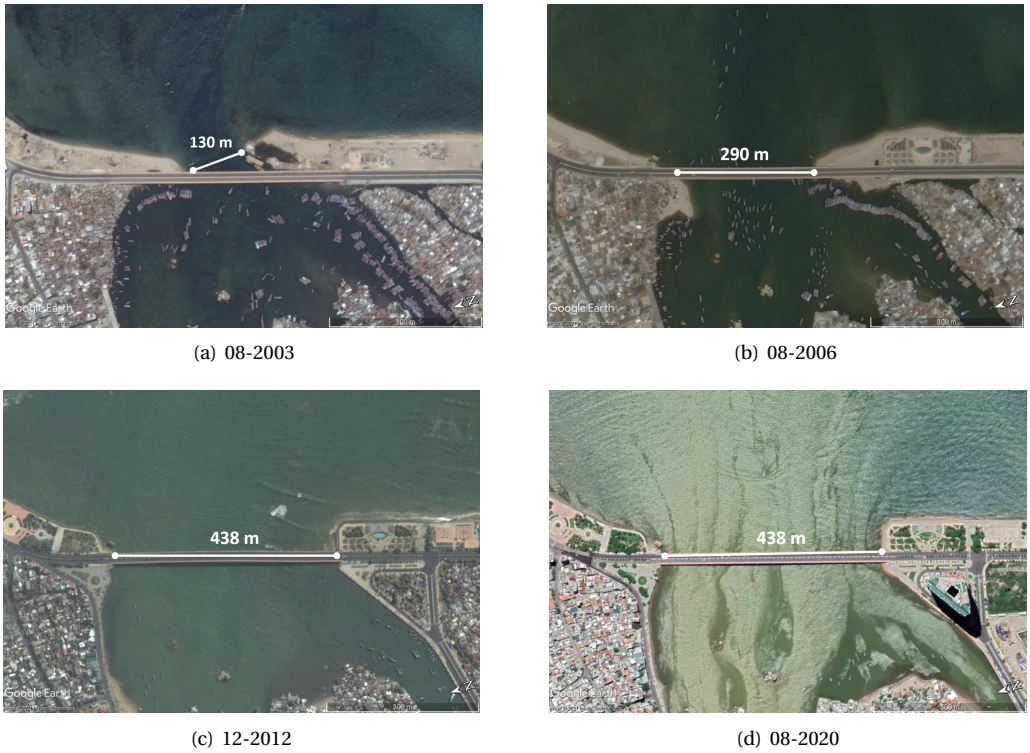

(a) 08-2003 (b) 08-2006

(c) 12-2012 (d) 08-2020

Figure 3.5: Change Over Time in Width of the Cai River Mouth in Nha Trang Obtained From Google Earth.

Due to this sea level rise, the bathymetry could adapt itself to the future sea level. As the sea level rises, water depth increases and therefore the flow velocities decrease. The river will then adjust itself to a new equilibrium condition. Furthermore, changes in discharge and dredging activities could change the bathymetry of the river. As there is no data on how the bathymetry has changed over time, no accurate projections can be made for the changes in bathymetry. The width of the river is restricted by structures and it was assumed that these structures are not removed in the future.

3.4. Saltwater Intrusion Dam

In order to mitigate the problem of the saltwater intrusion into the Cai River, the local government has decided to build a saltwater intrusion dam. The dam, which will be built 75 metres downstream of the existing railway bridge Cau Sat Nha Trang, is expected to be delivered by the end of 2022 [40]. An impression of the dam is shown in Figure 3.6. The dam is both to prevent saltwater intrusion and to improve water management capabilities [10].

The dam will have a total length of 173 m consisting of 5 compartments and a shipping lock on one side. The shipping lock will be located on the right side of the figure. The total stream width will be 150 m interrupted by pillars with a width of 3 m. When fully opened, the top of the gates will be at -4.50 m for the middle compartments or at -3.50 m for the boundary compartments relative to the national datum. When fully closed, the top of the gates will be at +1.5 m. The height of the gates can be adjusted to all intermediate values. Three potential locations for the dam were identified as shown in Figure 3.7. The authorities chose location 1 as the optimal location [39].

3.5. Conclusions on the Boundary Conditions

The boundary conditions are important input parameters for the analytical and numerical model. Enough data was collected on the sea level to accurately model the tidal signal and seasonal differences at the river mouth. The available bathymetry data did not give any information on the changes over time, but the data was sufficient to use as input for the models. Historical images provided some insights on the change in bathymetry in the last 20 years, but it was insufficient to draw conclusions on its effect on the saltwater in-

trusion. The climate change projections also provided enough data to predict future sea levels and assess the changes in saltwater intrusion. The plans for the proposed dam were of great detail and enabled the implementation in the model.

Figure 3.6: An Impression of the Saltwater Intrusion Dam at Nha Trang. [39]

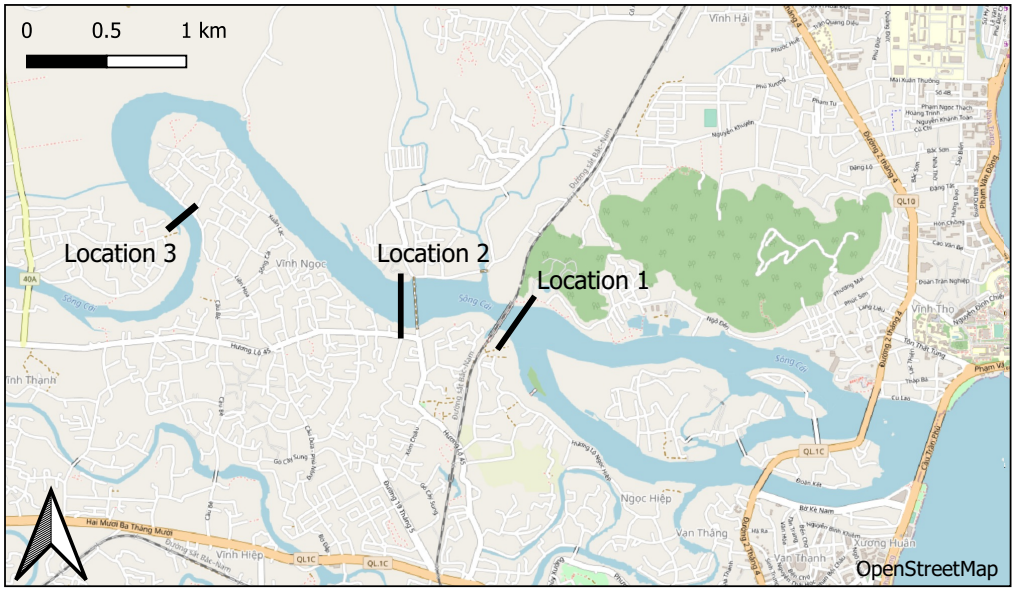

Figure 3.7: The Potential Locations of the Saltwater Intrusion Dam as Presented in the Technical Dam Report [39].

4

Saltwater Intrusion

This chapter explains the phenomenon of saltwater intrusion and its situation in the Cai River. Firstly, Section 4.1 treats the theoretical background of saltwater intrusion in general and the main drivers. Secondly, the Cai River estuary is classified and salinity measurements are presented in Section 4.2. Lastly, Section 4.3 gives some concluding remarks about the collected data.

4.1. Theoretical Background

An estuary is the transition zone between a river and an ocean. In this transition zone, influences from both the river and the ocean are present. There are tides and the water is brackish. These estuaries are a unique habitat for many organisms [13]. With saltwater intrusion, the saltwater of the ocean enters a river. The seaward movement of freshwater in the river limits the length of the intrusion. In this section different types of intrusion mechanisms, mixing mechanisms, intrusion shapes and the most important factors influencing the intrusion will be explained.

4.1.1. Types of Intrusion Mechanisms

The saltwater intrusion mechanism can be divided into three types: the stratified (or saline wedge), the partially mixed and the well-mixed type (Figure 4.1). In general, an estuary is stratified if the river discharge is large compared to the tidal flows. A stratified estuary is characterized by a large vertical salinity gradient, while a well-mixed estuary has a vertical gradient close to zero. The intrusion length increases as the estuary is better mixed. Hence, the saline wedge, where the freshwater and saltwater meet, only occurs in a stratified estuary and near the river mouth. [35]

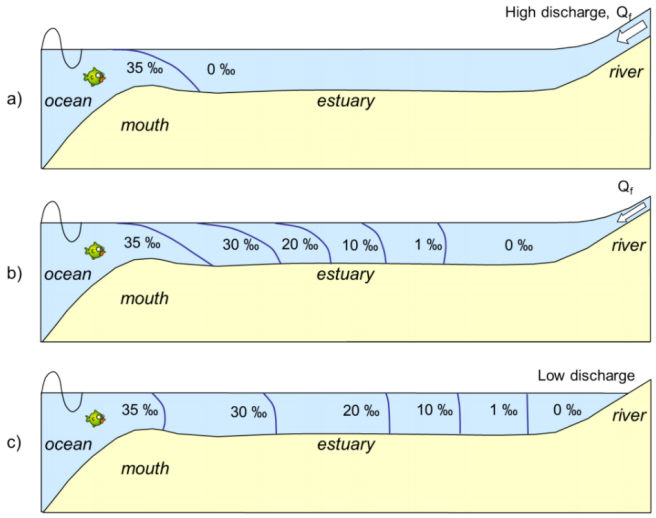

Figure 4.1: Saltwater Intrusion of the Stratified Type (a), the Partially Mixed Type (b) and the Well-mixed Type (c). [35]

4.1.2. Types of Mixing

Salification of an estuary is a natural process caused by different types of mixing between freshwater and saltwater. Wind, tides and density differences are the main drivers for mixing. Mixing by wind has only a small contribution to saltwater intrusion [25] and will therefore be neglected in this report.

Tides are a source of potential as well as kinetic energy. Mixing happens because the tides push the water in the estuary back and forth. Tide-driven circulation includes six types of mixing mechanisms: turbulent mixing, tidal shear, spring-neap interaction, trapping of water, residual currents and exchange between ebb and flood channels. Generally, a larger tidal range causes better mixing in the estuary. [35]

Density-driven or gravitational circulation is dependent on the longitudinal salinity gradient, because a salinity gradient causes a density gradient which is a source of potential energy within the estuary [35]. In the Cai River estuary, the saltwater is 2.1% denser than the freshwater. In stratified estuaries this can cause a saline wedge: the saltwater flows below the freshwater (visible in Figure 4.1a). The hydrostatic forces cause the tidally averaged (TA) flow to be downstream in the upper part of the channel and upstream in the lower part of the channel. In well-mixed estuaries, gravitational circulation (the vertical mixing process) is the dominant consequence of the density difference. This is caused by the moment M:

$$M = \frac{1}{12}\frac{\partial \rho}{\partial x} g h^2 \tag{4.1}$$

where $\frac{\partial \rho}{\partial x}$ is the longitudinal density gradient and $h = h_1 = h_2$ is the water depth (see Figure 4.2).

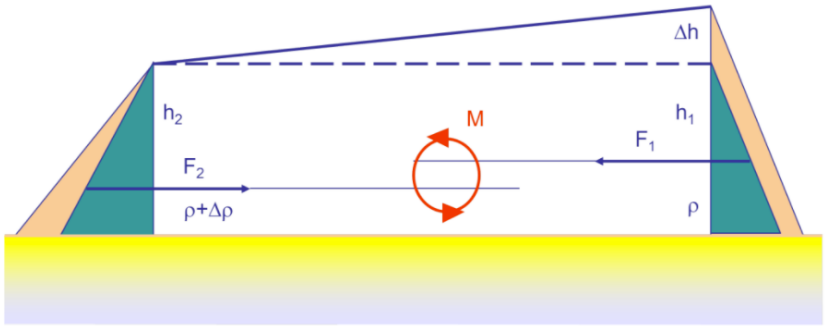

Figure 4.2: Resultant Hydrostatic Forces Driving Vertical Net Circulation. The Left-hand Side of the Figure Is Downstream. [35]

The Estuarine Richardson number reflects whether the mixing in the estuary is predominated by tide-driven circulation or gravitational circulation (the equation can be found in Appendix A.6). An estuary with a large Estuarine Richardson number ($N_R > 0.8$) is characterized by gravitational circulation and is stratified, while an estuary with a low Estuarine Richardson number ($N_R < 0.08$) is well-mixed mainly by tide-driven circulation. [35]

4.1.3. Types of Intrusion Curve Shapes

In well-mixed estuaries, the saltwater intrusion curve can take different shapes depending mainly on the estuary geometry. The four types are:

- Type 1: recession shape
- Type 2: bell shape
- Type 3: dome shape
- Type 4: humpback shape

The different types are visualised in Figure 4.3. Type 1 has a convex shape. This type is found in estuaries that are close to prismatic, straight and narrow. Type 3 is concave shaped and occurs in wide estuaries with relative short convergence lengths. Type 2 is a mixture of type 1 and 3: it happens in estuaries with a clear inflection point, the location of which the geometry of the estuary is upstream significantly different than downstream. Type 4 can occur in estuaries with a rainfall deficit or an evaporation excess. [35]

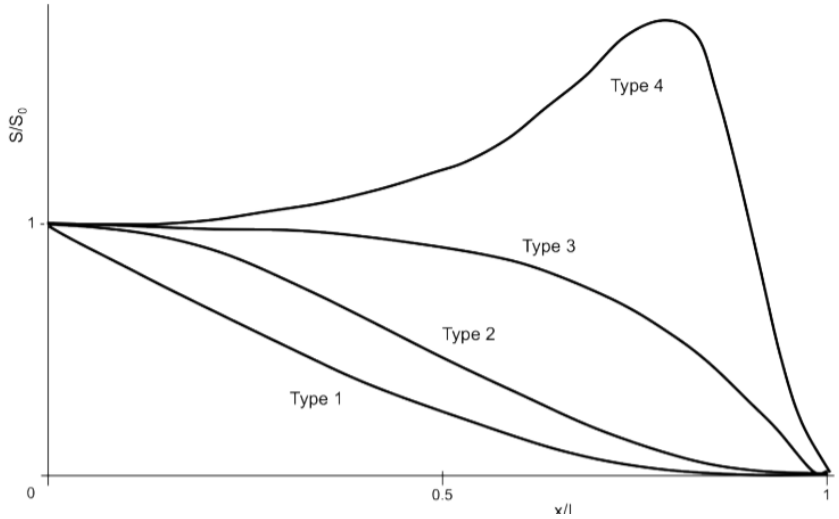

Figure 4.3: The Different Types of Saltwater Intrusion Curve Shapes. [35]

4.2. Salinity Measurements and the Situation in the Cai River

Identifying the characteristics of the estuary is important to understand the saltwater intrusion thoroughly. An estuary can be classified on several different topics. In this research the Cai River was classified based on two relevant topics, starting with the classification on the basis of the Estuarine Richardson number. Taking all parameters at the river mouth and a river discharge of 10 m^3/s, one obtains $N_R = 0.09$ (the specification of the parameters can be found in Appendix A.6). In this situation, the Cai River estuary is partially mixed, practically well-mixed, and tide-driven circulation is the dominant type of mixing. Estuaries can also be classified based on tidal range. The Cai River estuary is a micro-tidal estuary (tidal range $H < 2$ m). Micro-tidal estuaries generally have a smaller excursion length [35].

There have been four salinity measurement campaigns in the Cai River in the past. Data sets with salinity measurements are available from April 1998 [26], June 2005 [10, 11], 2006 [10] and February to July 2016 [10]. The in situ salinity measurements were used to calibrate and validate the saltwater intrusion models made in this research. Figure 4.4 shows the salinity distribution at high water slack (HWS) of April 1998. From these measurements only the vertical distribution is available. Figure 4.5 presents the salinity measurements of 2005, 2006 and 2016. The locations of the measurements are not completely reliable, as they were specified by names instead of coordinates. It is believed that the chosen locations are mostly correct, but they cannot be assumed to be faultless. The dataset of 2005 is obtained during HWS and low water slack (LWS) in June and was measured at 6 locations along the river for both cases. The 2006 dataset also consists of HWS and LWS. The error bars in the figures indicate the 'min' and 'max' values specified in the source, although it is not specified what these mean exactly. In the measurement campaign of 2016, salinity was measured on 26 different days in a period from February to July. The measurements were taken at 4 locations along the river. The measurements shown in Figure 4.5 are averages of all 26 days. The error bars indicate one standard deviation.

All measurements are recorded under different circumstances. Before the data could be used to calibrate the models, the actual river discharge and sea state needed to be taken into account. Figure 4.6 shows the discharges at the time of measurements. It should be noted that this is the discharge measured at Dong Trang, so the river discharge at the river mouth can differ because of reservoir outflow.

The saltwater intrusion looks stratified in 1998. In 2005, 2006 and 2016 the measurements show a salinity curve of the well-mixed type. The spatial resolution of the measurements is too low to be certain about the type of the intrusion curve shape. However, the data show characteristics of a type 2 shape.

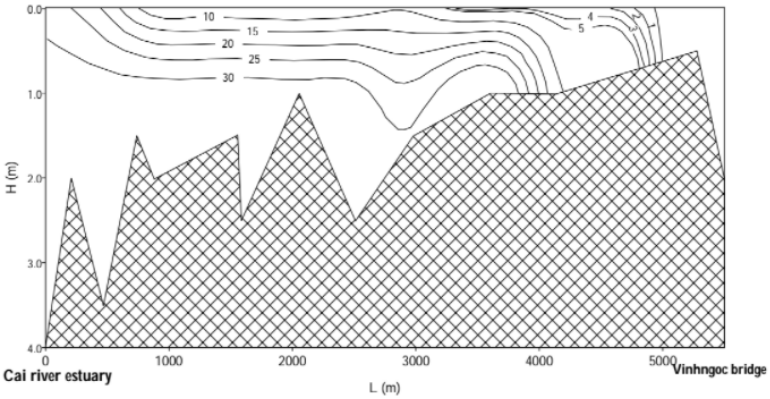

Figure 4.4: The Vertical Salinity Distribution Along the Cai River at HWS in 1998 [26].

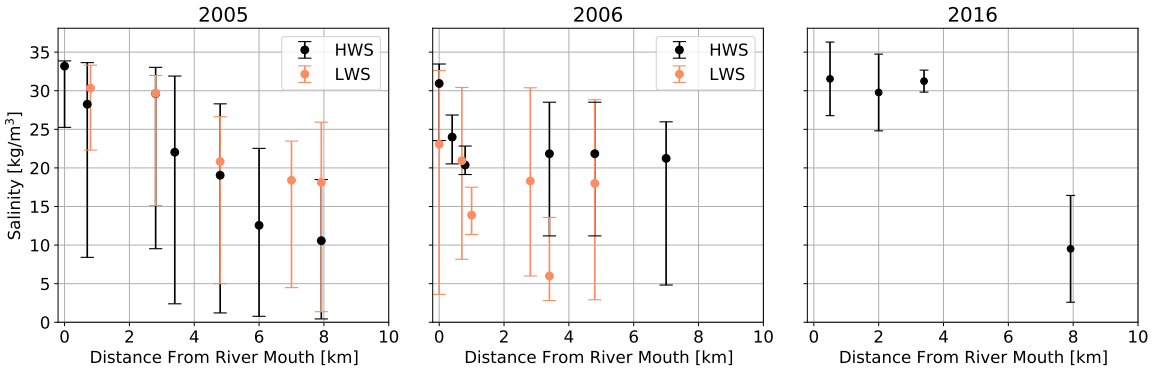

Figure 4.5: Salinity Measurements in 2005, 2006 and From February to July 2016 [10, 11].

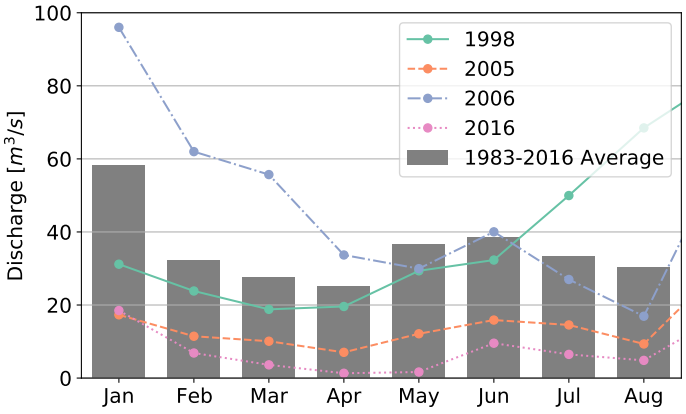

Figure 4.6: Monthly Averaged Discharge in 1998, 2005, 2006, 2016 Compared to Long Term Average [1].

4.3. Conclusions on the Saltwater Intrusion Data

The first research question of this report was about the change in saltwater intrusion length over the past 30 years. The available salinity measurements do not suffice to draw clear conclusions about that. They were recorded under different circumstances and believed not to be perfectly reliable. However, some measurements could be used to calibrate and validate the analytical and numerical model. The models are presented in the next chapter. In that chapter, attention is paid to the calibration process using the in situ data.

5

Analytical and Numerical Models of Saltwater Intrusion

This research presents two models of saltwater intrusion in the dry season. The results of the analyses and boundary conditions as obtained in the previous chapters served as input for the models. This chapter introduces both an analytical and a numerical model. The analytical model was used both to investigate the influence of input parameters on the intrusion length and as extra validation for the numerical model. Section 5.1 presents an analytical model applied to the Cai River estuary. Secondly, in Section 5.2 a numerical model in Delft3D is explained.

5.1. Analytical Model

In the past, multiple predictive analytical models for saltwater intrusion have been proposed. Examples are Van der Burgh (1972), Rigter (1973), Fischer (1974), Van Os & Abraham (1990), Prandle (2004) and Savenije (1993, 2005) [25]. All methods are semi-empirical and assume a steady-state situation of the intrusion in the estuary. The methods of Van der Burgh, Rigter, Fischer and Van Os & Abraham simplified the estuary by assuming a constant cross-section. Prandle and Savenije gained accuracy by taking into account the estuary geometry. Prandle described the bathymetry as a power function (but this is assumed to be unrealistic [25]) and Savenije described it by an exponential function. Except for the geometry, all methods require similar input variables. Figure 5.1 shows that the analytical model of Savenije is the most accurate. Since bathymetry data of the Cai River is available, the analytical model in this research is based on Savenije's method. Later this method was revised by Savenije [35] and adapted by Cai [5] and Zhang [44].

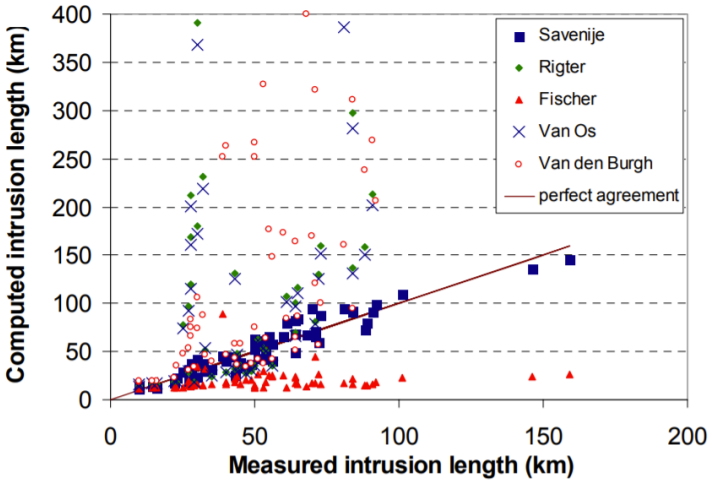

Figure 5.1: Salinity Intrusion Length Computed by Several Methods. [25]

5.1.1. Derivation and Application

The revised and adapted analytical model of Savenije [5, 35, 45] is a 1D predictive steady-state model in which the estuary is assumed to be well-mixed. The Cai River estuary was divided into two reaches where the downstream part features short convergence lengths and the upstream part features long convergence lengths (here the estuary is more prismatic) [5, 27, 44]. The transition point between the two reaches is called the inflection point. Savenije derived the following differential equations for the river salinity, assuming that the saltwater intrusion and the freshwater flow are time-invariant. Equation 5.1a represents the downstream reach and Equation 5.1b the upstream reach. One can obtain Equation 5.1b from Equation 5.1a by integration under the boundary conditions $S = S_f$ and $\partial S/\partial x = 0$ when $x \to \infty$. [35]

$$Q_f \frac{\partial S}{\partial x} + \frac{\partial}{\partial x}\left(AD\frac{\partial S}{\partial x}\right) = 0 \tag{5.1a}$$

$$Q_f (S - S_f) + AD\frac{\partial S}{\partial x} = 0 \tag{5.1b}$$

where Q_f is the freshwater river discharge, S is the depth-averaged salinity, S_f is the freshwater salinity (which is close to 0), A is the effective cross-sectional area of the estuary and D is the dispersion coefficient. One boundary condition and two interface conditions are necessary to solve the system of differential equations of Equation 5.1. The boundary condition is $S(0) = S_0$ where S_0 is the salinity of the South China Sea, which is 33.0 kg/m^3, whereas the interface conditions at the inflection point are $S_d = S_u$ and $\partial S_d/\partial x = \partial S_u/\partial x$, where subscript d indicates downstream and subscript u indicates upstream relative to the inflection point. The assumption was made that the river has no bottom slope.

In this model, the geometry of the estuary is described by convergence lengths. Therefore, the effective river width B and the effective cross-sectional area A are assumed to be described by exponential functions as shown in Equations (5.2a) and (5.2b). Herein, a and b represent the convergence lengths of the width and the cross-sectional area, respectively, with B_1 and A_1 referring to the values at the inflection point x_1. This is a location where a clear change in convergence lengths is observed.

$$B = B_1 \exp\left(-\frac{x}{b}\right) \tag{5.2a}$$

$$A = A_1 \exp\left(-\frac{x}{a}\right) \tag{5.2b}$$

where $A_1 = B_1 h$. For Equation 5.2b, a is calculated by $a = bd/(b+d)$ and is different for both reaches. The effective water depth h was assumed to have a constant value of 3.81 m (depth convergence length $d \to \infty$), but the effective width B has a funnel shape with a clear inflection point around 7 km upstream. The Cai River has multiple channels in the first part of the estuary. Since this model assumes single-channel estuaries, the width of the estuary was taken to be the sum of the width of the channels. The width convergence length and the exact location of the inflection point x_1 were estimated by fitting a line through the measurements (Figure 5.2). Table 5.1 presents the outcomes of the least squares regression.

Table 5.1: Estuary Geometry Parameter Estimations.

Parameter		Value	Unit
x_1	Inflection point	$7.0 \times 10^3 \pm 6.1 \times 10^2$	m
b_0	Width convergence length downstream of x_1	$6.0 \times 10^3 \pm 3.0 \times 10^2$	m
b_1	Width convergence length upstream of x_1	$1.8 \times 10^5 \pm 3.1 \times 10^5$	m

Another prominent factor in Equation 5.1 is the dispersion. Dispersion is a real physical mechanism comprising all different types of mixing mechanisms as described in Subsection 4.1.2. Dispersion leads to the mixing of the freshwater and saltwater if there is a density gradient in the water. The dispersion along the estuary was calculated by a 1D predictive equation [35, 44]:

$$\frac{D}{D_1} = 1 - \beta\left(\exp\left(\frac{x}{a}\right) - 1\right) \tag{5.3}$$

where D_1 is the dispersion at the inflection point and β is dispersion reduction rate:

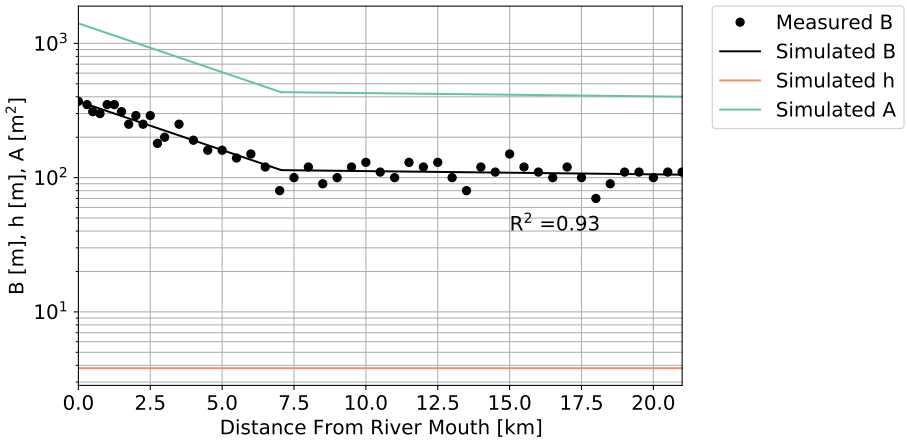

Figure 5.2: Semi-logarithmic Plot of the Estuary Geometry With the Measured Width and Simulated Width B and Depth h in m and Cross-sectional Area A in m^2 Along the Estuary Axis.

$$\beta = \frac{KQ_f a}{A_1 D_1} \tag{5.4}$$

where K is the Van der Burgh's coefficient. The coefficient has a domain from 0 to 1 and has a relatively high value if the mixing is mainly density-driven [44]. The van der Burgh's coefficient is seen as "a sort of 'shape factor', influencing the shape of the saltwater intrusion curve" [35]. K was assumed to be constant along the estuary length. In the analytical model, D_1 and K can be calibrated if sufficient salinity data is available. In this research, the Van der Burgh's coefficient could not be calibrated because the salinity measurements as presented in Section 4.2 have a too low spatial resolution to be able to draw conclusions about the shape of the saltwater intrusion curve. Therefore, an empirical coefficient for K by Zhang was used in this report. He concluded that the Van der Burgh's coefficient is highly related to the estuary geometry and proposed the following predictive equation [44]:

$$K = 0.18\left(\frac{b_1}{B_0}\right)^{0.15} \tag{5.5}$$

where b_1 is the width convergence length upstream of the inflection point and B_0 the width of the river mouth.

5.1.2. Calibration

The dispersion at the inflection point (D_1) was possible to calibrate with the measurements in contrast to the Van der Burgh's coefficient. In literature, a couple of relations between the dispersion coefficient at the inflection point and the river discharge were found [14, 34, 44]. They are of the form:

$$D_1 = C_1\sqrt{Q_f} \tag{5.6a}$$

$$D_1 = C_1 Q_f^K \tag{5.6b}$$

$$D_1 = C_1 Q_f^{C_2} + C_3 \tag{5.6c}$$

where C_1, C_2 and C_3 are constants. This research continued with a relation of the form of Equation 5.6a. Equation 5.6b is dependent on K, a parameter with high uncertainty, and Equation 5.6c adds two extra variables without gaining significant accuracy according to the model.

All salinity measurements in 1998, 2005 and 2006 did not specify the date on which measurements were done, so no accurate discharge data was available. Therefore, 2016 data was used for the determination of C_1. For each of the measurement days, a non-linear optimization was done to determine the optimal D_1. These results, together with their estimated accuracy, were then used for weighted calibration of Equation 5.6a, with the results visualized in Figure 5.3. That resulted in the following relation between D_1 and Q_f ($R^2 = 0.62$):

$$D_1 = 19\sqrt{Q_f} \tag{5.7}$$

The constant $C_1 = 19 \pm 1.6$ $m^{0.5}s^{-0.5}$ is dependent on multiple characteristics of both the estuary and the adjacent sea. Parameters such as estuary shape, mean water height, tidal excursion length, tidal velocity amplitude and the Estuarine Richardson number are included in the constant. With all presented equations, the length of the saltwater intrusion L can be found using the following equation [35]:

$$L_{\mathrm{TA}} = x_1 + a_1 \ln\left(\frac{1}{\beta_1} + 1\right) \tag{5.8}$$

One can move between LWS, TA and HWS by shifting the intrusion curve by half the excursion length E [35]. So for the intrusion length during HWS, one obtains:

$$L_{\mathrm{HWS}} = x_1 + a_1 \ln\left(\frac{1}{\beta_1} + 1\right) + \frac{E}{2} \tag{5.9}$$

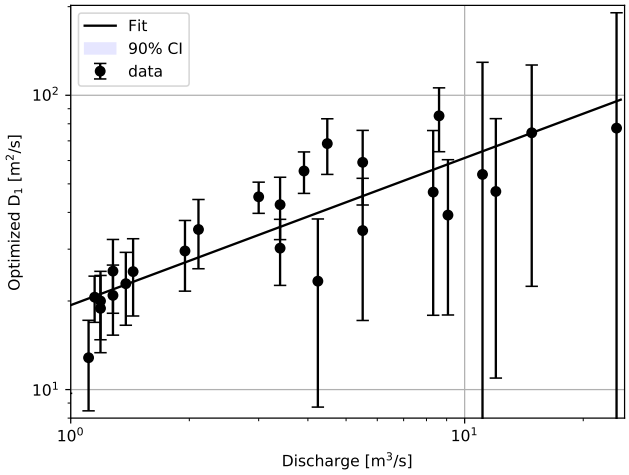

Figure 5.3: Logarithmic Plot of the Optimized Dispersion at the Inflection Point and the Discharge

5.2. Numerical Model

Besides the analytical model, a numerical model made with Delft3D4 modelled the saltwater intrusion into the Cai River. Morphological changes in the river were beyond the scope of this project and were therefore not computed with the numerical model. This section describes the numerical model and some of its input parameters. A full overview of the input parameters of the model can be found in Appendix A.7.

5.2.1. Computational Grid

A computational grid was created based on the land boundaries obtained from images. Due to the complex geometry of the river, with different branches near the river mouth, the domain had to be decomposed into two different grids. The decomposed grid allows for a different spatial interval for the upper and lower branch. This made it possible to increase the timestep and therefore reduce the simulation time. The timestep is limited by the spatial interval because the courant number ($C = u\Delta t/\Delta x$) should not exceed a value of 1. The program computed an optimal time step for the model of 2.4 seconds. [9]

The arrangement of the variables on the computational grid is called an Arakawa C-grid and is shown in Figure 5.4 [4]. The water level is defined at the centre of the cells and the velocity components are perpendicular to the grid cell faces where they are situated [9]. A constant number of layers divided the grid in the vertical direction. The thickness of the layers was defined as a percentage of the total water depth (σ-grid in Delft3D) and not a constant layer thickness. The model required multiple layers to accurately model the density-driven currents of the saltwater. Increasing the number of layers increases the simulation time, as all

flow and transport equations have to be solved for each layer separately. The choice was made for a model with 10 layers so that all the necessary simulations could be performed in time to process the results with enough accuracy.

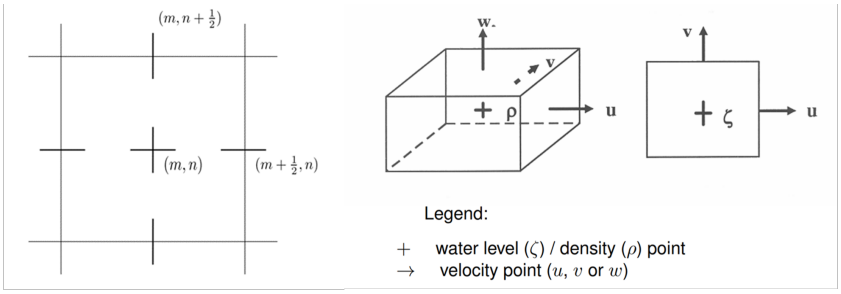

Figure 5.4: Overview of the Arrangement of Variables in the Staggered Arakawa C-grid. [9]

All grid cells require a bottom level to model the flow in the computational grid. Bathymetry data was merged onto the grid by triangular interpolation between the depth samples (see Section 3.2). The bathymetry used for the model can be seen in Figure 5.5. The bottom level is specified at the grid cell corners and the maximum depth of the corners of a cell determined the cell centre depth. The bottom levels are all relative to the national datum, the mean sea level of the tide gauge in Hon Dau.

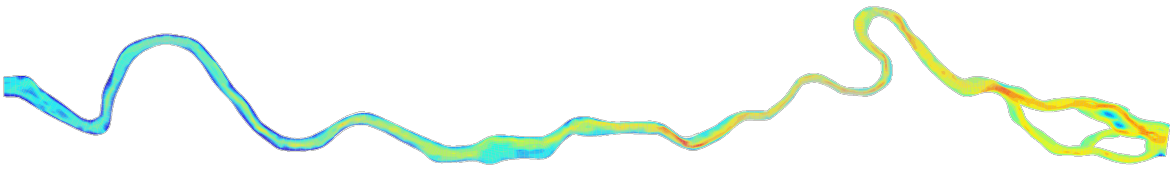

Figure 5.5: Map of the Bathymetry of the Delft3D Model.

5.2.2. Boundaries

The numerical model contained four boundaries, two open boundaries and two closed boundaries. The boundaries on both sides of the river were closed so that no water could flow outside the embankments of the river. This could happen during the wet season but this model only simulates part of the dry season when saltwater intrusion into the estuary is maximum and no flooding is expected to occur.

The open boundary conditions specified at the upstream and downstream ends of the grid allowed water to flow through. The upstream boundary generated a discharge through the river coming from the upstream part of the basin. The downstream boundary condition generated an astronomical tidal signal at the river mouth, based on the tidal constituents determined in Section 3.1 (see Table 3.1). The input for the seaward side boundary condition is shown in Figure 5.6. The simulation time was set in February, which has the highest mean sea level of the dry season. The duration of the simulation covered one cycle between two neap tides so that the developments during spring tide could clearly be seen.

5.2.3. Physical Parameters

The model needed the input of some physical parameters to accurately model the flow in the estuary. Gravitational acceleration and water density were kept at the default values as the program computes the density differences via the salinity. The average sea surface temperature was found to be 25 °C using the Hybrid Coordinate Ocean Model.

The bed roughness was determined based on the bed composition samples collected in the estuary. The derivation of the Chézy coefficient that was used as input for the numerical model can be found in Appendix A.2. The model used a constant Chézy coefficient for all grid cells with a value of 65 $m^{0.5}/s$.

The input for the background viscosity and diffusivity are specified to compute the transport functions. These values had to be calibrated with in situ measurements so that the model simulates the actual flow and transport as good as possible. Due to the small availability of calibration data, this was not possible and

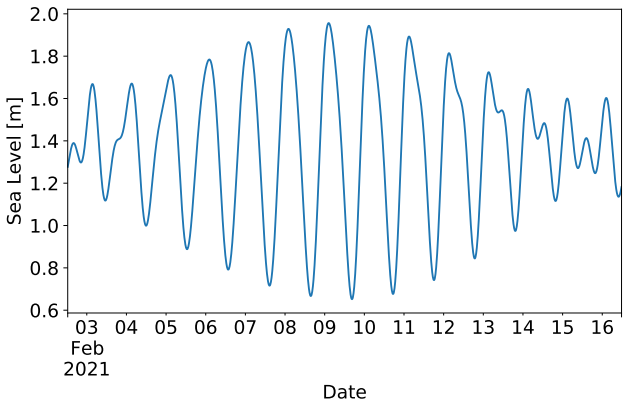

Figure 5.6: Input for the Boundary Condition on the Seaward Side of the Model Based on the Tidal Constituents.

therefore the default values of the program were used. The 3D turbulence model determines the vertical mixing between the different layers. This was done in the program by the $\kappa - \epsilon$ model.

5.2.4. Simulations

Many simulations were run to obtain results for different sea levels and discharges. All simulations had observation points at every kilometre and measured the flow conditions and salinity every 12 minutes. The specified discharge at the upstream boundary was varied to investigate its effect on the saltwater intrusion. The downstream boundary had a varying mean sea level to investigate the effect of sea level rise. The simulation time of the model had to be long enough to guarantee that the model reached a steady-state.

Models with an adapted bathymetry based on Figure 3.5 investigated the effect of the river mouth width on the saltwater intrusion. The bottom level of multiple grid cells was raised high above the maximum water level so that the river mouth width decreased to the desired widths, the adapted grids can be seen in Figure 5.7. Because there was no available data on the actual bathymetry at these moments, the bathymetry was slightly adjusted to include a tidal channel to the river mouth.

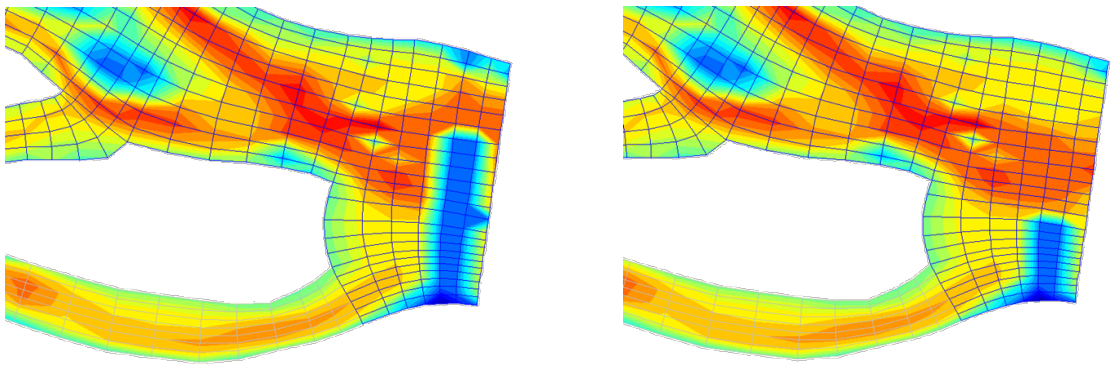

(a) River Mouth Width of 130 Metres (2003).

(b) River Mouth Width of 290 Metres (2006).

Figure 5.7: Adapted Bathymetries for the Different River Mouth Widths in the Numerical Model.

5.2.5. Modelling of the Dam

The numerical model was also used to model the saltwater intrusion prevention dam. Delft3D4 only allows the modelling of thin dams that completely block the flow in the specified direction. In the case of the dam, water is allowed to flow over the gate to maintain a discharge through the dam. Therefore, the dam was modelled by raising the bottom level for an entire row of cells to the height of the gates. Hence, it was not possible to model the dam with only some of the gates raised. It was not possible to reduce the size of the

cells to widths close to the actual thickness of the gate because the grid size is limited by the time step. The adapted grids for the three different locations of the dam can be seen in Figure 5.8. For the locations of the dam in the estuary see Figure 3.7.

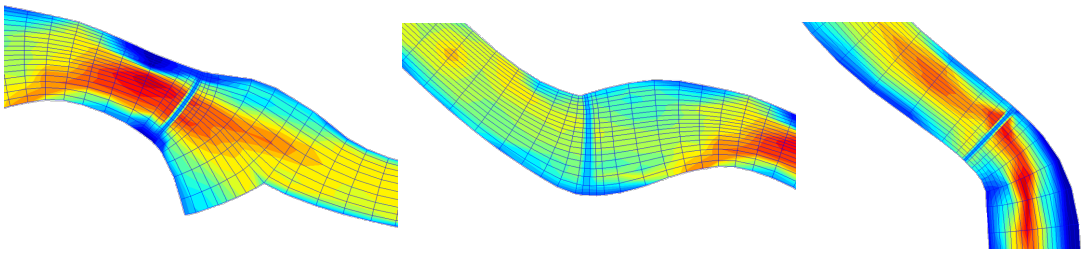

(a) Location 1 (b) Location 2 (c) Location 3

Figure 5.8: Grid Adaptions for the Different Dam Locations.

6

Results of the Models and Discussion

This chapter shows the results of the models as presented in Chapter 5. Firstly, the results of the analytical model are discussed in Section 6.1. After that, Section 6.2 presents the results of the numerical models. Often a reference situation with a discharge of 10 m^3/s is chosen. The average discharge in the dry season is 30 m^3/s, but saltwater intrusion is more prominent for lower discharges. Therefore, the decision was made to use 10 m^3/s as the reference situation, even though this occurs on only 7% of the days. The results of the analytical and numerical models are compared to each other and to the in situ measurements in Section 6.3. This section also provides a discussion on the results.

6.1. Analytical Model

Table 6.1 shows all input parameters of the analytical model. The length of the TA saltwater intrusion only depends on the geometrical parameters of the estuary, because the dispersion at the inflection point D_1 was calibrated by measurements.

Table 6.1: Initial Values of the Parameters Used in the Analytical Model.

Parameter		Value	Unit
Q_f	River discharge	10	m^3/s
x_1	Inflection point	7.0×10^3	m
a_0	Cross-sectional convergence length downstream of x_1	6.0×10^3	m
a_1	Cross-sectional convergence length upstream of x_1	1.8×10^5	m
A_1	Effective cross-sectional area at x_1	4.33×10^2	m^2
b_1	Width convergence length upstream of x_1	1.8×10^5	m
B_0	Effective width at river mouth	3.70×10^2	m
E	Tidal excursion length	1.0×10^4	m

Figure 6.1 displays the depth-averaged tidal average (TA) saltwater intrusion curve, which was obtained by solving the system of differential equations of Equation 5.1. Additionally, the figure shows salinity curves during low water slack (LWS) and high water slack (HWS). The LWS and HWS curves result from shifting the TA curve by half the tidal excursion length along the x-axis. Obtaining the excursion length in the Cai River estuary was difficult due to insufficient measurements. However, according to H.H.G. Savenije (personal communication, June 2021) estuaries such as the Cai River estuary typically have an excursion length of around 10 km. Therefore, the TA saltwater intrusion curve was shifted 5 km left and right to obtain respectively the LWS and HWS curve.

Figure 6.1 shows that the modelled intrusion curve is bell-shaped (type 2, Figure 4.3). The clear inflection point x_1 caused this shape. Downstream of the inflection point (short convergence lengths) the curve is dome-shaped and upstream of the inflection point the curve is recession-shaped. This observation is consistent with the theory as explained in Subsection 4.1.3.

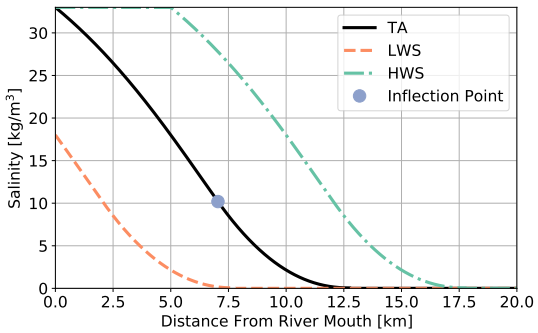

Figure 6.1: Analytically Computed Saltwater Intrusion Curves of TA, LWS and HWS With the Parameters in Table 6.1 as Input Values. The inflection point of the TA curve is indicated in the figure.

6.1.1. Varying Input Parameters

The sensitivity of the input parameters on the intrusion length is different for all parameters. Some of the parameters are fixed for the Cai River estuary (x_1 and b_1), the other parameters can vary. Figures 6.2 to 6.4 show the effect of changes in Q_f, A_1, B_0 and a_0 on the saltwater intrusion curve.

Discharge Figure 6.2 shows the effect of changes in the river discharge. The model suggests that the intrusion length is sensitive to changes in discharge. In the case of a low discharge ($Q_f < 20$ m^3/s), a small change causes a significant change in the intrusion length. Discharge influences the length as well as the shape of the curve. The larger the discharge, the more stratified the estuary is.

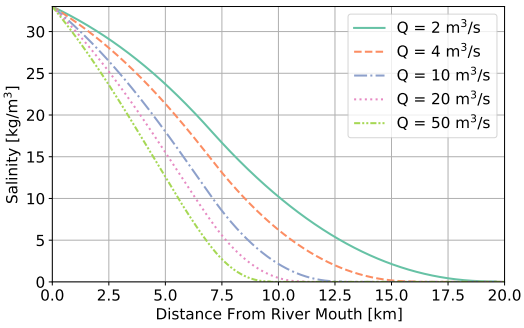

(a) TA Salinity Curves for a Varying River Discharge.

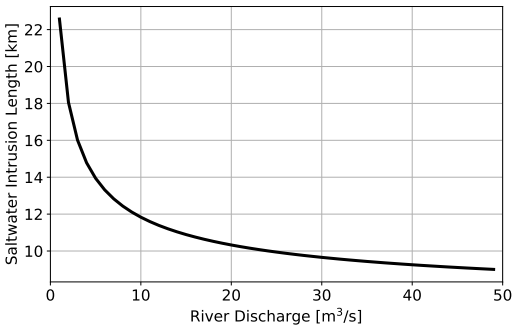

(b) Saltwater Intrusion Length Versus the River Discharge.

Figure 6.2: The Analytically Modelled Effect of Changes in River Discharge Q_f on the Salinity.

Water Depth Figure 6.3 shows the influence of changes in the cross-sectional area of the river at the inflection point A_1 according to the analytical model. The model assumes the width of the river at the inflection point to be fixed, so only the water depth influences A_1. Both dredging and a rising sea level can increase the mean water depth and therefore the cross-sectional area. A change in water depth only influences the modelled length of the intrusion. In this model, there is a linear relationship between the water depth and the saltwater intrusion length. The model suggests that a larger mean water depth increases the intrusion length.

River Mouth Width Figure 3.5 shows that the width of the estuary mouth has changed significantly over the past 20 years. The model suggests that the width of the mouth influences the convergence length downstream of the inflection point. An increasing mouth width reduces the convergence length. A changing mouth width also influences the tidal excursion length, but this effect was not taken into account in the analytical model since a solid quantification was impossible because of insufficient measurements. Figure 6.4 illustrates the

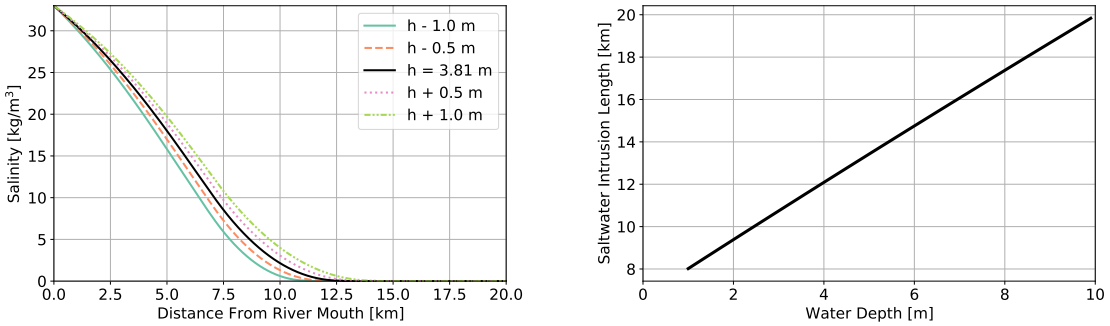

(a) TA Salinity Curves for a Varying Mean Water Depth.

(b) Saltwater Intrusion Length Versus the Mean Water Depth.

Figure 6.3: The Analytically Modelled Effect of Changes in Mean Water Depth h on the Salinity.

results of the analytical model with a changing estuary mouth width. The change only influenced the salinity at the inflection point and therefore the shape of the saltwater intrusion curve. The intrusion curve is more dome-shaped if the estuary mouth is wide. Here, mixing downstream of the inflection point is predominated by tidal-driven circulation instead of gravitational circulation. The change in intrusion length is negligible according to the analytical model.

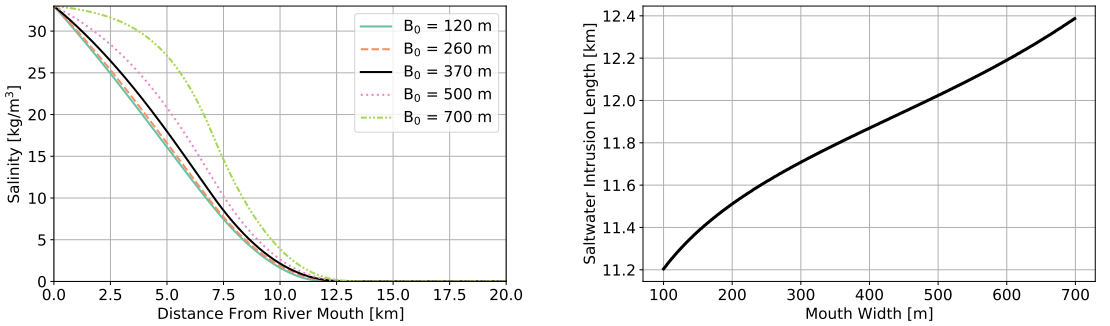

(a) TA Salinity Curves for a Varying River Mouth Width.

(b) Saltwater Intrusion Length Versus the River Mouth Width.

Figure 6.4: The Analytically Modelled Effect of Changes in the Effective River Mouth Width B_0 on the Salinity.

6.1.2. Sensitivity and Uncertainty Analysis

A sensitivity analysis was conducted to get insight into the importance of different input parameters. The analysis recalculated the maximum saltwater intrusion length L_{HWS} (Equation 5.9) whilst varying only one parameter at the time. Figure 6.5 and Table 6.2 show the results of the sensitivity analysis. The mean values for the parameters that correspond to the point '1.00' on the x-axis can be found in Table 6.1. The saltwater intrusion length is most sensitive to parameters with the largest absolute slope at (1, 1) in the graph. However, it should be noted that the expected standard deviation of the parameters plays a large role. If the slope is significant but the standard deviation is minimal, the saltwater intrusion length is not expected to change much due to a change in that parameter. The slope of the parameters at (1, 1) is given in Table 6.2. It shows that the most sensitive parameters are the tidal excursion length, the location of the inflection point and the effective cross-sectional area of the river at the inflection point. A change in the convergence lengths only changed the saltwater intrusion length marginally. One can note parameter a_0 is not included in the analysis. This is because, in the model used, this parameter only influenced the shape of the saltwater intrusion and not the length.

The sensitivity analysis showed that the relative change of certain parameters can have a large influence on the saltwater intrusion length. Without the standard deviation or the uncertainty of the parameters, it

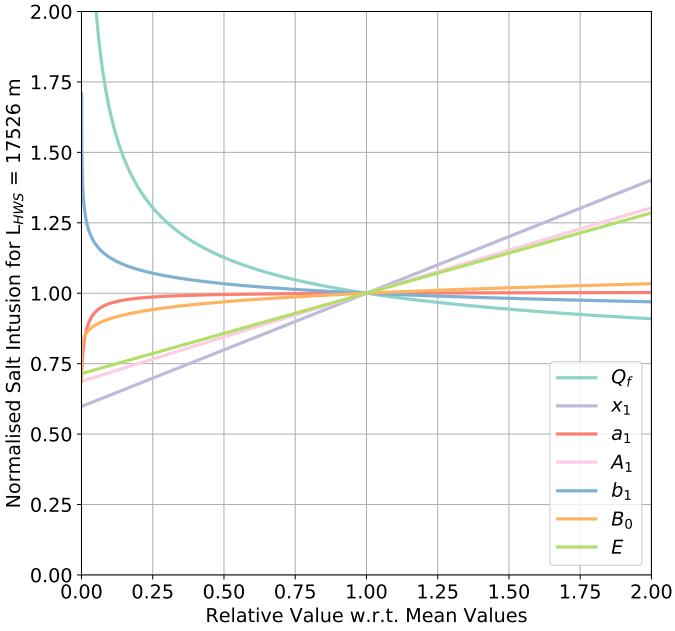

Figure 6.5: Results of the Sensitivity Analysis for the Analytical Model With on the X-axis the Normalised Parameter Value and on the Y-axis the Normalised Saltwater Intrusion Length. Table 6.1 provides a description of the symbols.

Table 6.2: Slopes of the Parameters at (1, 1).

Parameter	Slope
Q_f	-0,117
x_1	0,402
a_1	0,003
A_1	0,306
b_1	-0,037
B_0	0,040
E	0.285

was impossible to identify the true importance and influence of a parameter. The remainder of this section presents an uncertainty analysis performed in Prob2B, in which all parameters are described by a probabilistic distribution. The analysis described the saltwater intrusion length as a mean value with a standard deviation Then, it identified which parameters contribute most towards the final uncertainty of the saltwater intrusion computed, using the analytical model. Table 6.3 shows the parameters with corresponding distributions. The parameter distribution included the spread in the parameter due to measurement, model and prediction uncertainties. The discharge Q_f was kept as deterministic, as this parameter was a fixed input parameter during further analysis in this report. Appendix A.8 provides a complete explanation for the choice of distributions.

Table 6.3: Parameters and Distributions for the Uncertainty Analysis.

Parameter	Distribution type	Distribution parameters	
Q_f	Deterministic	10	
x_1	Normal	$\mu = 7.0 \times 10^3$	$\sigma = 6.1 \times 10^2$
b_1	Weibull	$u = 1.8 \times 10^5$	$k = 1.2$
A_1	Normal	$\mu = 4.33 \times 10^3$	$\sigma = 30$
a_1	Normal	$\mu = 1.8 \times 10^5$	$\sigma = 3.1 \times 10^5$
B_0	Normal	$\mu = 3.70 \times 10^2$	$\sigma = 10$
E	Normal	$\mu = 1.0 \times 10^4$	$\sigma = 4.0 \times 10^3$

A First-Order Reliability Method (FORM) and Monte Carlo analysis were performed. The FORM obtained α-values of the parameters, indicating the relative contribution towards the total uncertainty of the saltwater intrusion length. The performed Monte Carlo analysis obtained an accurate probabilistic representation of the saltwater intrusion length in the form of a graph and numerical data. The relative contribution to the total uncertainty of the i^{th} variable (α_i) adds up to one with the following relation:

$$\sum_{i=1}^{N} \alpha_i^2 = 1 \tag{6.1}$$

where N is the total number of variables in the analytical model. The results of the analysis can be found in Figure 6.6 and Table 6.4. The resulting α-values from the FORM suggested that the tidal excursion length has the most significant contribution to the uncertainty of HWS saltwater intrusion length L_{HWS}. After that, the inflection point and the effective cross-sectional area at the inflection point contributed most to the total uncertainty. It can be seen from Figure 6.6 that a significant error range existed around the computed HWS saltwater intrusion L_{HWS}, mainly caused by the uncertainty in the tidal excursion length. In grey, the probability distribution for the TA saltwater intrusion length L_{TA} is given, which shows a significant decreased spread and an increased accuracy. The standard deviations for L_{HWS} and L_{TA} are 2.2×10^3 m and 9.4×10^2 m respectively.

Table 6.4: α-values for the Relative Contribution to the Total Uncertainty of the Saltwater Intrusion Length Resulting From the FORM.

Parameter	**α-value**
Q_f	0
x_1	2.7×10^{-1}
A_1	1.8×10^{-1}
b_1	-3.0×10^{-1}
B_0	1.1×10^{-2}
E	9.0×10^{-1}

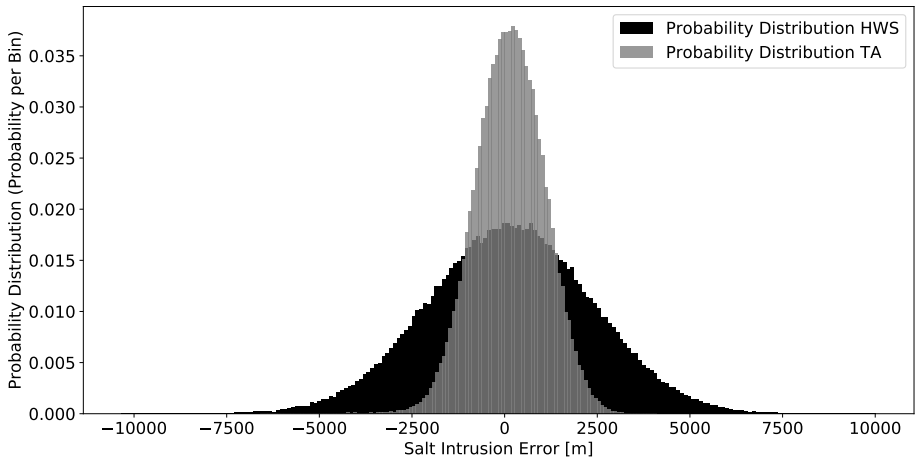

Figure 6.6: Probability Density of the Error of the TA and HWS Saltwater Intrusion Length Computed Using a Monte Carlo Analysis.

6.2. Numerical Model

Besides the analytical model, the numerical model computed the saltwater intrusion for different input parameters as well. The numerical model had to be sampled at certain locations in order to perform data analyses. It was chosen to sample salinity at 1 km intervals from the river mouth because a higher number of sample locations would require substantially more post-processing. Figure 6.7 shows the saltwater intrusion curve simulated by the numerical model for a discharge of 10 m^3/s. The curve shows similarities to the dome shape and the saltwater intrusion extends to 10 km.

Unlike the analytical model, the numerical model is 3-dimensional. This also allowed for assessing the shape of the saltwater wedge.Figure 6.8a displays the saltwater concentration for a discharge of 10 m^3/s. The figure indicates that the numerically modelled estuary was well-mixed, which was in accordance with assumptions made earlier for the analytical model.

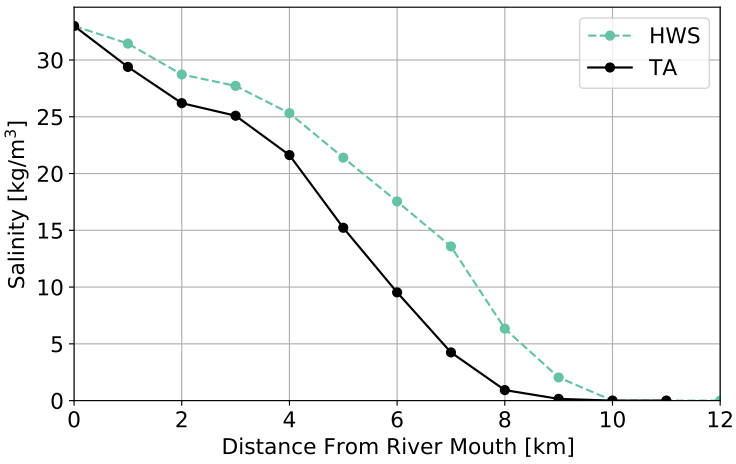

Figure 6.7: Numerical Simulation of the Depth Averaged Saltwater Intrusion Curve.

6.2.1. Varying Input Parameters

In a similar manner as in Subsection 6.1.1, the model assessed the impact of changing input parameters on the saltwater intrusion. This subsection describes the model output from these different variations of input parameters.

Discharge Whether an estuary is well-mixed or more stratified often depends on the discharge. Figure 6.8b displays the salinity again, but for an increased discharge of 50 m^3/s. It is visible that the salinity gradient in the used model was larger for a higher discharge as compared to Figure 6.8a, but also the spatial pattern over depth is different. For a higher discharge, the estuary was more stratified, but could still be considered well-mixed. Figure 6.9 shows the correlation between the discharge and the saltwater intrusion.

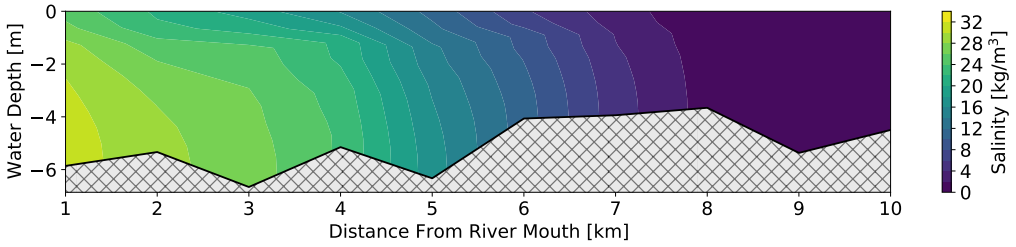

(a) $Q_f = 10$ m^3/s.

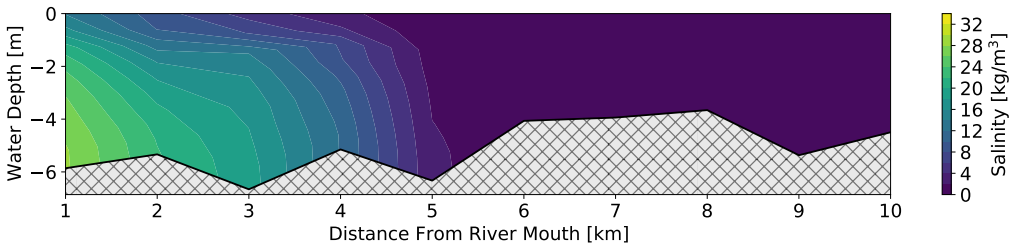

(b) $Q_f = 50$ m^3/s.

Figure 6.8: Numerical Simulation of the TA Saltwater Intrusion for Two Different Discharges Q_f.

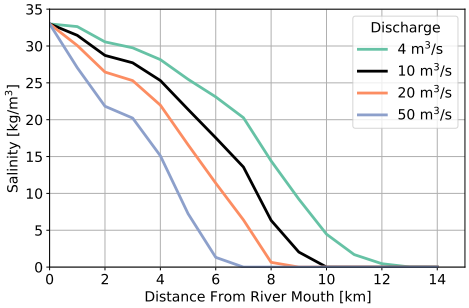

(a) The TA Salinity Curves for a Varying River Discharge.

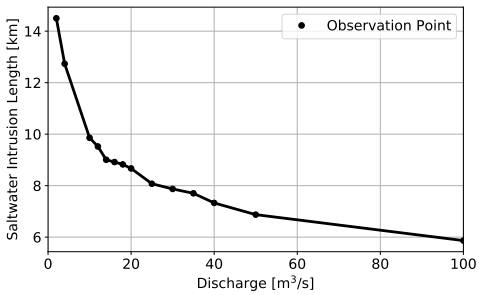

(b) The HWS Saltwater Intrusion Length Versus the River Discharge.

Figure 6.9: The Numerically Modelled Effect of Changes in River Discharge Q_f on the Salinity.

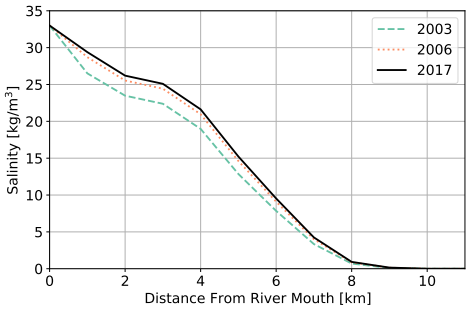

Figure 6.10: Numerically Modelled TA Salinity Curves for Three Different Widths of the River Mouth.

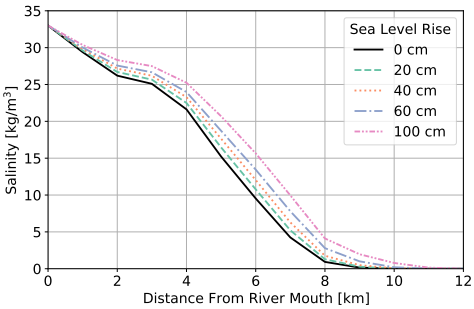

Figure 6.11: Numerically Modelled TA Salinity Curves for Different Values of Sea Level Rise.

River Mouth Width The river mouth width has increased over the past 20 years, as described in Section 3.2. The 2020 situation, with a width of 438 m, was compared to the 2003 situation, with a width of 130 m. Figure 6.10 displays the numerical results. The results shown in the figure suggest that a change in river mouth width had a slight influence on the shape of the salinity curve, but not so much on the total saltwater intrusion length.

Sea Level Rise The effect of the rising sea level was investigated by changing the boundary condition at the river mouth and modelling the saltwater intrusion. Figure 6.11 shows the expected salinity curves for different levels of sea level rise. The saltwater intruded further land inward for higher sea levels in the numerical results, as expected from the theory and the analytical model. With a sea level increase of 60 cm, the simulated saltwater intrusion length increased by approximately 1 km.

Saltwater Intrusion Prevention Dam A dam to prevent saltwater intrusion was proposed, as elaborated on in Chapter 3. The model computed the saltwater intrusion for three different locations and for different crest heights of the dam. Figures 6.12 and 6.13 show the results of the model for locations 1 and 2, which are 2.7 and 3.5 km from the river mouth respectively, with crest heights of +1 m and +1.5 m above the national datum. Both locations were effective mainly for a crest height of 1.5 m. Figure 6.14 shows a comparison of the three different locations of the dam. These simulations all used a crest height of +1 m. In the models used, the dam was most effective when built at location 1. Figure 6.15 shows contour plots of the salinity for different crest heights of the dam at location 1, to get more insight into the exact effect. Figure 3.7 elaborate on the exact locations of the dam.

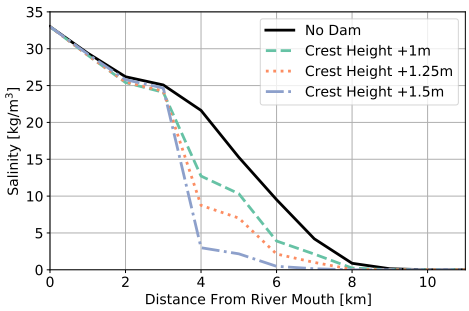

Figure 6.12: Numerically Modelled TA Salinity Curves for Different Dam Levels at Location 1.

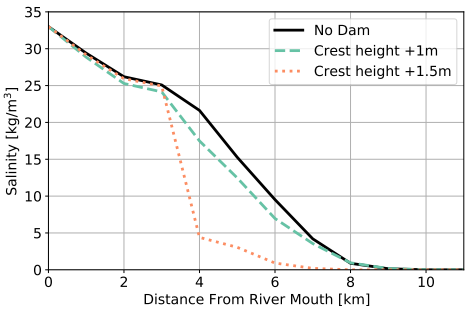

Figure 6.13: Numerically Modelled TA Salinity Curves for Different Dam Levels at Location 2.

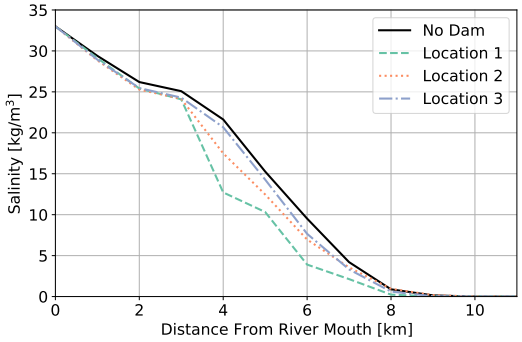

Figure 6.14: Numerically Modelled TA Salinity Curves for Different Dam Locations With a Crest Height of +1 m.

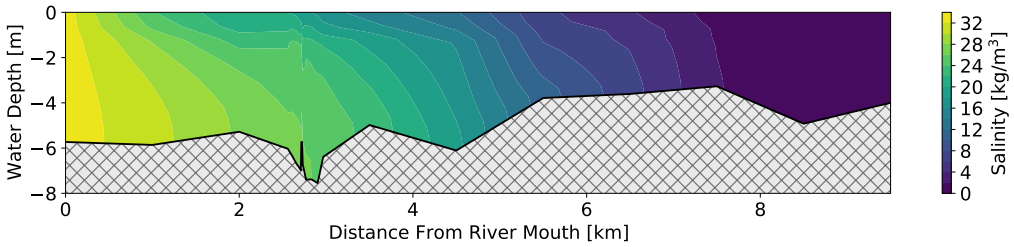

(a) All Gates Opened.

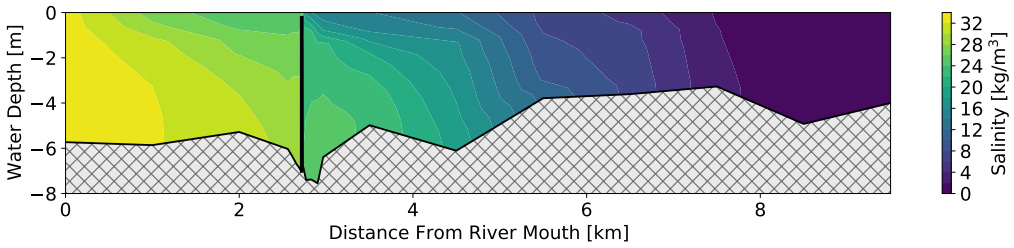

(b) Crest Height at a Level of 1 m.

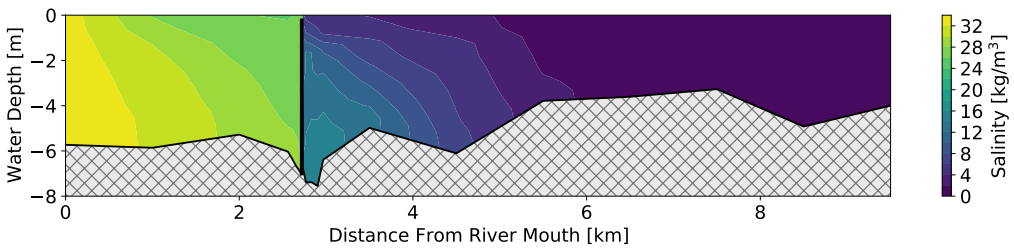

(c) Crest Height at a Level of 1.5 m.

Figure 6.15: Numerical Simulation of the TA Saltwater Intrusion for Different Dam Levels at Location 1 for a Discharge of 10 m^3/s.

6.3. Discussion of the Results and Limitations

Sections 6.1 and 6.2 presented all results of the simulations. This section compares the results of both models to each other and to in situ measurements to assess the reliability of the models and to draw conclusions where possible. Limitations of the methods used and the data available are discussed throughout the section.

6.3.1. Validation of the Numerical and Analytical Model

Figure 6.16 compares the results of the numerical and the analytical model to the in situ measurements for TA and HWS. The models used the initial values as shown in Table 6.1 as input (so $Q_f = 10\ m^3/s$). The results were compared with the measurements from 2016 obtained when the river discharge was between 8 and 12 m^3/s. One can notice several similarities and differences in Figure 6.16.

First, the intrusion curves of both the numerical and analytical models were bell-shaped. This shape was also in line with the HWS in situ data, through which also a bell-shaped line could be drawn. The TA in situ data shows a rather remarkable course since the salinity increased from the mouth into the first part of the estuary. Furthermore, the TA results from the analytical and numerical model show remarkable similarities which increases the trustworthiness of the models.

Secondly, it became clear that during HWS the analytical model overestimated the saltwater intrusion length compared to the numerical model. Comparing the results of the analytical model to the in situ measurements, one can conclude that the salinity is both constant in the first kilometres from the river mouth, which is in contrast to the numerical model. Further from the river mouth, however, the analytical model also overestimates the salinity. Two potential causes for the overestimation were identified. The bottom slope of the Cai River can play a role for an intrusion length larger than 10 km. The analytical model assumed no bottom slope, while bathymetry data showed there is a bottom slope from 10 km from the estuary mouth. An uphill gradient is likely to decrease the intrusion length. Another reason for the difference can be an overestimation of the tidal excursion length. Shifting the outcome of the analytical model over half the excursion length to obtain the HWS salinity curve changes the output significantly (as can be seen in the uncertainty analysis in Figure 6.6). This research used a rough estimation of the excursion length, because of insufficient measurements, which makes it an uncertain input parameter. Due to both causes listed above, it is recommended to use only the TA values of the analytical model because the uncertainty is significantly lower. This despite the fact that extreme values (during HWS) are the most interesting when investigating nuisance caused by salification of the estuary.

Thirdly, inaccuracies in the numerical model could exist because it computed the vertical and horizontal mixing by a 3D turbulence model and background values specified by the user. The background values were not calibrated to reflect the actual situation. The actual dispersion in the river could therefore differ from the dispersion computed by the model. The numerical model also did not properly compute the bed shear stress. A uniform Chézy coefficient is specified on the grid, while this should be a depth-dependent parameter.

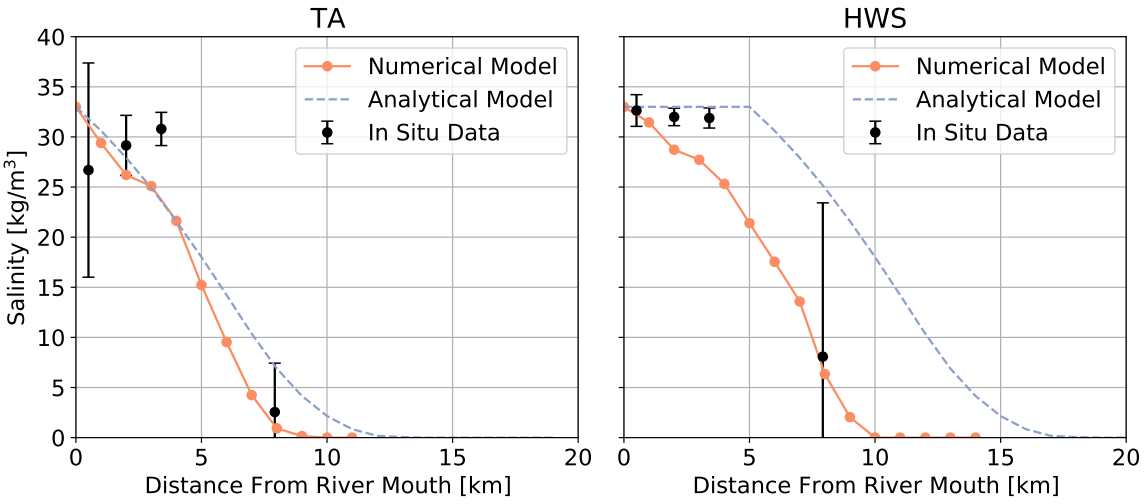

Figure 6.16: The TA and HWS Results of the Analytical Model and the Numerical Model Compared to the In Situ Measurements.

Lastly, the in situ measurements show a varying salinity at the river mouth as visible in Figure 6.16. In both the analytical and numerical model, however, the assumption is made that the salinity at the river mouth is always 33 kg/m^3. This is not necessarily true: freshwater outflow from the river, ocean currents and temperature can influence the salinity of the sea.

It should be noted that also the in situ measurement data is not fully reliable. Below, three reasons are mentioned. Firstly, the in situ data, measured in Dong Trang, referred to a min, max and mean value but it was not mentioned whether this concerns tidal averages, daily averages or other ways of determining the mean. Figure 6.16 displays the mean and max values, as these are assumed to have the highest similarity with respectively TA and HWS. This lack of knowledge is a big source of uncertainty itself already and should be taken into account in the interpretation of the results.

Secondly, both the analytical and numerical models use a freshwater discharge of 10 m^3/s at the mouth. In Subsection 2.4.4, it was already discussed that the discharge at Dong Trang is likely to be different than at the river mouth. Especially in the dry season, this difference can be substantial due to the outflow of the water reservoirs. The in situ data used in Figure 6.16 are based on five days in 2016 when the discharge measured at Dong Trang was between 8 and 12 m^3/s. It is, however, likely that the discharge at the river mouth was higher than those values. Therefore, it should be noted that the salinity values could possibly be higher when the discharge at the mouth equals 10 m^3/s.

Lastly, there are documents that report the existence (and the failing) of temporary dams in the Cai River. However, because information about the location, moment in time and technical details were missing, it was not included in this report. Still, the dams could have impacted salinity measurements used for calibration and validation.

6.3.2. Result Interpretation

Some interpretation can be done on the effect of certain parameters on the saltwater intrusion within the limitations of the models. Comparing the predictions of both models to changes in input can point out the strengths and weaknesses of each method.

First, both models suggested that there was a strong dependence on river discharge, which was in line with the literature. To get a more thorough understanding of the predicted correlation between saltwater intrusion length and discharge, the predictions of both models were normalized and compared. Figure 6.17 shows results of both models, both normalized to the saltwater intrusion length at a discharge of 10 m^3/s to allow for a better comparison.

The figure indicates that the analytical model predicted a stronger response than the numerical model to changes in discharge. The analytical model can be argued to be more accurate in predicting the relative increase in saltwater intrusion length because it was calibrated using in situ data. Even though the in situ data can also be argued to have high uncertainties, using those is likely to improve a model compared to a completely uncalibrated analytical model. Dispersion in the numerical model was hard to calibrate correctly and this can have lead to inaccurate results. Therefore, it is expected that the simpler analytical model based on real physical processes is more reliable in predicting the effect of discharge, especially when little calibration data is available.

The models indicated that discharges below 10 m^3/s would cause pumping stations up to 10 km from the river mouth to close since the salinity values here would exceed the maximum value of 0.25 kg/m^3. It should be noted that these indications were for the TA salinity, so for HWS, the saltwater was expected to reach even further. However, it has been pointed out that the models for HWS are not as reliable as for TA, so these results have to be validated more to be able to give more accurate predictions. This result can be recognised in the real situation: as written in the introduction the pumping stations within 15 km of the river mouth have had to shut down occasionally because of too high salinity.

Sea level rise is another parameter that was investigated in the models. In the analytical model, the sea level could not be changed as input, but only the mean water depth was altered. The numerical model agreed on the effect of the salinity curve shifting land inward. However, the numerical predictions showed a stronger effect of sea level rise. An increase of 1 m already showed an extension of the saltwater intrusion of more than 2 km. It is also valuable to look at the salinity at a fixed point; Figure 6.18 displays a comparison of the analytically and numerically modelled sensitivities to sea level rise of salinity 6 km from the river mouth. Both are normalized with respect to the current sea level. The numerical model showed an up to three times

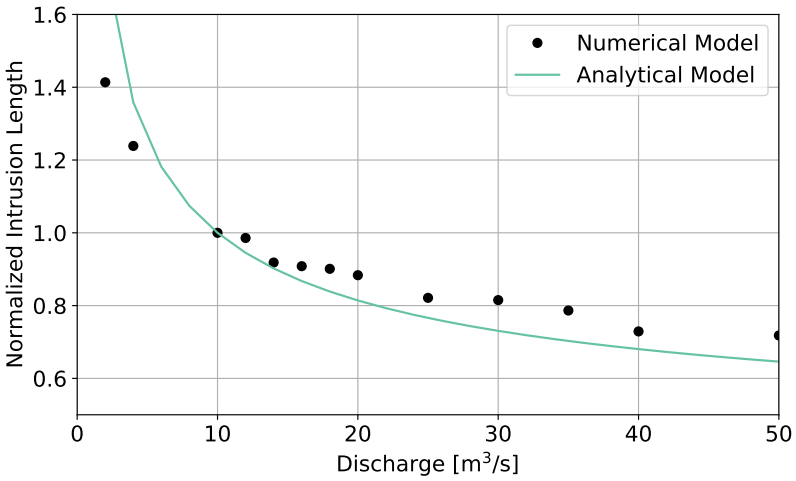

Figure 6.17: Modelled Saltwater Intrusion Length Normalized at Q_f = 10 m^3/s Against Discharge.

higher sensitivity, but both models agreed on the linear relationship.

The maximum projected sea level rise in Vietnam for 2070 is 43 cm. The numerical model suggested that this will increase the salinity at some parts of the Cai River by 20%, and will increase the saltwater intrusion length by approximately 0.5 km.

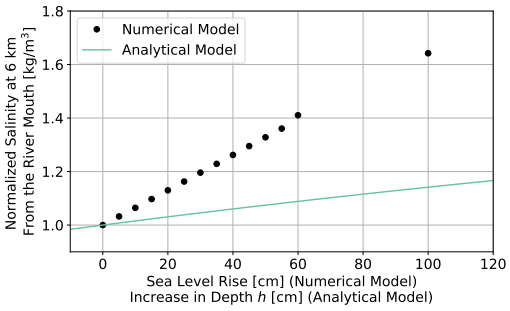

Figure 6.18: Comparison of Analytical and Numerical Model Sensitivity to Sea Level Rise or Water Depth Increase.

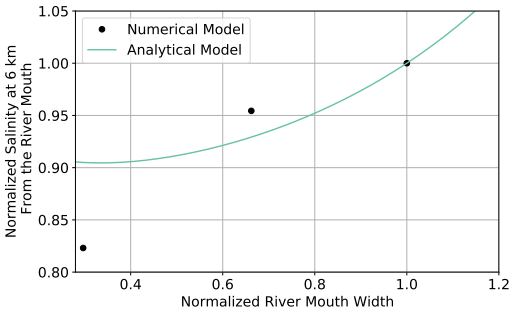

Figure 6.19: Comparison of Analytical and Numerical Model Sensitivity to River Mouth Width.

The change in river mouth width was explained in Chapter 3. The analytical model can change the parameter for effective mouth width B_0 and showed that mainly the shape of the intrusion curve changes. The numerical model performed three simulations for different mouth widths and seemed in agreement with the analytical model that the increment in salinity mainly was present in the middle part. Therefore, it seems likely that the widening of the river mouth from 130 to 438 m has mostly increased salinity values in the middle part of the estuary. The analytical model shows a maximum increase of 2 kg/m^3 between 2 and 7 km from the river mouth. The numerical model predicted an increase of up to 3 kg/m^3 on the section between 2 and 4 km from the river mouth. Both models also agreed that the length of the saltwater intrusion does not change significantly with increased river mouth width. Figure 6.19 shows a comparison of the modelled sensitivities to river mouth width. The analytical and numerical model agreed on an expected increased salinity for an increase in mouth width. The exact relation resulting from the models showed bigger differences, with both the shape and slope being different.

In a similar manner as was explained for the increase in sea level, the analytical model did not seem the more accurate method for modelling changes in bathymetry. Changing one input parameter in the analytical model does not match the changed bathymetry exactly, because the analytical model is based on the assumption of an exponential convergence. Changing the river mouth width also requires changing estimated convergence lengths, which introduced more errors. The shape of the analytical sensitivity to river mouth

width seems parabolic, which is not expected based on theory. The analytical model in its used form is not fit for assessing a geometry in one point only. Therefore, it is recommended to use the numerical model for assessing the effect of bathymetry changes, as this is more likely to produce more reliable results.

However, bathymetry changes also have some notable limitations in the numerical model. In this research, the models assumed the river bathymetry to be constant in time because only bathymetry data of a particular moment in 2017 was available. It is not documented if before or after this moment in time there have been dredging activities or if the river is locally narrowed or broadened (except for the river mouth). The models that were used to investigate the effect of the river mouth width also used the bathymetry from 2017 with slight adjustments. It is not possible to accurately assess the effect of the changes, since the current bathymetry has adjusted itself to the current situation. Calibration of the models may be performed using parameters resulted from an altered river bathymetry. Despite the limitations of both methods, it is encouraging that the analytical and numerical models are in agreement about the direction of the change of each input parameter. Only for the quantification of the effect, more validation is needed for obtaining more reliable results.

At all locations, the effect of the dam is clearly visible for the highest possible crest height. The salinity curve showed a drop at the dam for each location and a decrease is visible in the contour plots. A higher dam also showed higher effectiveness, which is to be expected; the higher the dam, the more the water is prevented from getting past the dam. For a dam height of 1 m, the salinity was reduced only slightly upstream, but the saltwater intrusion length remained roughly the same. For the highest dam height, the saltwater intrusion barely went past the dam. However, this is a logical effect, since the dam prevents almost all water from passing either way if it is completely raised with a crest level of 1.5 m above the reference level. The models showed the highest decrease in salinity and intrusion lengths when the dam is located at location 1, 2.7 km from the river mouth.

An important aspect influencing the effectiveness of the dam is the stratification of the water column. In Sections 4.2 and 6.2, the analytical model and the numerical model show that the estuary is well-mixed, especially for lower discharges. This means that only stopping convection in the lower part of the water column could prove to be less effective compared to more stratified estuaries.

It should be noted that these results are obtained with a constrained set of calibration points. They could not be validated with measurements nor analytical results because the saltwater intrusion prevention dam cannot be modelled in the analytical model used for this research. Furthermore, the numerical model also had limited ability to model the effect of the dam. The exact geometry of the dam is hard to input in the version of Delft3D used for this report. In the actual design, the dam consists of vertical gates, but the bathymetry was adjusted to the height of the dam and therefore a slope exists in the model. This could have decreased the effectiveness against saltwater intrusion in the model, so the actually proposed dam could possibly cause a higher drop in salinity than the results shown in this report. Because the dam was modelled as a change in bathymetry and not as a structure, turbulence around the structure is not computed by the numerical model. The eddies around the structure can affect the mixing of water and transport through the dam which in turn influences the saltwater intrusion.

7

Conclusions and Recommendations

This research aimed to analyse the development of the saltwater intrusion in the Cai River in Nha Trang, Vietnam. This was accomplished by performing a hydrological analysis of the river basin and by making both an analytical and a numerical model of the saltwater intrusion. Section 7.1 shows the conclusions of this research after which Section 7.2 gives recommendations for further research and possible ways to mitigate the problem of saltwater intrusion.

7.1. Conclusions

The goal of this research was to make a quantitative hydrological analysis of the development of saltwater intrusion in the Cai River in Nha Trang, Vietnam over the past 30 years and a view on the future. Research question 1, *How has the saltwater intrusion changed in the Cai River over the past 30 years?*, was not answered in detail in this research because of limited available salinity data. However, enough data was collected to be able to calibrate the analytical model and to compare the results of both models with in situ measurements.

Next, answers to research questions 2, 3 and 4 identified the possible drivers of saltwater intrusion providing an assessment of the current situation and past changes in local climate, freshwater use and bathymetry. Data suggested that the river discharge has remained roughly constant in the past 30 years. Furthermore, the water use within the Cai River basin is such a small fraction of the incoming water, that the influence on a yearly basis is limited. However, water usage can have a notable impact on the discharge during the dry season, when precipitation and therefore river discharge is low. Reservoir management partly compensates this. One major change in bathymetry was observed: the width of the river mouth has increased substantially from 130 to 438 m.

Both an analytical model and a numerical model were set up to answer research question 5, *To what extent do (future changes in) freshwater use, local climate and bathymetry influence the saltwater intrusion in the Cai River?* Both freshwater use and local climate influence the saltwater intrusion through the river discharge. Precipitation is expected to increase by approximately 9 to 16% in the basin (depending on the scenario), which can possibly increase the discharge by 14 to 24%, assuming the evapotranspiration to remain constant. This conversion from precipitation to discharge, however, cannot be considered to be of high accuracy, because of the imbalance in the water balance model.

The models showed that discharge is likely to be the most important driver of saltwater intrusion. The water usage is substantially smaller than the availability. Due to reservoir outflow in the dry season being of greater magnitude than the water usage, one can conclude that the influence of water usage in the Cai River on saltwater intrusion is likely limited. The saltwater intrusion in the wet season is less due to higher discharges but could decrease further due to increased discharge in the future. The numerical model indicated that the observed bathymetry change at the river mouth had a measurable effect on the modelled salinity values in the river. The analytical model supported this, but interestingly only the shape of the salinity curve was affected, not the intrusion length. It is expected that the salinity has increased between 2003 and 2020 due to the widening of the river mouth but this could not be supported by measurements.

With the same models, answers were obtained to research question 6, *What is the expected future change in saltwater intrusion in the Cai River (e.g. by the realisation of a saltwater intrusion dam)?*. Modelling of the projected sea level rise in Vietnam estimated an increase in the saltwater intrusion length by approximately 0.5 km in 2070.

Furthermore, the effect of the saltwater intrusion prevention dam seemed significant in the model used, but only for the highest position of the gate. At a crest height of +1 m, the dam did decrease the salinity upstream, but the intrusion length remained roughly the same. However, for the maximum level of +1.5 m, the dam was very effective in keeping the saltwater only downstream of the dam.

Combining all answers to the research questions, one can draw conclusions on the development of saltwater intrusion and its main drivers. The change in sea level and river mouth width are the most likely causes for any changes in saltwater intrusion in the past 30 years. However, this is not a solid conclusion, since not enough data was available to verify whether the salinity had changed at all. Water usage has and probably will have a limited effect on saltwater intrusion based on all analysed drivers. Possible future changes in discharge are likely to have a substantially larger effect. A proposed saltwater intrusion prevention dam is presumably effective in decreasing the length of the saltwater intrusion, but the well-mixed character of the estuary requires high crest heights to reach substantial effects in the model used.

7.2. Recommendations

The authors propose several ways towards improving the results of this research and possible follow-up researches. First, more elaborate in situ measurements of the salinity would contribute greatly to the accuracy of both models. Current data lacked in both temporal and spatial resolution, but also did not include information on the measurement conditions. Salinity data without specification of the tidal level or measurement depth are substantially less useful. A measurement campaign providing salinity measurements at a known depth at high water slack and low water slack would improve the analytical and numerical model, because it allows for enhanced calibration of constants and validation of the results. If the data source of the currently used values can be interpreted in more detail, this would already resolve some of the knowledge gaps.

One of the highest contributors to uncertainties in the results of the analytical model is currently the excursion length. Any in situ measurement campaign or research that provides a more reliable way to determine this excursion length would help to improve the HWS and LWS salinity estimates. A set of accurate salinity measurements can provide this, but also cross-sectional averaged velocity measurements over one tidal cycle would suffice.

Both this report and literature have shown that the salinity is highly dependent on the river discharge. However, the discharge at the river mouth is unknown in this area. Therefore, the authors also recommend a discharge measurement station at the river mouth at Nha Trang to provide daily discharge data for a period of several months for improved calibration and validation of the models. This is especially important if a field campaign is set up for salinity measurements. In that case, it is recommended to measure daily averaged discharge at least in the weeks before the salinity measurements. Discharge measurements at the river mouth are also helpful in improving the water balance model and possibly finding causes for the imbalance.

Next to acquiring more in situ data, more accurate predictions of the future saltwater intrusion can be obtained by improving the models themselves. The current numerical model does not include real-time operations, i.e. it does not change the status or height of the gates based on discharge or salinity measurements. A saltwater prevention dam is likely to be most effective when it can react to real-time in situ measurements. The effect of a dam can therefore be investigated in more detail if a new numerical model can be created, in which the status and heights of the gates are changed depending on certain real-time inputs. In this way, also different operation modes can be compared to obtain an optimal criterion for opening and closing parts of the dam.

The current models also do not take the water reservoirs into account. In the dry season, the discharge is very dependent on water reservoir operation. Including several river branches and water reservoirs in the model would improve the accuracy of the predictions. Furthermore, in a similar way as for a possible dam, a model can be used to optimize reservoir management for preventing saltwater intrusion.

Another possible topic for further investigation could be the (future) trend in extreme droughts and their influence on saltwater intrusion. Long term droughts will decrease the discharge substantially, while also increasing the water demand. This research has not focused on these events, but modelling these can be of

great value.

The former recommendations were about improving this specific research. This last paragraph contains recommendations about the measures to mitigate the problem of saltwater intrusion and some recommendations for possible follow-up researches in the Cai River basin.

Since it is likely that the magnitude of the saltwater intrusion increases in the future, the authors have looked into multiple solution strategies to mitigate the problem of saltwater intrusion so that the salinity at the freshwater pumping stations (the first one is 6 km upstream of the river mouth) is lower than the threshold value. Firstly, the local government already maintains a minimum discharge in the Cai River with the help of reservoirs. This research agrees that this is an effective way of pushing back the saltwater. However, the models suggest a rather high minimum discharge of 50 m^3/s is necessary to push back the saltwater enough. This is more than currently available in the dry season. So, the reservoir management would need an update. Another proposed measure is building a saltwater intrusion dam. The numerical model in this research suggests that this will be a good measure. A crest height of minimal +1.5 m with respect to the national datum is recommended in case of low river discharge (< 20 m^3/s). Thirdly, the local government could look into new options. Strategies involving nature-based solutions such as reduced water depth or artificial meanders could help to lower the saltwater intrusion length [16].

Lastly, some more comments can be made about the Cai River basin in general. Saltwater intrusion is not the only hydrological problem existing in the basin. As stated in the introduction in Chapter 1, also floods, coastal erosion and excessive sediment deposition pose a threat to the Cai River basin. Integrated Water Resources Management requires all these issues to be investigated to function optimally. Especially follow-up researches on floods and sediment deposition are closely related to this research. The numerical model could be extended to include these processes in the model.

References

[1] Discharge measured at dong trang from 1983-2012, and 2017. Provided by Dr. Dinh Nhat Quang from Thuyloi University, Vietnam.

[2] Rainfall data from 172 weather stations in vietnam. http://web.archive.org/web/20080207010024, 2017. Accessed: 2021-04-01.

[3] J.T. Abatzoglou, S.Z. Dobrowski, S.A. Parks, and K.C. Hegewisch. Terraclimate, a high-resolution global dataset of monthly climate and climatic water balance from 1958–2015. *Scientific data*, 5(1):1–12, 2018.

[4] A. Arakawa and V. R. Lamb. Computational design of the basic dynamical processes of the ucla general circulation model. *General circulation models of the atmosphere*, 17(Supplement C):173–265, 1977.

[5] H. Cai. *A new analytical framework for tidal propagation in estuaries*. PhD thesis, TU Delft, 2014.

[6] Center for International Earth Science Information Network - CIESIN - Columbia University. Gridded Population of the World, Version 4 (GPWv4): Population Count, Revision 11, 2018. URL https://doi.org/10.7927/H4JW8BX5.

[7] Center for International Earth Science Information Network - CIESIN - Columbia University, International Food Policy Research Institute - IFPRI, The World Bank, and Centro Internacional de Agricultura Tropical - CIAT. Global Rural-Urban Mapping Project, Version 1 (GRUMPv1): Population Count Grid, 2011. URL https://doi.org/10.7927/H4VT1Q1H.

[8] X. Cheng and Y. Qi. Trends of sea level variations in the south china sea from merged altimetry data. *Global and Planetary Change*, 57(3-4):371–382, 2007.

[9] Deltares. Delft3d-flow, user manual. August 2018.

[10] Viet nam công ty co phân tu vân t27 Don vi tu vân: liên danh vien khoa h c thuy loi. Tap 6 báo cáo tính toán thuy van thuy luc. 2017.

[11] P.X. Duong. Modelling of the salinity penetration at cal river in niiatrang in tile dry season using 1d and 2d models. *Vietnam Journal of Marine Science and Technology*, pages 36–50, 2008.

[12] Khanh Hoa Ministry for Agriculture & Rural Development & Institutes of Water Resources Planning. Báo cáo quy hoach cap nuoc, 2015.

[13] Y. Friocourt, K. Kuijper, and N. Leung. Salt intrusion, 2014. URL https://www.stowa.nl/deltafacts/zoetwatervoorziening/delta-facts-english-versions/salt-intrusion.

[14] J.I.A. Gisen, H.H.G. Savenije, and R.C. Nijzink. Revised predictive equations for salt intrusion modelling in estuaries. *Hydrol. Earth Syst. Sci.*, 19:2791–2803, 2015.

[15] 2030 Water Resources Group. Vietnam: Hydro-economic framework for assessing water sector challenges, 2017.

[16] G.G. Hendrickx, S.G.J Aarninkhof, and P.M.J. Herman. Nature-based solutions to mitigate salt intrusion. https://www.nck-web.org/boa-2021/423-nature-based-solutions-to-mitigate-salt-intrusion, 2021. Accessed: 29-06-2021.

[17] B. Hong and J. Shen. Responses of estuarine salinity and transport processes to potential future sea-level rise in the chesapeake bay. *Estuarine, Coastal and Shelf Science*, 104:33–45, 2012.

[18] Hydro-meteorological and Environmental Station Network Center. Quinhon. URL https://www.psmsl.org/data/obtaining/stations/1449.php.

[19] H.M. Le, Jessica R. P. Sutton, D.D. Bui, J. D. Bolten, and V. Lakshmi. Comparison and bias correction of tmpa precipitation products over the lower part of red–thai binh river basin of vietnam. *Remote Sensing*, 10(10), 2018. ISSN 2072-4292. doi: 10.3390/rs10101582. URL https://www.mdpi.com/2072-4292/10/10/1582.

[20] M. Le, H. Kim, H. Moon, R. Zhang, V. Lakshmi, and L. Nguyen. Assessment of drought conditions over vietnam using standardized precipitation evapotranspiration index, merra-2 re-analysis, and dynamic land cover. *Journal of Hydrology: Regional Studies*, 32:100767, 2020. ISSN 2214-5818. doi: https://doi.org/10.1016/j.ejrh.2020.100767. URL https://www.sciencedirect.com/science/article/pii/S221458182030241X.

[21] M. Milano, D. Ruelland, A. Dezetter, J. Fabre, S. Ardoin-Bardin, and E. Servat. Modeling the current and future capacity of water resources to meet water demands in the ebro basin. *Journal of Hydrology*, 500: 114–126, 07 2013.

[22] R. Mohammed and M. Scholz. Critical review of salinity intrusion in rivers and estuaries. *Journal of Water and Climate Change*, 9(1):1–16, 2018.

[23] T. Ngo-Duc, C. Kieu, M. Thatcher, D. Nguyen-Le, and T. Phan-Van. Climate projections for vietnam based on regional climate models. *Climate Research*, 60(3):199–213, 2014.

[24] X. Ngoc. Vietnam province cuts four hydropower projects out of environmental concerns, 2020. URL https://e.vnexpress.net/news/news/vietnam-province-cuts-four-hydropower-projects-out-of-environmental-concerns-4180022.html.

[25] A.D. Nguyen. *Salt Intrusion, Tides and Mixing in Multi-channel Estuaries.* PhD thesis, TU Delft, 2008.

[26] B.X. Nguyen and P.H.C. Tong. The characteristics of distribution and change of the seawater temperature and salinity of cai river estuary and northern part of nha trang bay in the dry and rainy seasons. *Collection of Marine Research Works*, pages 14–20, 2000.

[27] D. H. Nguyen, M. Umeyama, and T. Shintani. Importance of geometric characteristics for salinity distribution in convergent estuaries. *Journal of Hydrology*, pages 1–13, 2012.

[28] P.K. Nguyen. Climate change, sea level rise scenarios for vietnam. *Ministry of Natural resources and Environment. Hanoi, Vietnam*, 2009.

[29] T.L. Nguyen, T.T. Tran, H.S. Nguyen, V.V. Than, and Y. Lacroix. Estimation of shoreline changes of the cai river estuary in vietnam. In *Proceedings of Vietnam-Japan Workshop on Estuaries, Coasts and Rivers*, 2015.

[30] Khanh Hoa Department of Planning and Investment. Khanh hoa potential and prospects. http://khanhhoainvest.gov.vn/blog/article/khanh-hoa-potential-and-prospects, 2017. Accessed: 29-06-2021.

[31] Intergovernmental Panel on Climate Change. Ipcc special report - emissions scenarios, 2000. URL https://www.ipcc.ch/site/assets/uploads/2018/03/sres-en.pdf.

[32] P. Reig. What's the difference between water use and water consumption?, 2013. URL https://www.wri.org/insights/whats-difference-between-water-use-and-water-consumption#:~:text=%E2%80%9CWater%20use%E2%80%9D%20describes%20the%20total,its%20source%20to%20be%20used.&text=%E2%80%9CWater%20consumption%E2%80%9D%20is%20the%20portion,water%20source%20after%20being%20withdrawn.

[33] S. Running, Q. Mu, and M. Zhao. Mod16a2 modis/terra net evapotranspiration 8-day l4 global 500m sin grid v006 [data set], 2017.

[34] H.H.G. Savenije. Predictive model for salt intrusion in estuaries. *Journal of Hydrology*, 148:203–218, 1993.

[35] H.H.G. Savenije. *Salinity and Tides in Alluvial Estuaries.* Elsevier Publications, 2012.

[36] G.J. Schiereck. *Introduction to Bed, Bank and Shore Protection*. TU Delft, Department Hydraulic Engineering, Delft, The Netherlands, 1993-09-01.

[37] P.T. Shaw and S.H. Chao. Surface circulation in the south china sea. *Deep Sea Research Part I: Oceanographic Research Papers*, 41(11):1663–1683, 1994. ISSN 0967-0637. doi: https://doi.org/10.1016/0967-0637(94)90067-1. URL https://www.sciencedirect.com/science/article/pii/0967063794900671.

[38] W. Szczuciński, R. Jagodziński, T. Nguyen, A. Kubicki, and K. Stattegger. Sediment dynamics and hydrodynamics during low river discharge conditions in nha trang bay, vietnam. *Meyniana*, 57:117–132, 01 2005.

[39] T.N. Thien. Du an xay dung dap ngan man tren song cai nha trang. 2020.

[40] K. Thoa. Vietnamese province set to build dam-bridge over cai river in nha trang. https://tuoitrenews.vn/news/society/20200829/vietnamese-province-set-to-build-dambridge-over-cai-river-in-nha-trang/56456.html, 2020. Accessed: 2021-06-10.

[41] T. Thuc, N. Van Thang, H. T. L. Huong, M. Van Khiem, N.X. Hien, and D.H. Phong. Climate change and sea level rise scenarios for vietnam. *Ministry of Natural resources and Environment. Hanoi, Vietnam*, 2016.

[42] N.T. Viet, N.V. Duc, V.C. Hoang, H. Tanaka, T.T. Tung, J.P. Lefebvre, and R. Almar. Investigation of erosion mechanism on nha trang coast, vietnam. *Proceedings of the 19th IAHR-APD, Hanoi, Vietnam*, 2014.

[43] C. Wang, W.G. Wang, D. Wang, and Q. Wang. Interannual variability of the south china sea associated with el niño. *Journal of Geophysical Research: Oceans*, 111(C3), 2006.

[44] Z. Zhang. *A theoretical basis for salinity intrusion in estuaries*. PhD thesis, TU Delft, 2019.

[45] Z. Zhang and H.H.G. Savenije. The physics behind van der burgh's empirical equation, providing a new predictive equation for salinity intrusion in estuaries. *Hydrology and Earth System Sciences*, 21(7):3287–3305, 2017.

A

Appendix

A.1. Freshwater Demand per Sector

Table A.1: Water Demand per Sector per Month of the Year in mm.

		January	February	March	April	May	June	July	August	September	October	November	December	***Total***
2015	***Vùng LV Sông Cái Nha Trang***	***25,98***	***25,45***	***21,56***	***35,62***	***23,43***	***22,94***	***27,89***	***21,14***	***2,58***	***3,39***	***12,78***	***3,96***	***226,71***
1	Irrigation	8,61	8,98	4,07	18,55	5,84	5,97	10,12	3,46	0,71	1,47	10,94	2,07	80,78
2	Aquaculture	0,00	0,20	0,12	0,08	0,06	0,00	0,24	0,16	0,04	0,02	0,00	0,00	0,93
3	Livestock	0,08	0,07	0,08	0,07	0,08	0,07	0,08	0,08	0,07	0,08	0,07	0,08	0,89
4	Domestic	1,32	1,24	1,32	1,28	1,32	1,28	1,32	1,32	1,28	1,32	1,28	1,32	15,64
5	Tourism	0,32	0,32	0,32	0,48	0,48	0,48	0,48	0,48	0,32	0,32	0,32	0,32	4,64
6	Industry	0,17	0,16	0,17	0,16	0,17	0,16	0,17	0,17	0,16	0,17	0,16	0,17	2,01
7	Minimum DC	15,48	14,48	15,48	14,98	15,48	14,98	15,48	15,48	0,00	0,00	0,00	0,00	121,83
	Water inflow	26,95	12,83	15,28	7,79	7,30	13,50	6,65	5,81	48,65	117,50	281,77	160,94	704,97
	Difference	0,97	-12,62	-6,28	-27,82	-16,12	-9,45	-21,25	-15,33	46,07	114,11	269,00	156,98	478,26
														Total
2025	***Vùng LV Sông Cái Nha Trang***	***27,27***	***25,97***	***22,75***	***37,43***	***25,28***	***24,74***	***29,82***	***23,52***	***5,32***	***5,30***	***13,04***	***6,17***	***246,62***
1	Irrigation	8,07	7,91	3,55	18,11	5,39	5,42	9,92	3,62	1,67	1,58	9,39	2,45	77,08
2	Aquaculture	0,00	0,00	0,00	0,00	0,00	0,00	0,00	0,00	0,00	0,00	0,00	0,00	0,01
3	Livestock	0,13	0,12	0,13	0,13	0,13	0,13	0,13	0,13	0,13	0,13	0,13	0,13	1,55
4	Domestic	1,96	1,83	1,96	1,89	1,96	1,89	1,96	1,96	1,89	1,96	1,89	1,96	23,09
5	Tourism	1,39	1,39	1,39	2,08	2,08	2,08	2,08	2,08	1,39	1,39	1,39	1,39	20,09
6	Industry	0,25	0,23	0,25	0,24	0,25	0,24	0,25	0,25	0,24	0,25	0,24	0,25	2,96
7	Minimum DC	15,48	14,48	15,48	14,98	15,48	14,98	15,48	15,48	0,00	0,00	0,00	0,00	121,83
	Water inflow	26,92	12,79	15,14	7,52	6,70	12,60	6,44	5,78	50,41	121,72	292,24	161,19	719,46
	Difference	-0,35	-13,18	-7,61	-29,91	-18,58	-12,14	-23,37	-17,73	45,09	116,42	279,21	155,02	472,85
														Total
2035	***Vùng LV Sông Cái Nha Trang***	***29,93***	***28,31***	***25,36***	***40,78***	***28,56***	***27,94***	***33,17***	***26,98***	***7,48***	***7,94***	***15,65***	***8,75***	***280,85***
1	Irrigation	8,06	7,67	3,50	18,12	5,29	5,29	9,89	3,71	1,21	1,55	9,38	2,37	76,03
2	Aquaculture	0,00	0,00	0,00	0,00	0,00	0,00	0,00	0,00	0,00	0,00	0,00	0,00	0,01
3	Livestock	0,16	0,15	0,16	0,16	0,16	0,16	0,16	0,16	0,16	0,16	0,16	0,16	1,92
4	Domestic	3,16	2,95	3,16	3,06	3,16	3,06	3,16	3,16	3,06	3,16	3,06	3,16	37,29
5	Tourism	2,81	2,81	2,81	4,22	4,22	4,22	4,22	4,22	2,81	2,81	2,81	2,81	40,81
6	Industry	0,25	0,23	0,25	0,24	0,25	0,24	0,25	0,25	0,24	0,25	0,24	0,25	2,96
7	Minimum DC	15,48	14,48	15,48	14,98	15,48	14,98	15,48	15,48	0,00	0,00	0,00	0,00	121,83
	Water inflow	26,91	12,77	15,11	7,46	6,55	12,41	6,40	5,77	51,10	123,63	296,66	161,36	726,12
	Difference	-3,02	-15,54	-10,25	-33,32	-22,01	-15,54	-26,77	-21,21	43,62	115,69	281,01	152,61	445,26

A.2. Bed Roughness Calculation

The bed roughness/smoothness was determined as input for the numerical model. It causes the resistance to the flow and therefore influences the flow speed, water depth and salt intrusion.

The roughness can be computed using the White-Colebrook formula and/or the Manning formula. In this report the White-Colebrook formula was used, but the Manning roughness was also computed from the Chézy roughness. The White-Colebrook formula for the determination of the Chézy roughness is:

$$C = 18 \log_{10} \frac{12R}{k_s}$$

Where R is the hydraulic radius and k_s is the equivalent sand roughness. The value of k_s is not well defined, but for a stable bed without transport a value of $3D_{90}$ is often used [36]. The relation between the Manning roughness and the Chézy roughness is:

$$n = R^{\frac{1}{6}} / C$$

Measurements were conducted in the past as a study for the planned salt intrusion prevention dam [10]. The locations of the bed samples are shown in Figure A.1. The corresponding grain size distributions for the locations are given in Table A.2. Empty table cells correspond to no data for that particular grain size.

Figure A.1: Locations of the Bed Samples.

For the grain size distributions it was seen that measurement locations 8, 9 and 10 shows significantly different values that the other measurement locations. This could have been caused by dredging activities or excavations although the exact reason is unclear. Because of this local anomaly in the measurements, locations 8, 9 and 10 are deemed not representative for the remaining part of the river. The other points were analysed in order to compute the roughness of the Cai River.

As the grain size naturally becomes more coarse in upstream direction, the roughness also changes. However, due to the limited amount of measurement locations this effect could not be studied and it was assumed that the measured grain size distributions at these locations are representative for the remaining part of the Cai River that was analysed in this report.

In Table A.2 the average values and the cumulative values of the grain size distribution of points 1-7 and 11-16 are given. The cumulative values were plotted against the grain size in Figure A.2. From Figure A.2 the d_{90} was read, which is the grain size at the 90th percentage. 10% of the particles have a diameter larger and 90% of the particles have a diameter smaller that this d_{90}.

Table A.2: Bed Composition at the Different Measurement Locations and the Average and Cumulative Values.

	Grain size [mm]										
Loc. #	**<0,005**	**0,005-1**	**0,01-0,05**	**0,05-0,1**	**0,1-0,25**	**0,25-0,5**	**0,5-1**	**1,0-2,0**	**2,0-5,0**	**5,0-10,0**	**>10**
1	0,7	0,2	1,7	5,1	2	8,9	19	27,9	28,1	5,7	0,6
2	0,2	0,1	0,1	3,7	7,6	21,7	4,8	39,3	18,8	3,6	
3	0,2	0,1	0,1	3,7	7,6	21,7	4,8	39,3	18,8	3,6	
4	4,3	1,9	8,6	14,2	10,6	12,4	20,8	18,1	7,1	1,9	
5	0,2	0,1	0,1	4,8	19,9	29,4	27,8	12,2	5	0,4	
6	0,1		0,1	1,8	3,7	10,7	25,7	33,2	20,5	2,4	1,8
7	0,4	0,1	0,2	4,4	5,6	15	37,6	30,1	6,1	0,4	
8	37,3	13,5	31,7	9,7	7,6	0,2					
9	34,7	13	30,6	12,5	8,8	0,5					
10	31,4	12,2	29,2	13,8	13	0,5					
11	0,2	0,1	0,4	3,8	20,3	65,6	7,8	1,9			
12	0,1		0,2	17,5	29,4	49,7	2,5	0,5			
13	0,4	0,2	0,1	15,4	24	49,4	8,9	1,5			
14	6	4,1	9,7	6,9	1,7	8,9	15,5	26,8	18,1	2,5	
15	3,6	2,1	6,2	10,3	2,4	9,7	19,3	25,4	18,5	2,5	
16	0,2	0,1	0,1	3,9	6,9	16,1	34,6	26,6	9,6	1,8	
AVG	1,28	0,70	2,12	7,35	10,90	24,55	17,62	21,75	11,58	1,91	0,18
CUM	1,28	1,98	4,10	11,45	22,35	46,90	64,52	86,28	97,86	99,77	99,95

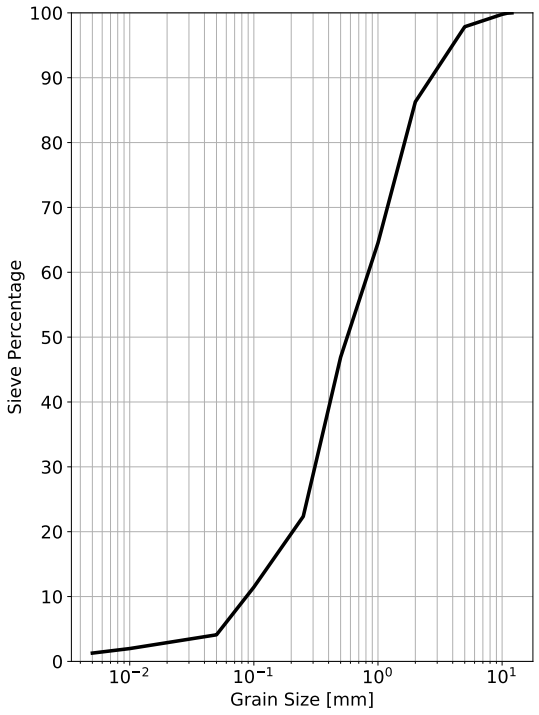

Figure A.2: Grading Curve of the Bed Composition in the Cai River.

The value read from Figure A.2 for the d_{90} is 2.68 mm. Together with the assumption that the hydraulic radius R is approximately the same as the water depth d for rivers, the values for the Chézy and Manning roughnesses were computed as a function of the water depth. The results can be found in Figures A.3 and A.4.

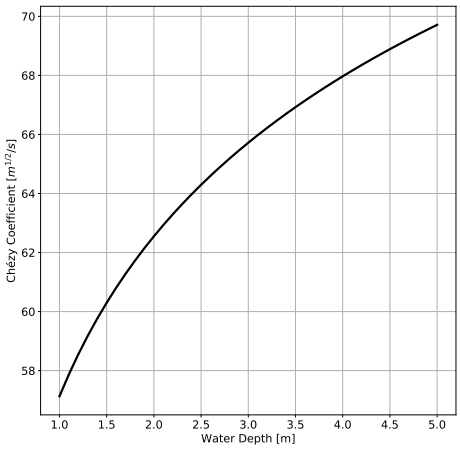

Figure A.3: Chézy roughness coefficient as a function of the water depth d.

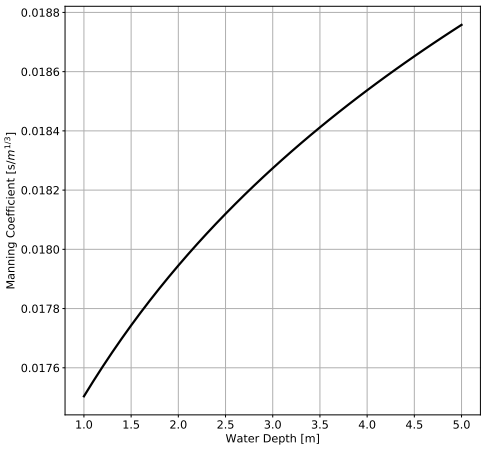

Figure A.4: Manning roughness coefficient as a function of the water depth d.

The water depth and bed composition throughout the numerical computation are not stationary in time and space and so the Chézy and Manning roughness change for every time step and location. However, the changes in water level are not that significant compared to the resulting relative change in the roughness. When considering the fact that the definition of k_s is not well defined, it means that the roughness was not determined to great precision. For these reasons, a Chézy roughness of 65 $m^{1/2}/s$ and a corresponding Manning roughness of 0.018 $s/m^{1/3}$ was chosen for every time step and for every place in the river during the numerical computations.

A.3. Input Data Processing

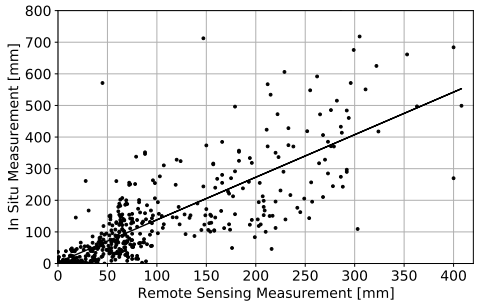

Figure A.5: Monthly Rainfall Measurements at Dong Trang From in Situ and Remote Sensing Data.

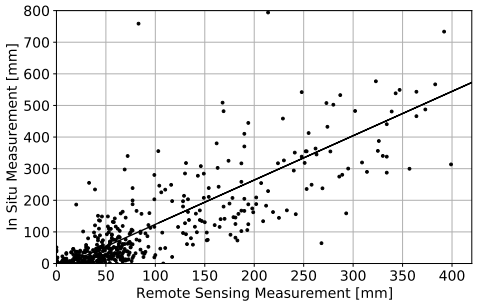

Figure A.6: Monthly Rainfall Measurements at Nha Trang From in Situ and Remote Sensing Data.

Table A.3: Correlation Between in Situ and Remote Sensing Rainfall Measurements.

	Slope [-]	Intercept [mm]	R^2
Dong Trang	1.35	3.57	0.63
Nha Trang	1.40	-16.5	0.69
Combined	1.38	-6.64	0.66

A.4. Water Demand Appendix

A.4.1. Domestic Water Use

The developments in domestic water use in a basin was estimated using population data and the mean domestic water demand per capita. The population data of the past 30 years was collected for the Cai River basin [6, 7]. In increments of five years the total population in the Cai River Basin is displayed in Figure A.7. The grey dotted line indicates a linear fit with an R^2-value of 0.989. It was concluded that the total population in the Cai River Basin has been growing constantly over the past 30 years and shows no signs of stagnation.

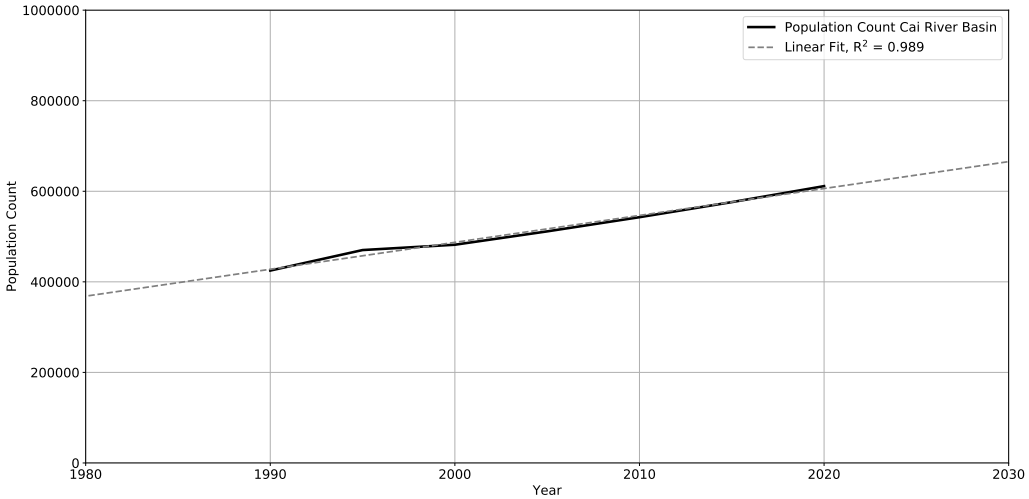

Figure A.7: Population Growth in the Cai River Basin.

A.4.2. Projections

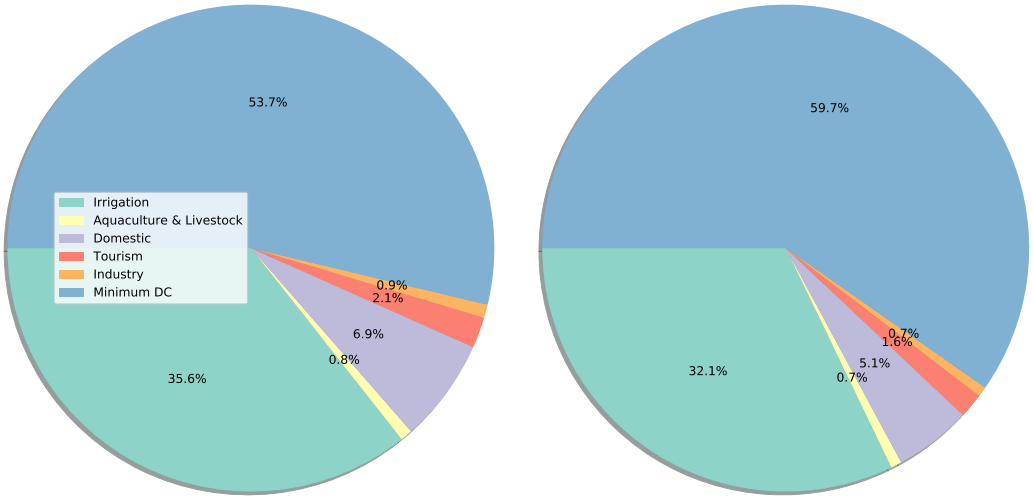

(a) 2015 Whole Year

(b) 2015 Dry Season

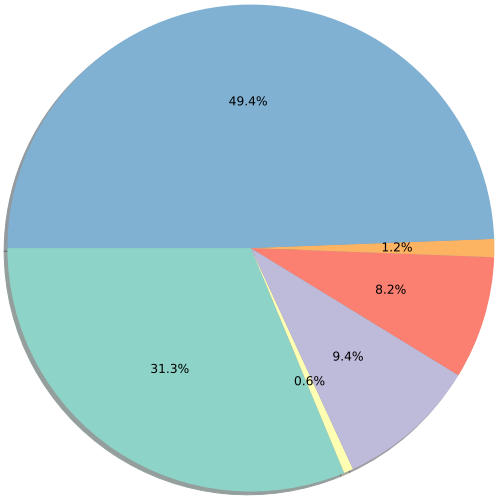

(c) 2025 Whole Year

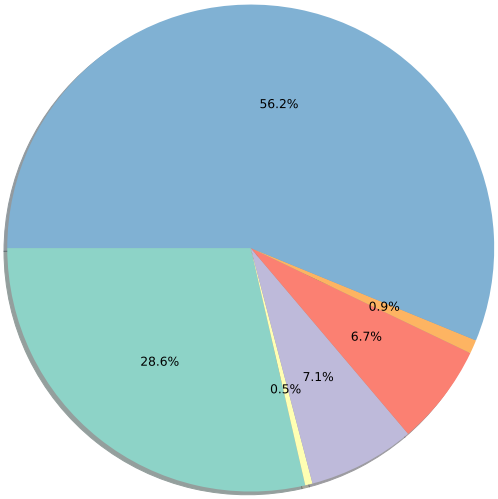

(d) 2025 Dry Season

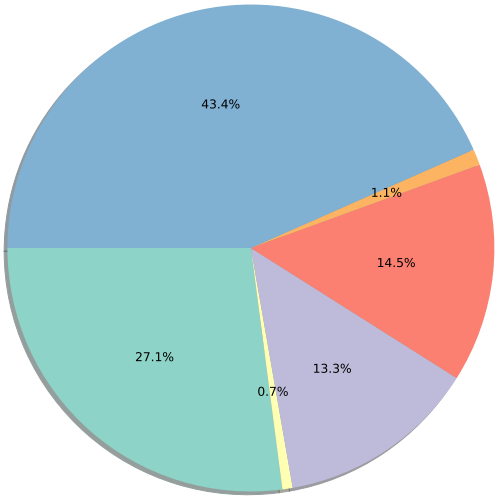

(e) 2035 Whole Year

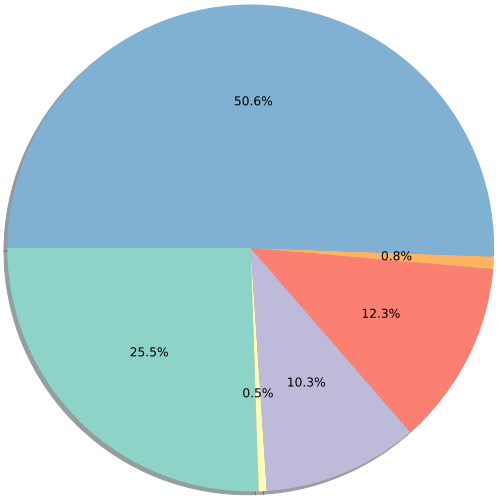

(f) 2035 Dry Season

Figure A.8: Distribution of the Freshwater Demand Per Sector Over the Whole Year and in the Dry Season (Jan-Aug) [12].

A.5. Tides

Figure A.9 shows the tidal spectrum off the coast of Nha Trang. Long-term, diurnal and semi-diurnal tidal constituents were clearly identified, whilst short-term constituents were of low magnitude and considered insignificant. For the remainder of this analysis, tidal constituents with an amplitude lower than 0.5 cm were neglected.

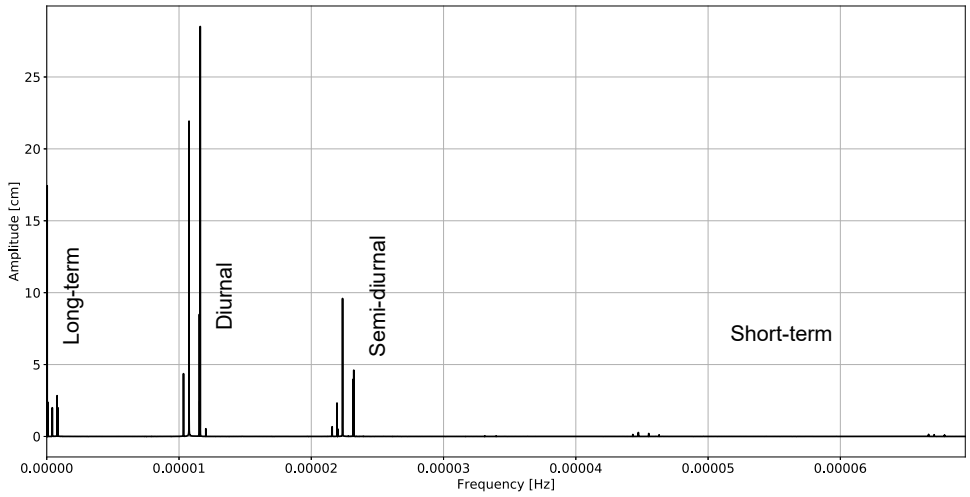

Figure A.9: Tidal Spectrum off the Coast of Nha Trang Showing the Tidal Constituents and Amplitudes.

Figure A.10 shows the tidal spectrum zoomed in for respectively the long term, the diurnal and the semi-diurnal tidal constituents and amplitudes. Table 3.1 summarises all the tidal constituents with amplitudes higher than 0.5 cm that have been found during the spectral analysis.

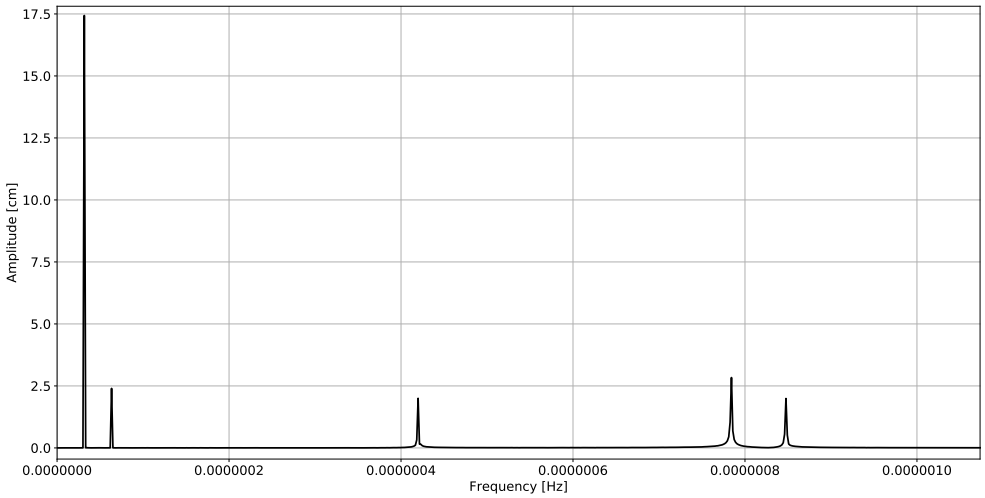

(a) Long Term

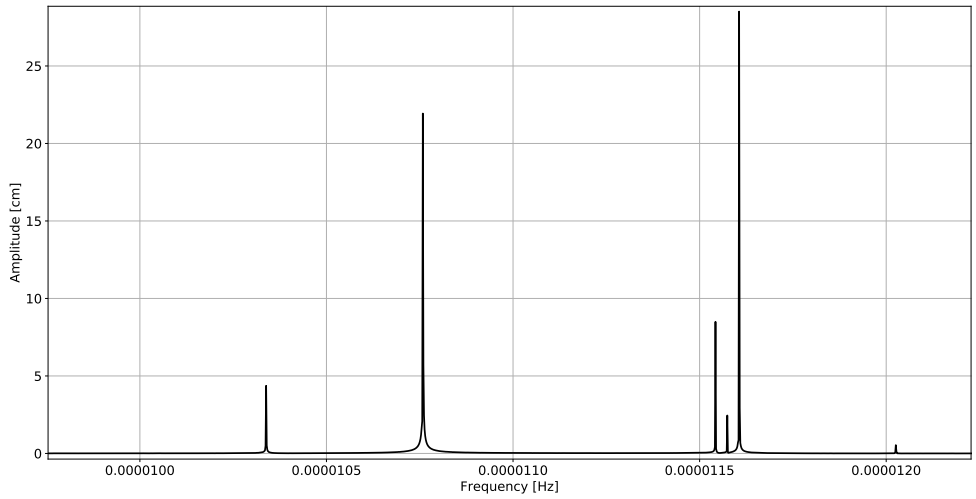

(b) Diurnal

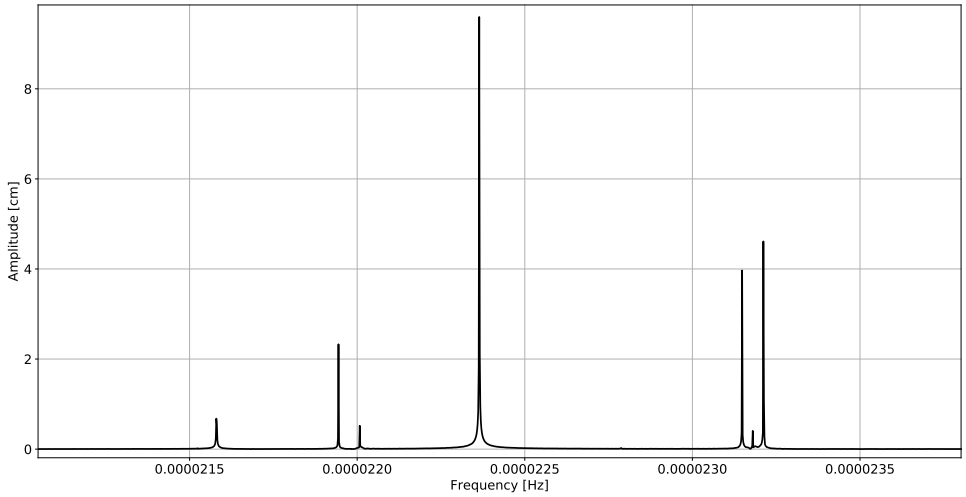

(c) Semi-Diurnal

Figure A.10: Tidal Constituents and Amplitudes measured off the coast of Nha Trang.

A.6. Estuarine Richardson Number

The estuarine Richardson number is calculated according the following formula:

$$N_R = \frac{\Delta\rho}{\rho_f}\frac{gh}{v^2}\frac{Q_f T}{EA_0} \tag{A.1}$$

where:

- $\Delta\rho = \rho - \rho_f$
- $\rho = 1021$ kg/m^3 is the saltwater density
- $\rho_f = 1000$ kg/m^3 is the freshwater density
- $g = 9.8$ m/s^2 is the gravitational acceleration
- $h = 3.81$ m is the mean water depth
- $v = \pi E/T$ [m/s] is the tidal velocity amplitude
- $E = 16000$ m is the tidal excursion length
- $T = 86400$ s is the tidal period
- $Q_f = 10$ m^3/s is the river discharge
- $A_0 = B_0 h$ [m^2] is the effective cross-sectional area of the river mouth
- $B_0 = 370$ m is the effective width of the river mouth

A.7. Delft3D Input

Many input parameters are required to model the estuary in Delft3D. Table A.4 gives an overview of all the input parameters of the model.

Table A.4: Input Parameters for the Numerical Delft3D Model.

Window	Tab	Parameter	Choice	Comment
Description	N/A	Textbox	Short description	Type of run, boundary conditions, simulation time, presence of the dam
Domain	Grid	Grid	Selected .grd file	The curvilinear grids created for this model are selected here
		Enclosure	Selected .enc file	Specifies the boundaries of the computational grid
		Latitude	12 degrees	The latitude of the area, needed to compute the coriolis force
		Orientation	0 degrees	Specifies the angle between the grid axis and the true North
		Number of layers	10 layers	Divides the grid in horizontal layers which is required to accurately model the transport of salt
		Layer thickness	10%	Same thickness for all layers
	Bathymetry	File	Selected .dep file	Depth file made by triangular interpolation between sample depth points
		Values specified at	Grid cell corners	The program used to create the bathymetry file uses this as default
		Cell center values computed using	Max	Kept at the default option
	Dry points	Location	None	
	Thin dam	Location	No thin dam used	Because thin dams block the flow completely, no thin dams were used. The dam was modelled by changing the bathymetry to the crest height of the dam
		Direction	N/A	No thin dam used
Time frame	N/A	Reference date	01 01 2021	Reference date at start of the year
		Start time	02 02 2021 00:00:00	Because February has the highest water levels of the dry season
		End time	17 02 2021 00:00:00	February 2nd till Feburary 17th covers a complete cycle between neap tide and the next neap tide so that the tidal averaged salinity and salinity during spring tide could be obtained.
		Time step	0.16 min	Depends on the grid size to obtain a good courant number, value suggested by the program
		Time step (dam simulations)	0.03 min	The timestep for simulations including dams had to be lower due to the smaller grid size around the dams.
		Local time zone	7+GMT	Local timezone in Vietnam
Processes	N/A	Active processes	Salinity	Only salinity is modelled for this research

Window	Tab	Parameter	Choice	Comment
Initial conditions	N/A	Water level	4 metres	Initial water level of 4 metres was used to create restart files for the actual simulations
		Salinity	0 ppt	Initial salinity of 0 ppt was used to create restart files for the actual simulations
Boundaries	Tide	Location	(M1, M2, N1, N2)= (1, 1, 4, 21)	Gives the grid points where the boundary of the sea water level starts and ends
		Type of boundary	Water level	The water level is specified on this boundary
		Reflection parameter alpha	0	This was kept on the default value
		Forcing type	Astronomical	The astronomical forcing was determined in Section A.5
		Transport conditions	Salinity of 33 ppt	The salinity in the sea was constant for all simulations and based on the mean value
	Discharge	Location	(M1, M2, N1, N2)= (242, 242, 4, 17)	Gives the grid points of the upstream boundary where the discharge was specified
		Type of boundary	Total discharge	The total discharge coming from the upstream part of the river was used as input for this boundary condition
		Reflection parameter alpha	0	This was kept on the default value
		Forcing type	Time-series	A time series with a constant discharge of 10 m^3/s was used for most simulations. Discharge was also varied to investigate the effect of the discharge on the salt intrusion
		Transport conditions	Salinity of 0 ppt	The water coming from the river was assumed to be fresh water
Phyiscal parameters	Constants	Gravity	9.81 m^2/s	Default gravitational acceleration
		Water density	1000 kg/m^3	Default value and density difference due to salinity is computed by the program
		Temperature	25 °C	Mean sea surface temperature at Nha Trang
	Rougness	Rougness formula	Chézy	Chézy values were determined in Section A.2
		Uniform	65 for U and V direction	This is the average value found in Section A.2
		Wall rougness	Free slip condition	Neglected due to large scale of the model
	Viscosity	Background horizontal eddy viscosity	1 m^2/s uniform	Kept at the default value, because parameter could not be calibrated
		Background horizontal eddy diffusivity	1 m^2/s uniform	Also set to 1 as this parameter could not be calibrated
		Model for 2D turbulence	None	Only the model for 3D turbulence was used

Window	Tab	Parameter	Choice	Comment
Phyiscal parameters	Viscosity	Background vertical eddy viscosity	0 m^2/s	Vertical eddy viscosity determined by 3D turbulence model
		Background vertical eddy diffusivity	0 m^2/s	Vertical eddy diffusivity determined by 3D turbulence model
		Ozmidov length scale	0 m	Only the 3D turbulence model was used
		3D turbulence model	κ-Epsilon	Most commonly used 3D turbulence model
Numerical parameters	N/A	Drying and flooding check at	Grid cell centres and faces	Kept at default option
		Depth at grid cell faces	Mean	Kept at default option
		Threshold depth	0.05 m	The threshold depth should be larger than $\frac{2\pi\|a\|}{N}$ with a the characteristic amplitude and N the number of timesteps per period. The threshold value for our model was just above 0.02 m and was rounded up to 0.05 m
		Marginal depth	-999	The marginal depth was not used in the model
		Smoothing time	60 min	Kept ath the default value
		Advection scheme for momentum	Cyclic	As suggested by Bas van Maren from Deltares
		Advection scheme for transport	Cyclic	As suggested by Bas van Maren from Deltares
		Forester filter	On for vertical and horizontal	Filters the negative concentrations which are physically impossible
		Correction for sigma-coordinates	Off	Kept at default option
Operations	N/A	No operations used		
Monitoring	Observations	Points	Observations points every kilometre	Model gave output for observation points with an interval of one kilometre and the dam models contained additional observation points
	Drogues	Drogues	None	No data required through drogues
	Cross-sections	Location	Cross-sections at the dams and river mouth	Only cross-sectional data on these locations was required
Additional parameters	N/A	No additional parameters used		
Output parameters	Storage	Map results start/stop time	Same as model start/stop time	The map results were only stored when needed to save storage space
		History interval	12 min	Must be a multiple of the timestep and short enough to create smooth graphs
		Restart interval	Dependent on required file	Only used when a specific restart file was required
		Other output parameters	Not used	The other output options were not used during this research

A.8. Distributions of the Uncertainty Analysis Parameters

The distributions used for all input parameters of the analytical model are found in Table A.5. The distribution are estimates because of a lack of data. An attempt was made to calculate the deviations but for some parameters only a rough estimate was possible. In this appendix gives an explanation for all distributions.

Table A.5: Parameters and Distributions for the Uncertainty Analysis.

Parameter	Distribution type	Distribution parameters
Q_f	Deterministic	10
x_1	Normal	$\mu = 7046$, $\sigma = 605$
b_1	Weibull	$u = 179639$, $k = 1.2$
A_1	Normal	$\mu = 433$, $\sigma = 30$
a_1	Normal (equal to b_1)	$\mu = 179639$, $\sigma = 313944$
B_0	Normal	$\mu = 370$, $\sigma = 10$
E	Normal	$\mu = 10000$, $\sigma = 4000$

$\boldsymbol{Q_f}$: This parameter was used as variable input in the models and was thus kept deterministic. The value for Q_f was altered and the resulting saltwater intrusion was observed from the models.

$\boldsymbol{x_1}$: This value and its standard deviation have been determined using regression analysis.

$\boldsymbol{b_1}$: A Weibull distribution was chosen for the width convergence length of the upstream part. From the regression analysis that determined the geometric parameters, standard deviations were determined as well. Because the bed is nearly flat upstream of the inflection point, the convergence length is very large (this can bee seen in Figure 5.2. A slight change in slope on a semi-logaritmic plot can lead to big changes in convergence length, which is why the standard deviation is so high. In order to prevent some samples of b_1 to be drawn lower than zero, a Weibull distribution was applied. The parameters were adjusted as such that it matches the calculated mean and standard deviation.

$\boldsymbol{A_1}$: The cross-sectional area at the inflection point was assumed normally distributed and has a standard deviation of approximately 30 m^2. The standard deviation was based on the standard deviation of the width of the river, but it was increased due to the large assumption in the water depth at the inflection point.

$\boldsymbol{a_1}$: See explanation of b_1. As the slope of the depth was assumed to be zero, the convergence length for the area is the same as the convergence length for the width.

$\boldsymbol{B_0}$: The effective width at the river mouth is a part of the total width of the river. The sides of the river are storage areas and the river bed has a slope, not the full width and full depth was thus available for conveyance of saltwater into the Cai River. Slight mistakes in the assumptions for the effective width resulted in the standard deviation as given in Table A.5.

$\boldsymbol{E}$: Because of the lack of in situ data, the tidal excursion length was guessed based on personal communication with H.H.G. Savenije (June, 2021), who wrote 10 km is a typical excursion length for estuaries like the Cai River estuary. However, this value can vary a lot for different estuaries. Therefore, a standard deviation of 4000 m was applied (comprising also a sufficient range of tidal velocity amplitude which is closely depended on the tidal excursion length).